Drought Analysis of the Lake Manyara Catchment:

Meteorological Drought Occurrence, Influence of Atmospheric Teleconnections and Impact on Lake Manyara

Tamara Keijzer

Universiteit Utrecht

Drought Analysis of the Lake Manyara Catchment:

Meteorological Drought Occurrence, Influence of Atmospheric Teleconnections and Impact on Lake Manyara

MSc Thesis

July-2020

Author: Tamara Keijzer

Student number: 4288165

E-mail: t.keijzer@students.uu.nl

First supervisor: Geert Sterk

Second supervisor: Niko Wanders

MSc Programme: Earth Surface and Water

Faculty of Geosciences

Department of Physical Geography

Utrecht University

Abstract

Lake Manyara is a terminal lake in northern Tanzania. As a destination of wildlife and part of a national park, it provides a booming tourism industry in the region. The lake also reflects water availability in the catchment used e.g. for agriculture. The catchment experiences a bimodal precipitation pattern, with a long rainy season in March-May and a short rainy season in October-December. Fluctuating lake levels, especially shrinkage of Lake Manyara during dry periods, raise concerns about the (future) water availability and potential disappearance of the lake. Possible mechanisms driving these fluctuations are: land use and land cover changes, sedimentation of the lake, irrigation water abstractions and climate change/drought. The aim of this study was to determine the impact of drought on the dynamics of Lake Manyara. The occurrence of drought over the past century in the Lake Manyara catchment (LMC), the influence of atmospheric teleconnections on LMC rainfall and the impact of drought on Lake Manyara are explored.

The occurrence of meteorological drought and characteristics (duration, severity and frequency) was studied using the Standardized Precipitation Index (SPI) and Standardized Precipitation Evapotranspiration Index (SPEI) with periods of 3 (short-term droughts) and 12 (long-term droughts) months. A literature study explored the relevant teleconnections influencing East African rainfall: the El Niño-Southern Oscillation, Indian Ocean Dipole, Madden-Julian Oscillation, Southern Annular Mode and North Atlantic Oscillation. Monthly, seasonal, lead-lagged, sliding and partial correlations between rainfall and teleconnections were applied. To determine the impact of drought on Lake Manyara available observations regarding its size were linked with meteorological variables and the drought indices.

In general, a drying trend was found in the LMC over the last century. The short rainy season does not show a clear drying or wetting trend. Precipitation of this season was found to be related to atmospheric teleconnections. Though overall correlations with the IOD, ENSO and MJO are quite strong, the relations between rainfall and teleconnections changed through time. These changes correspond with changes in the strength of Walker circulation cells of the Indian, Pacific and Atlantic Ocean. The long rainy season shows a drying trend. Rainfall during this season showed only weak influence by atmospheric teleconnections. Combined rainfall and evapotranspiration showed largest impact on changes in the volume of Lake Manyara ($r=0.56$). Though the drought indicators did not show strong relation, the strong influence of P-PET on changing lake volume does imply the impact of drought occurrence. This would decrease the value of P and P-PET, which can cause shrinkage of Lake Manyara. Models predict further increase in temperature, and thus evapotranspiration, in the future. This implies (long-term) shrinkage of the lake. However, future change in P is uncertain. Improvement of the models simulating future precipitation are important to estimate the magnitude of effort required to improve future water resource management in the Lake Manyara catchment.

Cover photo by Harry van den Bergh

Acknowledgements

When I first encountered this thesis subject I was immediately interested in and enthusiastic for both the subject matter and the opportunity to visit Tanzania for fieldwork. Things however did not go as planned. Therefore, first of all, I would like to thank Geert for understanding and keeping this subject reserved for me. I would also like to thank my supervisors for their help, advice, support and patience during the making of this thesis. Additionally, I am grateful to family and friends for their support, positivity and feedback. Unfortunately, I was not able to go to the Lake Manyara catchment to perform fieldwork. One day I will visit Tanzania and I look forward to exploring this catchment, the size of the lake at that time and its environment with my own eyes.

Table of contents

1. Introduction....1
1.1 Background information....1
1.2 Problem definition....2
1.3 Study objective....3
2. Study area....4
3. Methods....7
3.1 Literature study....7
3.2 Data....7
3.2.1 Precipitation and temperature....7
3.2.2 Atmospheric teleconnections....8
3.2.3 Lake Manyara....9
3.3 Analyses....11
3.3.1 Drought analysis....11
3.3.2 Influence of atmospheric teleconnections on LMC rainfall....13
3.3.3 Drought occurrence and Lake Manyara fluctuations....14
4. Results....15
4.1 Literature study of atmospheric teleconnections....15
4.1.1 Walker circulation....15
4.1.2 El Niño-Southern Oscillation....18
4.1.3 Indian Ocean Dipole....19
4.1.4 Madden-Julian Oscillation....20
4.1.5 Southern Annular Mode....22
4.1.6 North Atlantic Oscillation....23
4.1.7 Nonstationary relationship teleconnections and East African rainfall....25
4.1.8 Interrelations teleconnections....28
4.1.9 Conclusion....28
4.2 Drought analysis....30
4.2.1 Precipitation and temperature....30
4.2.2 SPI and SPEI....32
4.2.3 Drought characteristics....37
4.3 Influence of atmospheric teleconnections on LMC rainfall....39
4.3.1 Monthly correlation....39
4.3.2 Seasonal correlation....41
4.3.2 Sliding correlation....42
4.3.3 Partial correlation....44

4.4 Drought occurrence and Lake Manyara fluctuations 45
5. Discussion 51
5.1 Data limitations and method implications 51
5.2 Drought analysis 52
5.3 Influence of atmospheric teleconnections on LMC rainfall 53
5.4 Drought occurrence and Lake Manyara fluctuations 55
5.5 Recommendations 56
6. Conclusion 57
References 58
Appendices 67
Appendix A: Comparison precipitation datasets 67
Appendix B: Lake Manyara surface area observations 72
Appendix C: Yearly SPI-3 and SPEI-3 rainy seasons 73
Appendix D: Teleconnection correlations of the other months 74

List of Tables

Table 1: Location and available rainfall data of six weather stations in the LMC. All stations were used to form the In-situ dataset. Location of the stations is also shown in Figure 1. 8
Table 2: Overview of the precipitation products. * indicates the dataset is used to form the Reanalysis dataset. 8
Table 3: SPI-based classification of drought. 12
Table 4: Guidelines for interpretation of a correlation coefficient. Adapted from: Karadimitriou (2020). 13
Table 5: Results of Mann-Kendall Trend test applied to SPI and SPEI values of individual months for all 3-month SPI/SPEI and applied to all values (overall) for both 3- and 12-month SPI/SPEI. Plus indicates a positive trend. Minus indicates a negative trend. Significant trend (α=0.05) indicated by *. 36
Table 6: Results of Mann-Kendall Trend test applied to decadal drought characteristics. Plus means an increasing trend of the variable through the decades (1910/1930-2010), minus indicates a decreasing trend. Zero indicates no positive nor negative trend. Significant trend (α=0.05) indicated by * 38
Table 7: Correlation values between March-May rainfall and teleconnections for the period 1978-2010. Both partial and standard Pearson correlation values were calculated for comparison. Significance of the relation: * significant at α=0.10, ** significant at α=0.05. 44
Table 8: Correlation values between October-December rainfall and teleconnections for the period 1978-2010. Both partial and standard Pearson correlation values were calculated for comparison. Significance of the relation: * significant at α=0.10, ** significant at α=0.05 44
Table 9: Correlations values between several variables and the volume of Lake Manyara. No lag/lead applied. Significance: * significant at α=0.10, ** significant at α=0.05. 48
Table 10: Correlations values between several variables and the change in volume of Lake Manyara. Significance: * significant at α=0.10, ** significant at α=0.05. 50

List of Figures

Figure 1: Location and elevation map of the Lake Manyara catchment. Adapted from: Deus et al. (2013). Modified by the addition of rain gauge stations. 4
Figure 2: Annual precipitation and temperature variability. Adapted from: TMA (2019). 5
Figure 3: Mean location of the ITCZ and direction of surface winds during January, April, July and November. Adapted from: Dhonneur (1974). 6
Figure 4: Computation of lake volume. Left: bathymetric map adapted from Deus et al. (2013). Upper right: relation between surface area and depth with linear trend line. Bottom right: relation between surface area and volume according to Eq. 3. 10

Figure 5: Definitions of drought duration, drought severity and drought intensity by the run theory of Yevjevich (1967). Adapted from: Zhang et al. (2015). 12
Figure 6: Generalized Walker circulation (Dec-Feb) during normal conditions. Convection occurs at the rising branches. Adapted from: NOAA (2014). 15
Figure 7: Equatorial east-west atmospheric circulation: climatologies of a) all months, b) January, c) July for the period 1949-1999. In colour: areas of strong upward (positive values) and downward (negative values) motion. Adapted from: Lau & Yang (2003). The location of the LMC is indicated by the red line. 16
Figure 8: Vertical motion expressed by omega as a function of latitude averaged between 10° N- 10° S. Positive values represent subsidence and negative values ascent. Top diagram: October-November (short rainy season). Bottom diagram: March-April-May (long rainy season). Adapted from: Nicholson (2017). 17
Figure 9: Generalized Walker circulation (Dec-Feb) during ENSO-neutral conditions (upper), El Niño (middle) and La Niña (lower). Colours indicate anomalous ocean cooling (blue/green) and warming (orange). Adapted from: NOAA (2014) 19
Figure 10: Circulation pattern, equatorial thermocline and SST anomalies across the equatorial Indian Ocean during a neutral, positive and negative IOD phase. Adapted from: Commonwealth of Australia (2013). 20
Figure 11: Rainfall anomalies for all 1979-2012 November-March MJO events. The phases represent the grouped geographically based stages of the convection zone. Green shaded areas show above average rainfall (enhanced convection), while brown shaded areas show below-average rainfall (suppressed convection). The eastward movement of the shaded areas can be seen in each successive phase from top to bottom. Adapted from: Gottschalck (2014) 21
Figure 12: Changes around Antarctica during a positive SAM. Adapted from: Government of Western Australia (2019). 22
Figure 13: Mechanism of the influence of a positive SAM on October-December rainfall in East Africa. Replacing the red words with the antonym gives the mechanism of a negative SAM. 23
Figure 14: Influence of the NAO on East African wind fields. Lighter and darker grey zones represent statistical significance at the 95% and 99% confidence intervals. The red dot indicates the location of the LMC. A) Location of the five alternating bands of zonal wind strength. Values represent 300-hPa u-component wind velocity standardized regression coefficients associated with the NAO index. Negative isolines are broken. B) 850-hPa streamlines associated with a positive NAO index. Adapted from: McHugh & Rogers (2001). 24
Figure 15: Mechanism of the influence of a positive NAO on boreal winter rainfall in East Africa. Replacing the red words with the antonym, and Indian Ocean with Atlantic Ocean, gives the mechanism of a negative NAO. 25
Figure 16: Upper: 20-year mean October-November rainfall. Bottom: Sliding 20-year correlation between October-November rainfall and the IOD/Niño 3.4 index. Values are plotted at the final year of the 20-year interval. Vertical lines indicate regime shifts. Values exceeding ±0.38 are significant (α=0.05). Adopted from: Nicholson (2015). 26
Figure 17: Vertical motion expressed by omega as a function of latitude averaged between 10° N- 10° S over four time periods. Adapted from: Nicholson (2015) 26
Figure 18: 31-year running correlation between the SAM and East African October-December rainfall. Blue line represents the correlation values. Bars show the p-values. Adapted from Manatsa et al. (2016). 27
Figure 19: Total rainfall of the long rainy season (March-May) from 1900 up to and including 2018 according to the In-situ and Reanalysis datasets. A linear trend line is presented for both datasets. 30
Figure 20: Total rainfall of the short rainy season (October-December) from 1900 up to and including 2018 according to the In-situ and Reanalysis datasets. A linear trend line is presented for both datasets. 30
Figure 21: Annual rainfall from 1900 up to and including 2018 according to the In-situ and Reanalysis datasets. A linear trend line is presented for both datasets 31
Figure 22: CRU monthly mean temperature of the region 3-6° S, 35-37° E from 1901 up to and including 2018. 31
Figure 23: 3-month SPI and SPEI values through time for the In-situ and Reanalysis datasets 33
Figure 24: 12-month SPI and SPEI values through time for the In-situ and Reanalysis datasets. 34
Figure 25: 3-month SPI and SPEI values from 1990 to 2010 34
Figure 26: Differences between SPEI and SPI values for both 3- and 12-months period of interest and the In-situ and Reanalysis datasets. 35
Figure 27: Differences between the In-situ and Reanalysis datasets in SPI-3, SPI-12, SPEI-3 and SPEI-12 values. 35
Figure 28: Total drought duration (TDD), total drought severity (TDS) and average drought intensity (ADI) per decade for both SPI and SPEI, 3- and 12-months periods of interest and the In-situ and Reanalysis datasets 37
Figure 29: Total number of moderate, severe and extreme droughts per decade for each SPI and SPEI time-series 38

Figure 30: Correlations between rainfall and teleconnection indices with a maximum lead of 6 months for the separate months of the rainy seasons. Both Kendall and Pearson's correlations are shown for the In-situ and Reanalysis datasets. These figures for the other months can be found in Appendix E. 40
Figure 31: Correlations between rainfall and teleconnection indices with a maximum lead of 6 months for the long (March-May) and short (October-December) rainy season. Pearson's correlations are shown for the In-situ and Reanalysis datasets..... 41
Figure 32: Sliding 20-year correlations between March-May rainfall and the teleconnections IOD, MJO, NAO, SAM and ENSO. Values are plotted at the final year of the 20-year interval. The sliding correlations are calculated for both the In-situ and Reanalysis dataset. Values exceeding ±0.44 (indicated by dotted lines) are significant (α=0.05)..... 42
Figure 33: Sliding 20-year correlations between October-December rainfall and the teleconnections IOD, MJO, NAO, SAM and ENSO. Values are plotted at the final year of the 20-year interval. The sliding correlations are calculated for both the In-situ and Reanalysis dataset. Values exceeding ±0.44 (indicated by dotted lines) are significant (α=0.05). 43
Figure 34: Monthly SPI-3, SPEI-3, SPI-12, SPEI-12, P, P-PET and the volume of Lake Manyara plotted from 2000 to 2019. 46
Figure 35: Correlations between the volume of Lake Manyara and drought indicators with a maximum lead of 12 months. Both Kendall and Pearson's correlations are shown. 47
Figure 36: Volume of Lake Manyara plotted against SPI-3, SPEI-3, SPI-12, SPEI-12 values of the same month. Blue indicates evapotranspiration is not taken into account. Green indicates evapotranspiration is taken into account. Linear trend lines are also shown. R2 of this line is the squared of Pearson's r in Table 9. 47
Figure 37: Change in volume of Lake Manyara plotted against cumulative SPI-3, SPEI-3, SPI-12, SPEI-12 values between the observations. Blue indicates evapotranspiration is not taken into account. Green indicates evapotranspiration is taken into account. Linear trend lines are also shown. R2 of this line is the squared of Pearson's r in Table 10..... 49
Figure 38: Change in volume of Lake Manyara plotted against cumulative P and P-PET values between the observations. Blue indicates evapotranspiration is not taken into account. Green indicates evapotranspiration is taken into account. Linear trend lines are also shown. R2 of this line is the squared of Pearson's r in Table 10..... 49

1. Introduction

1.1 Background information

Water is the most fundamental natural resource of the world. However, over the last decades the demand for water has increased due to global population growth and increasing water consumption (WWAP, 2009). Water demands are expected to increase even more with predicted higher temperatures and longer dry periods due to (anthropogenic) climate change (Karl et al., 2009; Vörösmarty et al., 2010). This intensifying pressure on water availability can lead to below normal water availability, described as drought (Tallaksen & van Lanen, 2004). Droughts are characterized as a regionally extensive and sustained occurrence of below average values of variables as precipitation (meteorological drought), soil moisture (agricultural drought), streamflow or groundwater (hydrological drought, van Loon, 2015). Worldwide the spatial and temporal characteristics of drought vary, depending on climate and catchment characteristics (van Lanen et al., 2013). Due to the large scale direct and indirect environmental, economic and social impacts it affects more people globally than any other natural hazard (Schwabe et al., 2013). The most severe social consequences (e.g. decrease in drinking water availability, famine or conflicts) are present in arid and semi-arid regions, as in these regions the normal availability of water is already low and the vulnerability to drought is high (Tallaksen & van Lanen, 2004).

Tanzania is a country where vulnerability to droughts is high due to the reliance on rain-fed agriculture (Kijazi & Reason, 2009; Arndt et al., 2012). Agriculture provides a livelihood to more than 75% of Tanzania's population. The sector accounts for 29% of the Gross Domestic Product (GDP) (2017) and 95% of the national food requirements (Massoy, 2016; World Bank, 2017). Droughts between 1998 and 2005 caused food shortages as a result of crop failures and livestock losses. Another consequence was water rationing due to reduction in the water level of reservoirs (Kijazi & Reason, 2009; Rwehumbiza, 2014). These surface water reservoirs reflect both climatic and environmental changes. The impact of changes in the relationship between precipitation, water inflow and water loss due to evaporation, seepage and drainage is greatest on shallow lakes as a slight change in water volume has large areal effects (Simonsson, 2001).

Lake Manyara is an example of a lake that has fluctuated considerably in depth and area for thousand years and continues to fluctuate to this day (Simonsson, 2001; van Mens, 2016). It is located in the East African Rift in Tanzania, where the rift escarpments and volcanic highlands control the local climate and thus the precipitation in the lake basin (Yanda & Madulu, 2005). Lake Manyara is the terminal lake of a closed basin, making it sensitive to changes in local climate and catchment characteristics (UNEP, 2004). Although the saline-alkaline Lake Manyara itself is not a source of drinking water, the inputs to the lake are (Nonga et al., 2011). Therefore, the lake volume reflects the availability of usable water in the catchment. Frequently conflicts arise in the region because of competition for natural resources, including water. Water availability is important in the basin as both society (agriculture, tourism, drinking water) and wildlife depend on it (Ngana et al., 2004). The lake, when full, covers two-thirds of Lake Manyara National Park, which is a destination of herds of livestock in the dry season and a corridor for migrating wildlife. The lake itself is inhabited by (endangered) fish species and attracts various species of water birds. The presence of this wildlife results in the booming tourism industry present in the region (Ngana et al., 2004; Bayona, 2006; BirdLife International, 2019). Local people expressed their concerns about the shrinkage of Lake Manyara during dry periods and the possibility of disappearance of the lake (Ihucha, 2012; van Mens, 2016).

1.2 Problem definition

The fluctuating lake levels and the potential disappearance of Lake Manyara raise concerns about the (future) water availability in the region. Deus et al. (2013) showed a large variation of the lake surface area by mapping the water surface from 2000 to 2011 using remote sensing. The extent of Lake Manyara varied significantly from 520.25 km^2 in 2000 to 13.25 km^2 in 2005. In order to know what the future holds and to allow sustainable management of water resources in the catchment, the mechanisms driving the lake dynamics should be determined. Locals reported sedimentation, decreased rainfall and increased human activities near the rivers and lake as causes of decreased size, depth and water level (Nonga et al., 2010). Ihucha (2012) blamed global warming for the drying of the lake and siltation for a decrease of depth by up to two meters. According to literature, possible mechanisms driving the lake fluctuations include: land use and land cover changes, sedimentation of the lake, irrigation water abstractions and climate change. All these potential contributors to lake level change have to be quantified to understand the fluctuating lake levels and determine the chance of disappearance of Lake Manyara (Goerner et al., 2009; Nonga et al., 2010; Deus & Gloaguen, 2013; Deus et al., 2013; van Mens, 2016).

According to multiple studies, the number of farmers in the Lake Manyara region has increased since the 1950s due to population increase (Rohde & Hillhorst, 2001; Sechambo, 2001; Msoffe et al., 2011; Wynants et al., 2018). The proclaimed expanding shift from a predominantly pastoral zone to a populated agricultural landscape would comprise unsustainable land use practices, overgrazing and the clearing of vegetation. This could cause an increase in land degradation (e.g. lower soil fertility, gully formation, sheet and wind erosion) and changes in the hydrological regime (Rohde & Hillhorst, 2001; Nonga et al., 2010; van den Bergh, 2016; Wynants et al., 2018). An increase in run-off and soil erosion can lead to more sediment transportation causing siltation of Lake Manyara (Mwalyosi, 1992; Rohde & Hillhorst, 2001; Ngana et al., 2004; Yanda & Madulu, 2005; Nonga et al., 2010). Since the Lake Manyara catchment is a closed system, incoming sediments are never washed out. Therefore, enhanced siltation can decrease the depth of Lake Manyara. This could lead to lake disappearance (Sechambo, 2001; Choiński & Ptak, 2009). However, Verhoeve (2019) showed big variations and no significant trend in land use and land cover change over time, questioning the liability from previously mentioned studies regarding land use and land cover changes. Furthermore, the exact human impact on the sediment fluxes and the (variation in) soil erosion and siltation rates are not known (Yanda & Madulu, 2005; Munishi et al., 2017; Wynants et al., 2017).

Lake level fluctuations could also be caused by irrigation water abstractions. The abstraction of water from rivers for irrigation decreases the total inflow into the lake. Irrigation practices in the Lake Manyara catchment date back to 1955. Irrigated farming is common in the area: 75% (2011) of the households that grow crops enhance cultivation using river water. The importance of water availability arises here: 92% of the farmers proclaimed a shortage of water for irrigation and that these shortages lead to conflicts among farmers. They affirm that almost all river water is used for irrigation during dry seasons (Nonga et al., 2011). Van Mens (2016) showed that during dry years more water was indeed abstracted for irrigation. However, the influence of irrigation water abstractions on river discharge was minimal. Furthermore, van Mens (2016) noted the difficulty in quantifying a possible increase in irrigation water abstraction over time due to a lack of data. The largest part of the catchment is un-gauged and the inflow is unknown, which makes an estimate of Lake Manyara's water balance difficult (Deus et al., 2013).

The last suggested reason for change in lake dynamics is climate change. Global climate change can alter the magnitude, frequency and impacts of (extreme) meteorological events. Msoffe et al. (2011) argued that severe droughts become more frequent in the Lake Manyara region based on annual rainfall data. A questionnaire by van den Bergh (2016) showed that locals think it is drier and warmer nowadays and they reported more frequent periods of drought now compared to 10-20 years ago. The Tanzania National Adaptation Program of Action also listed prolonged dry spells as a vulnerability for the agricultural sector caused by climate change (United Republic of

Tanzania, 2007). More frequent droughts can lead to shrinking of Lake Manyara due to a reduced precipitation input and more output through higher evaporation. Deus et al. (2013) showed a strong relationship between the year to year change in Lake Manyara's surface area and annual meteorological parameters, suggesting the distinct impact of climate on Lake Manyara. Mercier et al. (2002) studied 12 larger continental lakes within the Rift Valley region. They identified the connection between interannual lake water balance variation and precipitation changes in the region, which were influenced by Sea Surface Temperatures (SST) of the Indian Ocean. Multiple studies indicated the relationship between East African rainfall and phenomena altering the atmospheric circulation patterns, including SST anomalies by atmospheric teleconnections (Black, 2005; Manatsa et al., 2008; Kijazi & Reason, 2009; Williams & Hanan, 2011; Tierney et al., 2013).

Hence, more frequent periods of drought, influenced by climate change, could be a reason for the fluctuations of Lake Manyara in size. However, a thorough understanding of (future) climate change, drought occurrence and its consequences in the Lake Manyara catchment is missing (WSDP, 2014). Climate change scenarios created by General Circulation Models (GCMs) suggest that the climate in Tanzania will become warmer, but there is no consensus whether the average precipitation will increase or decrease. Climate change is expected to vary widely within even countries. Therefore, higher spatial-resolution knowledge about the changing climate is necessary (Lobell et al., 2008; Arndt et al., 2012). Regarding drought occurrence, only annual data has been examined in the studies mentioned above, while the Lake Manyara experiences a bimodal rainfall pattern. A thorough investigation concerning the intra-annual variations in drought occurrence, the cause of these variations and the consequences has not been executed so far. Understanding gained from an analysis of historic drought events in the catchment offers possibilities for better drought management planning. In this way, the impacts of current and future droughts can be mitigated (Vicente-Serrano et al., 2012). Furthermore, the vulnerability of water resources to drought can be determined (Mishra & Singh, 2010).

1.3 Study objective

The aim of this study is to determine the impact of drought on the dynamics of Lake Manyara.

The following research objectives were defined:

- Analyse meteorological drought occurrence (duration, severity and frequency) in the Lake Manyara catchment from the 1900s until present (2019)
- Analyse the influence of atmospheric teleconnections on rainfall in the Lake Manyara catchment
- Study the impact of drought on the size fluctuations of Lake Manyara.

2. Study area

The study area of this research is the Lake Manyara catchment (LMC). Lake Manyara is located 126 km west of Arusha in northern Tanzania (3°25′–3°48′ S, 35°44′–35°53′ E). The LMC is the most southern basin in the eastern branch of the East African Rift System. It covers an area of 18.470 km² (3°03′–5°90′ S, 35°26′–36°40′ E) with elevations between 885 m and 3618 m a.s.l. (Figure 1). The topography is influenced by tectonic and volcanic activity in the area. In the west Lake Manyara is flanked by a deep escarpment. In the north of the LMC the Ngorongoro volcanic complex is present. In the east an undulating plain with volcanic cones is superseded by a peneplain surface (Simonsson, 2001; Deus & Gloaguen, 2013). The LMC is a closed basin with no natural outlet. Several springs and rivers, both perennial and seasonal, drain into Lake Manyara (Yanda & Madulu, 2005). It is a shallow (maximum depth 1.18m in June 2010) alkaline-saline lake. The present Lake Manyara is the remaining part of a much larger and deeper (300 m) paleolake (Casanova & Hillaire-Marcel, 1992; Somi, 1993; Deus et al., 2013).

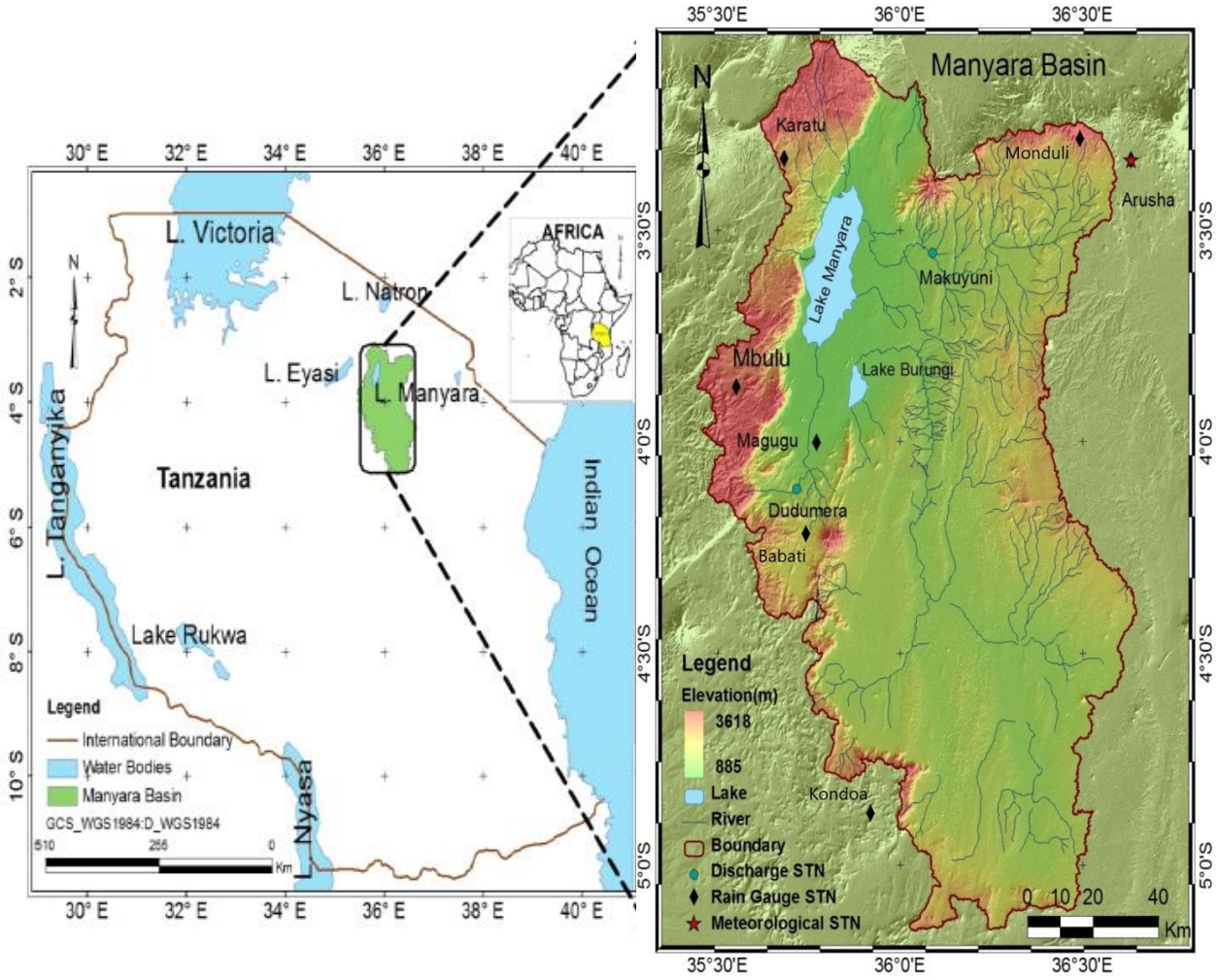

Figure 1: Location and elevation map of the Lake Manyara catchment. Adapted from: Deus et al. (2013). Modified by the addition of rain gauge stations.

The main vegetation of the LMC includes forest, acacia woodland, thicket woodland, alkaline grassland, cynodon grassland and swamps (AWF, 2003). On the elevated areas west of Lake Manyara mainly tropical semi-humid vegetation cover and highland forests are present. East of the lake and in the south of the catchment the environment is more semi-arid. Here vegetation is sparse and of savanna type (Yanda & Madulu, 2005; Bachofer et al., 2014; Verhoeve, 2019). The dominant types of land use are rain-fed agriculture, pastures and savanna (Maerker et al., 2015). In the Monduli District, located in the northern part of the LMC, more than 90% of the population is engaged in agriculture and livestock. The LMC is an attractive region for immigrants due to the fertile grounds and possibility of irrigated agriculture (Ngana et al., 2004). Crop types that are planted frequently include bananas, rice, maize and vegetables (Nonga et al., 2011; van Mens, 2016). Irrigated farming is applied in the Mto wa Mbu area during the dry season (Nonga et al., 2011). Another main economic activity is tourism due to the presence of wildlife and National Parks (MDC, 2014; Maerker et al., 2015). Pastoralism is the main land use activity of the Masai communities present in the region. They use the rivers, streams, dams and tap water as surface water sources and wetlands as pastures for their livestock. The river networks in the LMC provide water for domestic and agricultural uses (Yanda & Madulu, 2005; Nonga et al., 2011; Van Mens, 2016).

The LMC experiences a bimodal precipitation pattern (Figure 2). The short rainy season occurs from October to December, followed by a short and hot dry season (January-February). The long rainy season is from March to May. Then a long dry season lasts from May/June to October with cooler temperatures. Average air temperatures range from 14-30°C, being highest from December to March (Deus et al., 2013; TMA, 2019). Mean annual rainfall varies from 450 to 1200 mm, with an average of 750 mm rainfall annually (AWF, 2003; TMA, 2019). The lower areas receive on average less rainfall annually (500-700 mm) than the highlands (1000-1200 mm) (Prins, 1987; AWF, 2003; Bachofer et al., 2014; Quénéhervé et al., 2015).

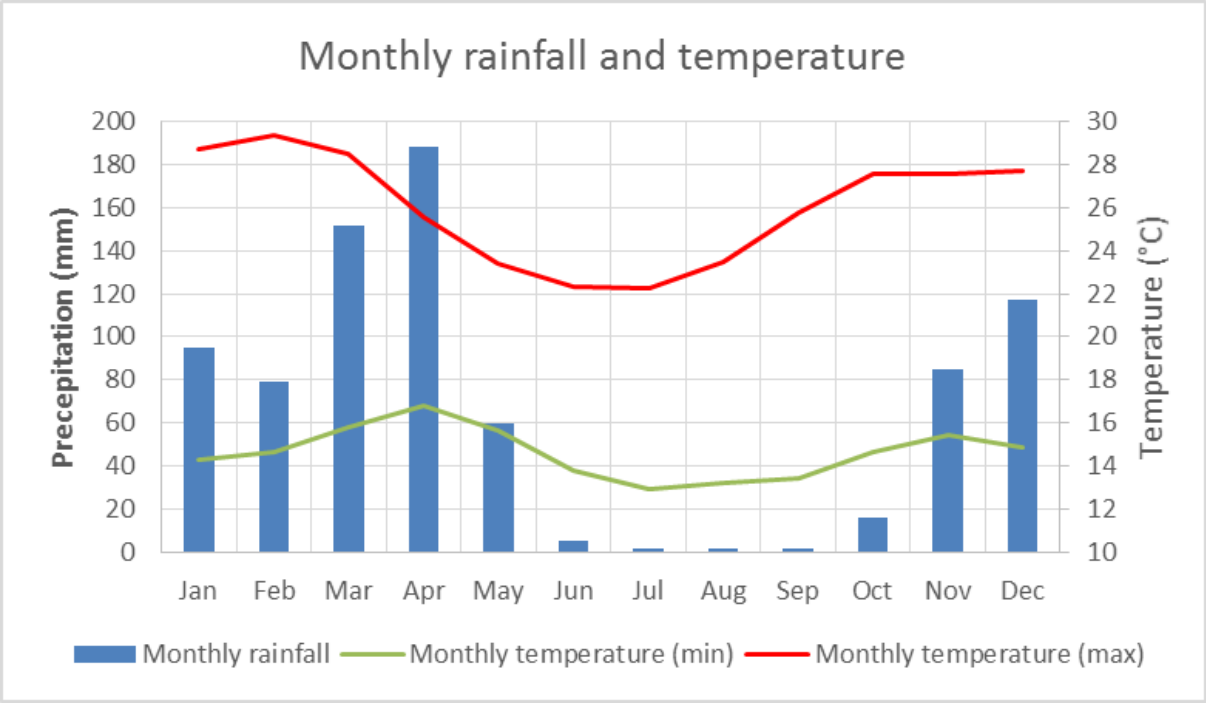

Figure 2: Annual precipitation and temperature variability. Adapted from: TMA (2019).

The existence of two rainy seasons in the study area is linked to the movement of the inter-tropical convergence zone (ITCZ) and the associated rain belt (Figure 3). The ITCZ generally takes longer to move northwards over the area in March-June than southwards in September-December and therefore generates the long- and short rainy seasons respectively (Henderson et al., 1949; Kijazi & Reason, 2009; Nicholson, 2018). Rainfall anomalies in northern Tanzania are often associated with atmospheric teleconnections as the El Niño-Southern Oscillation (ENSO), Indian Ocean Dipole (IOD) and Madden-Julian Oscillation (MJO) (Black, 2005; Kijazi & Reason, 2005; Manatsa et al., 2008; Kijazi & Reason, 2009; Williams & Hanan, 2011; Tierney et al., 2013).

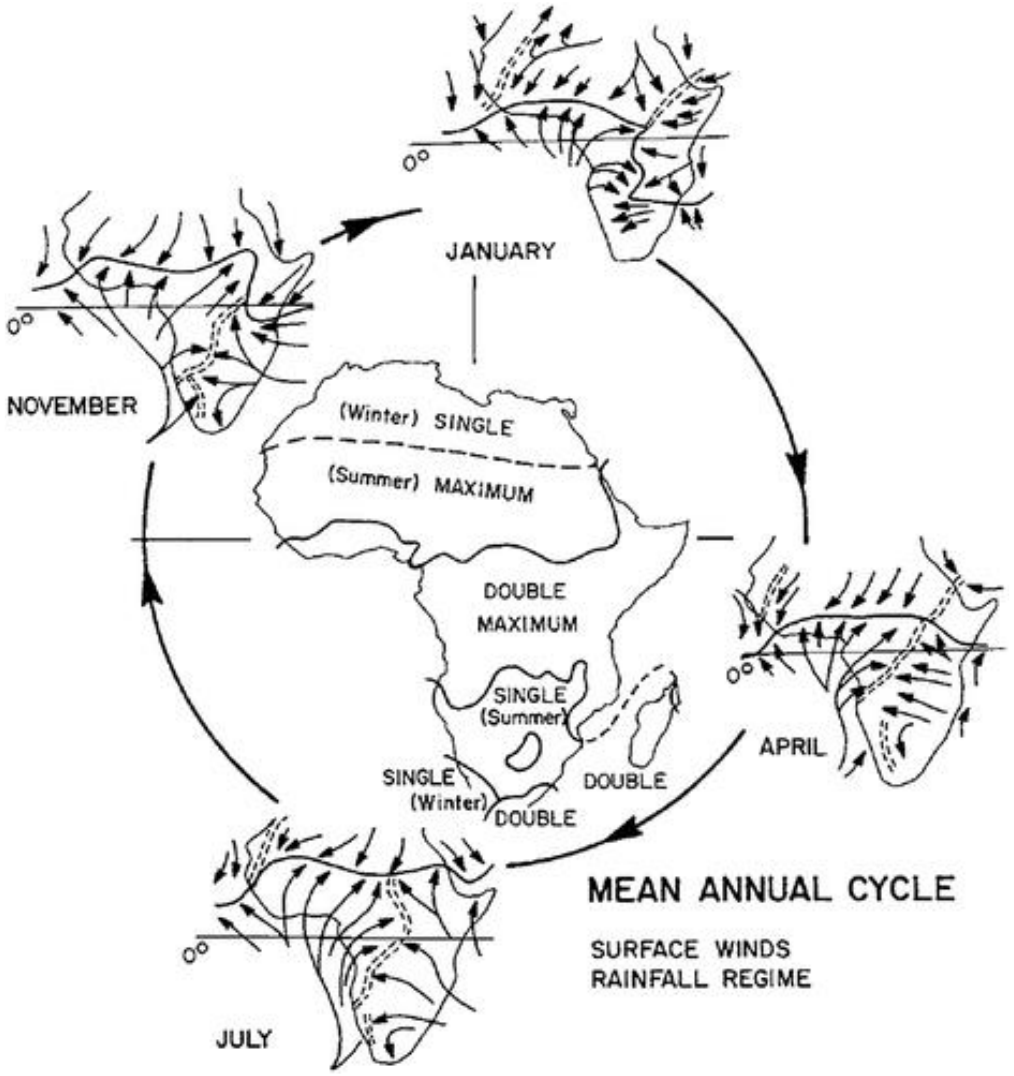

Figure 3: Mean location of the ITCZ and direction of surface winds during January, April, July and November. Adapted from: Dhonneur (1974).

3. Methods

3.1 Literature study

First a literature study was conducted exploring available research regarding connections between rainfall anomalies in northern Tanzania/East Africa and relevant atmospheric teleconnections. The potential relation between the discussed teleconnections was also examined. Using this review, it was determined which teleconnections were investigated to be related to rainfall anomalies in the LMC.

3.2 Data

Limited in-situ data is available for the LMC, as the lake is ungauged and the catchment poorly gauged. However, nowadays reanalysis and satellite-based techniques can provide continuous hydro-meteorological data. In this study, different types of data were used based on availability, frequency, range and suitability.

3.2.1 Precipitation and temperature

The in-situ data for precipitation was provided by the Tanzania Meteorological Agency (TMA) and the Climate Explorer of the Royal Dutch Meteorological Institute (KNMI). Monthly time series are available from 6 stations in or just outside the study area with varying temporal ranges. Within these ranges missing values are present. The amount of missing values differs for each station (Table 1; Figure 1). Due to the imperfection of the in-situ data regarding missing values, temporal aspects and the low and varying spatial distribution of the available stations in the region, other precipitation products were examined (Table 2). These combine in-situ observations, satellite measurements and/or climate reanalysis to create a precipitation dataset. The precipitation products were obtained through the Climate Explorer of the KNMI. The mean monthly precipitation of the area between coordinates ~3-6° S, ~35-37° E was taken for each product as drought is not a catchment confined phenomenon and the products are delivered grid sized.

All datasets were compared with each other (Appendix A). The temporal period for comparison was chosen when the datasets overlap (1981-1994). Both mean monthly and total annual values were compared. Dataset inter-comparison was performed using the coefficient of determination (R^2), root-mean-square-error (RMSE) and t- and F-tests. Based on this analysis two new datasets were formed. The average of all in-situ datasets was used in further analysis, as the average rainfall over the catchment is desired. This new time series is referred to as the In-situ dataset. It ranges from November 1902 up to and including December 2018. It contains 111 missing values (8%) of which 103 prior to 1922. Concerning the precipitation products, the average was taken of CHIRPS, CRU, GPCC and GPCP datasets for further analysis. ERA5 and ERA-interim were not included in further analysis as they showed large differences with the other precipitation products. The new time series is referred to as the Reanalysis dataset. It ranges from January 1891 up to November 2019 and has no missing values. Analyses were executed using both datasets to see whether there is large difference between the use of in-situ data or precipitation products.

The temperature data used in this study is the CRU TS4.03 monthly mean temperature obtained via the KNMI Climate Explorer. It is created using observations interpolated into 0.5° latitude/longitude grid cells combined with existing climatology to obtain absolute monthly values. As with the precipitation data the mean of the region 3-6° S, 35-37° E was used. The temporal range is 1901-2018 (Harris et al., 2014).

Table 1: Location and available rainfall data of six weather stations in the LMC. All stations were used to form the In-situ dataset. Location of the stations is also shown in Figure 1.

Name	Coordinates	Temporal coverage	Missing values (nr. / %)	Source
Arusha	-3.40N, 36.70E, 1372m	1922-1994	175/15.9	Climate Explorer
Babati	-4.21N, 35.75E, 1392m	1972-2018	134/23.8	TMA
Karatu	-3.33N, 35.66E, 1522m	1968-2009	39/7.7	TMA
Kondoa	-4.90N, 35.90E, 1386m	1902-1994	188/16.8	Climate Explorer
Mbulu	-3.90N, 35.60E, 1737m	1922-1994	8/0.91	Climate Explorer
Monduli	-3.30N, 36.50E, 1585m	1975-2018	22/4.2	TMA

*Table 2: Overview of the precipitation products. * indicates the dataset is used to form the Reanalysis dataset.*

Full name	Abbreviation	Data sources	Temporal coverage	Spatial resolution	Reference
Climatic Research Unit Timeseries version 4.03 (land)	CRU*	In-situ observations Existing climatology	1901-2018	0.5°	Harris et al. (2014)
Global Precipitation Climatology Project version 2.3 analysis	GPCP*	In-situ observations Satellite	1979-2019	2.5°	Adler et al. (2016)
Global Precipitation Climatology Center version 2018 analysis (land)	GPCC*	In-situ observations Reanalysis	1891-2016	0.5°	Schneider et al. (2018)
Centennial Trends (CenTrends) version 1.0 extended with Climate Hazards group Infrared Precipitation with Stations (CHIRPS) version 2.0	CHIRPS*	In-situ observations Satellite	1900-2019	0.2°	Funk et al. (2015)
European Centre for Medium-Range Weather Forecasts (ECMWF) Reanalysis (ERA) -Interim/Land atmospheric rain	ERA-Interim /ERAI	In-situ observations Satellite Reanalysis	1979-2016	79 km	Dee et al. (2011)
European Centre for Medium-Range Weather Forecasts (ECMWF) Reanalysis (ERA) - 5	ERA5	In-situ observations Satellite Reanalysis	1981-2019	31 km	Hersbach et al. (2019)

3.2.2 Atmospheric teleconnections

Several indices can be used to quantify atmospheric teleconnections and link them to rainfall pattern anomalies. A description of the teleconnections mentioned below and the way they can influence East African rainfall can be found in the literature study (4.1). When multiple indices were available for the same phenomenon, the choice was based on availability and range.

The Southern Oscillation Index (SOI) was used in this study to quantify the El Niño-Southern Oscillation (ENSO). It is defined as the normalized atmospheric pressure difference between Tahiti and Darwin (Ropelewski & Jones, 1987). Strong positive SOI values indicate a La Niña event and strong negative values indicate an El Niño event. The SOI data was obtained from the Climatic Research Unit (CRU), which provides a monthly SOI from 1866 to present.

To quantify the Indian Ocean Dipole (IOD), the Dipole Mode Index was used. The Dipole Mode Index is the difference between the western equatorial Indian Ocean (50E-70E and 10S-10N) and the south-eastern equatorial Indian Ocean (90E-110E and 10S-0N) SST anomalies. When the Dipole Mode Index is positive, a positive IOD event occurs and vice versa (Saji & Yamagata, 2003). The monthly Dipole Mode Index was obtained through the KNMI Climate Explorer. The temporal range is 1870-present and it is based on HadISST1 data. The absolute temperature difference is standardized by dividing by the standard deviation (Rayner et al., 2003).

The presence of the tropical convective anomalies described as the Madden-Julian Oscillation (MJO) was quantified using the MJO index developed by the Climate Prediction Center (CPC) of the National Oceanic and Atmospheric Administration (NOAA). This index uses the velocity potential at 200-hPa (CHI200) to construct a composite index for life cycles of the MJO. An extended Empirical Orthogonal Function (EEOF) analysis is applied to pentad velocity potential anomalies during weak- and neutral-ENSO winters. Ten MJO indices (longitudes 20°E, 70°E, 80°E, 100°E, 120°E, 140°E, 160°E, 120°W, 40°W and 10°W) are constructed by regressing daily CHI200 data onto ten time-lagged patterns of the first EEOF. Positive indices represent suppressed convection, while negative indices show enhanced convection (Xue et al., 2002; NOAA, 2019). The data is available from 1978 to present every 5 days. In this study the monthly average of the 20°E MJO index was used.

To represent the Southern Annular Mode (SAM), the monthly index developed by the British Antarctic Survey was used. It is available via the KNMI climate explorer and ranges from 1957 to present. This index is calculated using a total of twelve stations measuring sea level pressure at 40°S and 65°S. The index is defined as the difference in normalized mean sea level pressure of the latitudes. It indicates both the phase and strength of the SAM (Marshall, 2003).

The CRU provides a North Atlantic Oscillation (NAO) index ranging from 1851 to present. The NAO index is defined as the normalized pressure at the Gibraltar minus the normalized pressure at Iceland. Positive NAO index values indicate an anomalously high pressure-difference, thus a positive NAO event. The increased pressure difference can be due to anomalously high pressure over Gibraltar and/or anomalously low pressure over Iceland. The opposite results in a negative NAO index (Jones, 1997).

3.2.3 Lake Manyara

The surface area of Lake Manyara through time could be obtained using remote sensing. The Global Surface Water Dataset from the Joint Research Centre (JRC) was used in this study. To create this dataset water surfaces were mapped globally on three million orthorectified Landsat 5, 7 and 8 satellite images (resolution 30m) acquired from March 1984 up to and including December 2018. They were classified using an expert system. An expert system is a classifier that emulates the decision-making ability of a human expert. The classifier misses less than 5% of water and produces less than 1% of false water detection according to classification performance using over 4,000 reference points. The dataset contains monthly water presence and can be accessed and worked with freely in the Google Earth Engine platform (Pekel et al., 2016). For Lake Manyara 267 images with data were available. Many of these images show a relatively high percentage of no-data pixels. This can be due to the presence of clouds or technical difficulties of the sensor (e.g. the defect in the Scan Line Detector of Landsat 7). As this can influence the perception of the surface area of Lake Manyara, only images with less than 10% no data pixels were selected. This resulted in 83 usable images. 78 (94%) of these images were acquired between 2000 and 2019. 69% of the images were obtained between October and February. The values of the surface area of Lake Manyara vary from 13.9 to 547.1 km^2. The exact months and surface area values of the observations can be found in Appendix B.

The volume of Lake Manyara was calculated using the method of Busker et al. (2019). They combined lake surface area data obtained from the Global Surface Water Dataset and the satellite altimetry database DAHITI to obtain the linear hypsometry relationship:

$$h_i = a * A_i + b + \varepsilon_i \qquad (1)$$

with A_i and h_i as the surface area and water level observations respectively, a and b as the slope and intercept parameter and ε_i as the error term or residual for observation i. The intercept parameter b is the depth of the theoretical lake bottom from the linear regression at A=0. When the relation between depth and area is linear, the expected volume of the water body is calculated as:

$$V_i = \frac{(h_i - b) * A_i}{2} \qquad (2)$$

where V_i is the lake volume. By substituting Eq. (1) in Eq. (2) the volume can be calculated using only h or A:

$$V_i = \frac{(h_i - b)^2}{2a} = \frac{a * {A_i}^2}{2} \qquad (3)$$

Unfortunately, the DAHITI database does not provide data for Lake Manyara. No time series for the monthly depth of the lake were found. Instead, to obtain the relation between surface area and depth the bathymetric map of Deus et al. (2013) was used (Figure 4). The map was made using lake bathymetry measurements surveyed in 2010. The contours of this map were digitized providing observations of surface area and corresponding water depth. In this way the linear relation (R^2=0.975) between depth and area was obtained (Figure 4). Now the volume of Lake Manyara could be calculated for each surface area observation as:

$$V_i = \frac{1.84857 * 10^{-06} \times {A_i}^2}{2} \qquad (3)$$

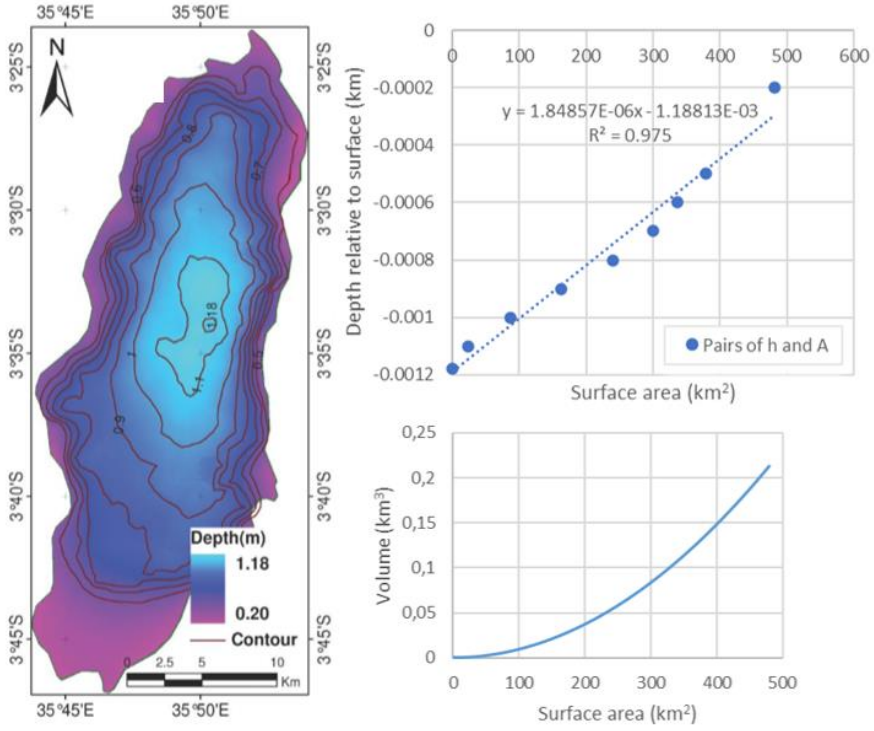

Figure 4: Computation of lake volume. Left: bathymetric map adapted from Deus et al. (2013). Upper right: relation between surface area and depth with linear trend line. Bottom right: relation between surface area and volume according to Eq. 3.

3.3 Analyses

3.3.1 Drought analysis

Due to the lack of stream flow, groundwater and soil moisture data in the study area, only the occurrence of meteorological drought was investigated. The Standardized Precipitation Index (SPI) developed by McKee et al. (1993) was used to indicate drought. The SPI is the commonly used meteorological drought indicator globally (Schwabe et al., 2013; EDO, 2019). It measures precipitation anomalies based on a comparison of observed total precipitation amounts for a period of interest (e.g. 1, 3, 6, 12, 48 months) with the long-term historical record of that period. It requires a monthly precipitation dataset, preferably continuous and 30 years or longer. For each month a SPI value is calculated using the month itself and a previous number of months, together equal to the period of interest. For instance: when calculating the SPI of March with a period of interest of 3 months, the cumulative precipitation of January, February and March (JFM) is used. This value is then compared with the long-term record of cumulative JFM precipitation.

The period of interest of the SPI represents typical time scales for precipitation deficits to affect different types of water sources. For example, the 1- or 3-months SPI represents short droughts and indicates immediate impacts as reduced soil moisture, while the 12- or 24-months SPI represents long droughts causing changes in reservoir storage (McKee et al., 1993; EDO, 2019). In this study the 3 months SPI (SPI-3) and 12 months SPI (SPI-12) will be used to represent short-term and long-term drought respectively. The former can furthermore be used to portray the seasonal rainfall in the study area.

To calculate the SPI, the precipitation record is fitted to a probability distribution (gamma) function. It is then transformed into a normal distribution with a mean of zero and a variance of one. The result is the SPI, which represents the number of standard deviations from the mean. For instance: an SPI-3 equal to -2 in JFM of a certain year, means that the cumulative JFM precipitation of that year is 2 standard deviations smaller than the long-term average of cumulative JFM precipitation. Positive SPI values indicate anomalous wetter periods, and negative values indicate drier periods (McKee et al., 1993; Maggione & Massari, 2019). The magnitude of the SPI gives a probabilistic measure of drought intensity. Table 3 shows SPI classes representing arbitrary drought intensity as defined by McKee et al. (1993).

To account for the influence of temperature on drought occurrence, the Standardized Precipitation Evapotranspiration Index (SPEI) was also calculated. The SPEI is an index for meteorological drought as well. The calculation is the same as for the SPI, with two adaptations. First, precipitation (P) minus potential evapotranspiration (PET) values are used instead of just precipitation. Secondly, a log-logistic distribution is used instead of the Gamma distribution to deal with possible negative values of P-PET (Vicente-Serrano et al., 2010). PET was calculated in this study using the Thornthwaite (1948) equation, available in the R SPEI package. It requires mean temperature and latitude as input values. Other equations (e.g. Hargreaves or Penman) require variables for which no data was found for the LMC. As the study area lies between 3-6° S, a latitude of -4.5° was used in the Thornthwaite equation. Furthermore, the mean temperature data of CRU was used.

Characteristics of a drought event such as duration, severity and intensity can be quantified using the SPI/SPEI. Drought events are defined according to the methodology of McKee et al. (1993): a drought event occurs when the index falls below -1, it begins when the index first falls below zero and ends when the index becomes positive after a value of -1.0 or less. Drought characteristics were identified using the theory of runs described by Yevjevich (1967). The duration of an event is equal to the number of months between the start (included) and end (not included; Figure 5). Drought severity is the absolute cumulative of the SPI/SPEI values during a drought event. Drought intensity can be calculated by dividing drought severity by drought duration. Drought

peak intensity is defined as the most negative SPI/SPEI value of a drought event. This peak intensity determines the drought class (Table 3).

To see whether there is a (significant) trend in drought characteristics, total drought duration (TDD), total drought severity (TDS), average drought intensity (ADI) and drought frequency (DF) were computed for every 10-year interval. TDD, TDS and total drought intensity (TDI) are the sum of duration, severity and intensity of drought events in the period respectively. ADI was calculated by dividing the TDI by the number of droughts occurring during the decade. DF is the number of events in the period. A linear trend analysis was performed over the decades. The non-parametric Mann-Kendall test was used to determine the sign and significance of trends (Mann, 1945; Kendall, 1975). The presence of a trend in the drought characteristics was tested for short-term (SPI/SPEI-3) and long-term (SPI/SPEI-12) droughts. To investigate whether there is a trend in SPI and SPEI values in general, the Mann-Kendall test was applied to all 3- and 12-month SPI and SPEI values. A possible trend in seasonal SPI and SPEI values was also examined.

The SPI-3, SPEI-3, SPI-12 and SPEI-12 were calculated for both the In-situ and Reanalysis datasets. The indices for the In-situ dataset were calculated with data from November 1922 to July 2011 as this is the longest period without missing values. The indices for the Reanalysis dataset were calculated with data from January 1901 to December 2018 as after January 1901 three instead of one precipitation product were taken into account and as the CRU temperature data ranges up to December 2018. The SPI and SPEI values were compared to see the effect of including evapotranspiration on the appearance of droughts. The difference in possible trends and drought characteristics when including/excluding evapotranspiration was also examined. The differences between the results of the In-situ versus the Reanalysis dataset were analysed as well.

Table 3: SPI-based classification of drought.

SPI	Classification	Expected probability (%)
0 to -0.99	Mild drought	34.1
-1.00 to -1.49	Moderate drought	9.2
-1.50 to -1.99	Severe drought	4.4
≤ -2.00	Extreme drought	2.3

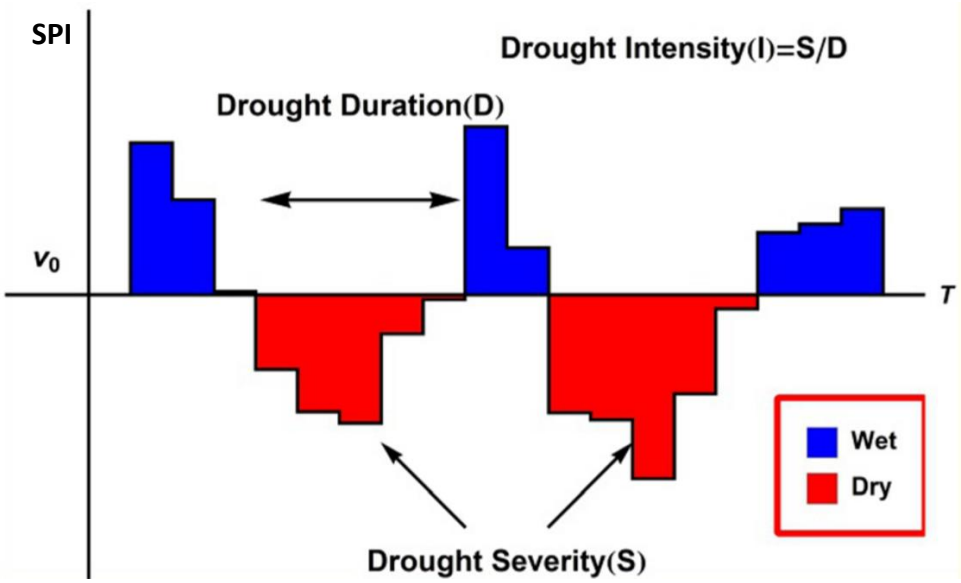

Figure 5: Definitions of drought duration, drought severity and drought intensity by the run theory of Yevjevich (1967). Adapted from: Zhang et al. (2015).

3.3.2 Influence of atmospheric teleconnections on LMC rainfall

Many studies focus on relating atmospheric teleconnections to anomalies of the rainy seasons in East Africa (Heijenk, 2013; Black, 2005; Kijazi & Reason, 2009). However, both Camberlin & Philippon (2002) and Nicholson (2017) showed that especially the long rainy season is not coherent. The character, causal factors and teleconnections were found markedly different in each month. The causes of rainfall anomalies during the season would thus be less clear when using seasonal anomalies. Therefore, first monthly rainfall anomalies were correlated to teleconnections in this research. The techniques described below were executed for both the In-situ and Reanalysis precipitation datasets.

For each separate month, the precipitation datasets were correlated with each teleconnection index. Not all monthly time series of the correlated variables are normally distributed according to the Shapiro-Wilk test and histograms. Therefore, both Kendall and Pearson correlations were calculated. The Kendall Rank correlation is a non-parametric test that uses a rank correlation and does not require a normal distribution. The Pearson correlation is a parametric test that measures the linear correlation between variables and assumes normally distributed variables. As many papers use Pearson correlation, calculating this correlation as well enables comparison with the results of these papers. The correlations have a value of -1 for a perfect negative correlation and a value of 1 for a perfect positive correlation. Guidelines of Karadimitriou (2020) were used to interpret the strength of the relationship (Table 4). A lead-effect was also applied. Correlations between rainfall and teleconnection indices of up to six months in advance were calculated.

Furthermore, seasonal correlations were calculated. These could be compared with the monthly correlations to determine the impact of using monthly or seasonal variables. For this seasonal correlation, 3-month cumulative teleconnection indices were calculated. The SPI-3 values were used to represent seasonal rainfall. These are by definition normally distributed time series of cumulative precipitation of 3 months. In this way May SPI-3 represents March-May rainfall for example. As the time-series are normally distributed, only Pearson's correlation was calculated.

The correlations described above are based on the whole range of available data. It is also interesting to know whether the relationship between rainfall and teleconnections has changed with time during the analysis period. It can indicate strengthening or weakening of the influence of the teleconnections on rainfall in the study area. To examine the long-term changes in the relationship, a sliding correlation was established between each teleconnection and rainfall of the rainy seasons using a 20-year window (as in Gershunov et al. 2001, Ashok et al., 2003, Manatsa et al., 2008, Wu & Kinter, 2008 and Nicholson, 2015). A sliding correlation is the correlation coefficient calculated between two time-series for all points within a window. This window is moved along the data and correlation is calculated at every fixed interval.

Partial correlation was also applied since the teleconnections may be susceptible to contamination of each other in their influence on LMC rainfall variability. Partial correlation measures the strength and direction of a relationship between two variables while controlling the effect of one or more other variables. Using this approach, the strength of the relationship between precipitation and one teleconnection (e.g. the ENSO) without the influence of other teleconnections (e.g. the IOD, MJO, SAM and NAO) can be determined. To include the possible influence of each teleconnection, this correlation was calculated for the period 1978-2010. During this period, all teleconnections indices have observations.

Table 4: Guidelines for interpretation of a correlation coefficient. Adapted from: Karadimitriou (2020).

Correlation coefficient			**Association**
-0.3 < r < 0.3			Weak
-0.5 to -0.3	or	0.3 to 0.5	Moderate
-0.9 to -0.5	or	0.5 to 0.9	Strong
-1 to -0.9	or	0.9 to 1	Very strong

3.3.3 Drought occurrence and Lake Manyara fluctuations

To test the relation between drought occurrence and fluctuations in the volume of Lake Manyara several correlations were examined. As it was unknown which moment during the month an observation of Lake Manyara is exactly from, the effect on correlations of including/ excluding the month the observations were taken in was considered. First the correlations (with a lead-lag effect) between the volume of Lake Manyara and the SPI/SPEI-3/12 were analysed. This could determine to which extent Lake Manyara fluctuations are influenced by short-term (SPI/SPEI-3) as well as long-term (SPI/SPEI-12) droughts. The influence of extreme wet events was also taken into account as this is indicated by high positive SPI/SPEI values. Furthermore, monthly P and P-PET values of the same month and the cumulative of several months prior to the observation were correlated with the volume of Lake Manyara. In this way the dependence on rainfall in general and the effect of evapotranspiration could be examined. The link between the change in volume of Lake Manyara and P, P-PET and cumulative SPI-3, SPI-12, SPEI-3 and SPEI-12 was also inspected. Gaps of several months existed between some observations. Therefore, for each variable the cumulative from one observation (included) to the next observation (excluded) was taken and compared to the change in lake volume between these observations. The last month was excluded as it was unknown which moment during the month an observation is exactly from. In this way they were all assumed to be taken at the beginning of the month to prevent the inclusion of events which might not have happened yet.

4. Results

4.1 Literature study of atmospheric teleconnections

In this chapter current knowledge about the influence of atmospheric teleconnections on rainfall in the LMC is reviewed. The NOAA (2020) defines teleconnections as: "spatially and temporally large-scale anomalies that influence the variability of the atmospheric circulation". These spatial patterns in the atmosphere can explain climate anomalies occurring in widely separated regions across the globe, which cannot be accounted for by local physical processes (Liu & Alexander, 2007; Feldstein & Franzke, 2017).

As the interannual variability is larger during the short rainy season (CV=77%) than during the long rainy season (CV=38%) more research is done regarding the causes of rainfall variability in the short rainy season (Camberlin et al., 2009). Furthermore, Camberlin & Philippon (2002) found the patterns of both rainfall variability and teleconnections to be dissimilar during the long rainy season. However, most existing studies highlight the connection between atmospheric phenomena and one or both rainy seasons. Therefore, this literature study will also predominantly discuss the influence of teleconnections on the seasonal rainfall. First, the most relevant circulation pattern is described. Then each of the teleconnections found to be influencing East African rainfall is explained and existing research about its influence reviewed. Hereafter the non-stationarity of the relations and possible interrelations of teleconnections is discussed, followed by a conclusion.

4.1.1 Walker circulation

Circulation patterns represent large-scale movement of air by which heat is distributed. They restore an imbalance in the energy budget of the climate system caused by differences in solar insolation, sea surface temperature (SST) anomalies and internal variability of the climate system (storms, gyre circulations) (Stan et al., 2017). The Walker circulation refers to the totality of east-west atmospheric circulation cells along the equator in the troposphere (Figure 6). It is driven by the difference in heat distribution over ocean and land (Mölders & Kramm, 2014). During the normal state of the Walker circulation a warm pool is present in the western Pacific. In this warm pool, air is unstable and convection occurs, which is a major driver of global atmospheric circulation. The air disperses in the tropopause, travels east and descends in the eastern Pacific. This causes a high-pressure area at the surface of the ocean. The resulting pressure gradient across the Pacific causes the low-level zonal wind from east to west. The existence of the low-level wind across the Pacific is amplified by the existence of trade winds due to Earth's rotation. The Walker circulation includes secondary circulation cells with rising branches over Africa and South America (Figure 6). These cells have a weaker vertical motion compared to the Pacific cell of the Walker circulation (Lau & Yang, 2003).

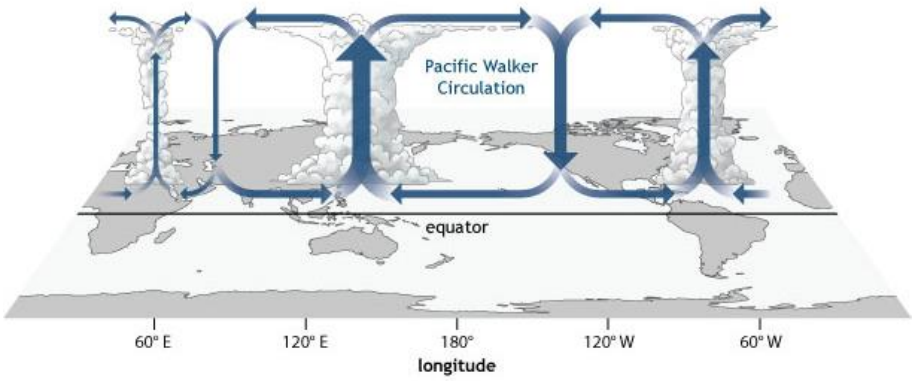

Figure 6: Generalized Walker circulation (Dec-Feb) during normal conditions. Convection occurs at the rising branches. Adapted from: NOAA (2014).

At the location of the rising branches precipitation ensues due to convection. The downward branches are characterized by lack of clouds and thus no precipitation. The location and intensity of these branches can change, leading to changes in rainfall (Kijazi & Reason, 2005; NOAA, 2014). As the Walker circulation is driven by temperature differences, these can change the location of the branches. According to Lau & Yang (2003), the annual cycle of incoming solar radiation causes a seasonal variation of the circulation. The resulting east-west swaying of the circulation cells is visible in Figure 7. A weak and shallow ascending branch is present over the study area during the rainy seasons (Figure 7b and 8).

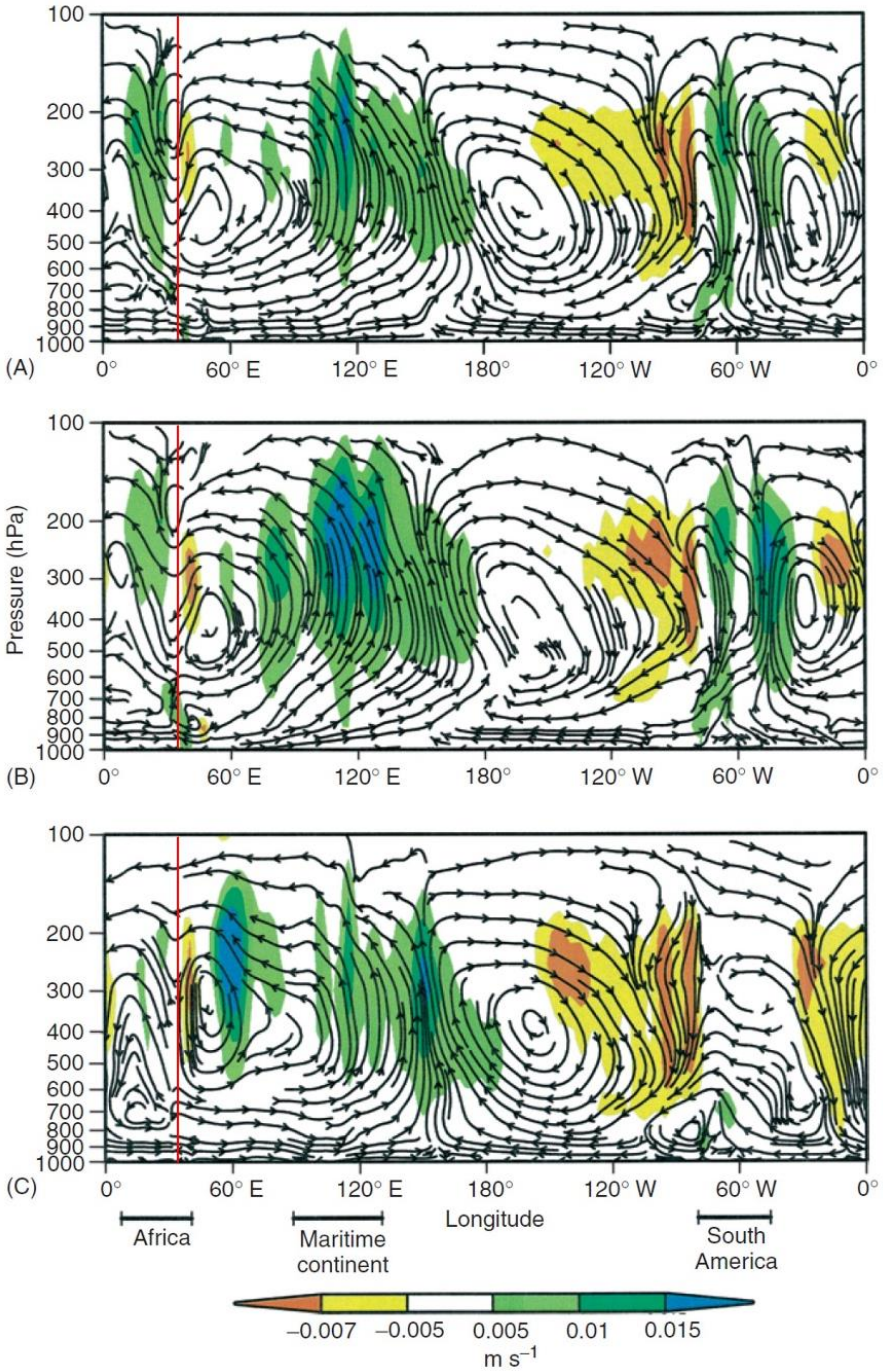

Figure 7: Equatorial east-west atmospheric circulation: climatologies of a) all months, b) January, c) July for the period 1949-1999. In colour: areas of strong upward (positive values) and downward (negative values) motion. Adapted from: Lau & Yang (2003). The location of the LMC is indicated by the red line.

The existence of the Indian Ocean Walker cell can also be seen in Figure 8. Air rises in the east of the Indian Ocean, travels to the west and descends there before flowing to the east again. It is relatively strong during the short rainy season compared to the long rainy season. Accordingly, the subsidence over East Africa at upper levels is also relatively strong during the short rainy season (Pohl & Camberlin, 2011; Nicholson, 2017). East African rainfall during this season is found strongly negatively related to the intensity of the Indian Ocean Walker cell. Mutai et al. (2012) correlated Kenyan rainfall with components of the Indian Ocean cell for the period 1958-1997. Subsidence over East Africa, defined by 500-mb omega vertical motion, had a correlation of -0.60 with rainfall. The ICOADS index of surface winds over the central equatorial Indian Ocean by Woodruff et al. (2011) showed even higher correlation with rainfall: -0.85. Nicholson (2015) found a correlation of -0.74 between this surface wind index and October-November rainfall in Uganda, Tanzania and Kenya for 1874-2012. If pressures reverse over the Indian Ocean, the winds can switch to easterly and enhance low-level convergence in East Africa causing increased rainfall. An increase in equatorial westerlies over the African continent (e.g. westerly flow out of the Congo basin) also enhances the low-level convergence in East Africa (Birkett et al., 1999; Dezfuli & Nicholson, 2013). These winds are positively associated with the East African rainfall, as it controls the location of the meridianally (north-south) oriented part of the ITCZ. If these winds increase, the meridional ITCZ will move more eastward, enhancing rainfall in East Africa (Camberlin & Philippon, 2002; Mafuru & Guirong, 2018). Lastly, atmospheric teleconnections can alter the Walker circulation on intra-seasonal to inter-annual timescales (Lau & Yang, 2003).

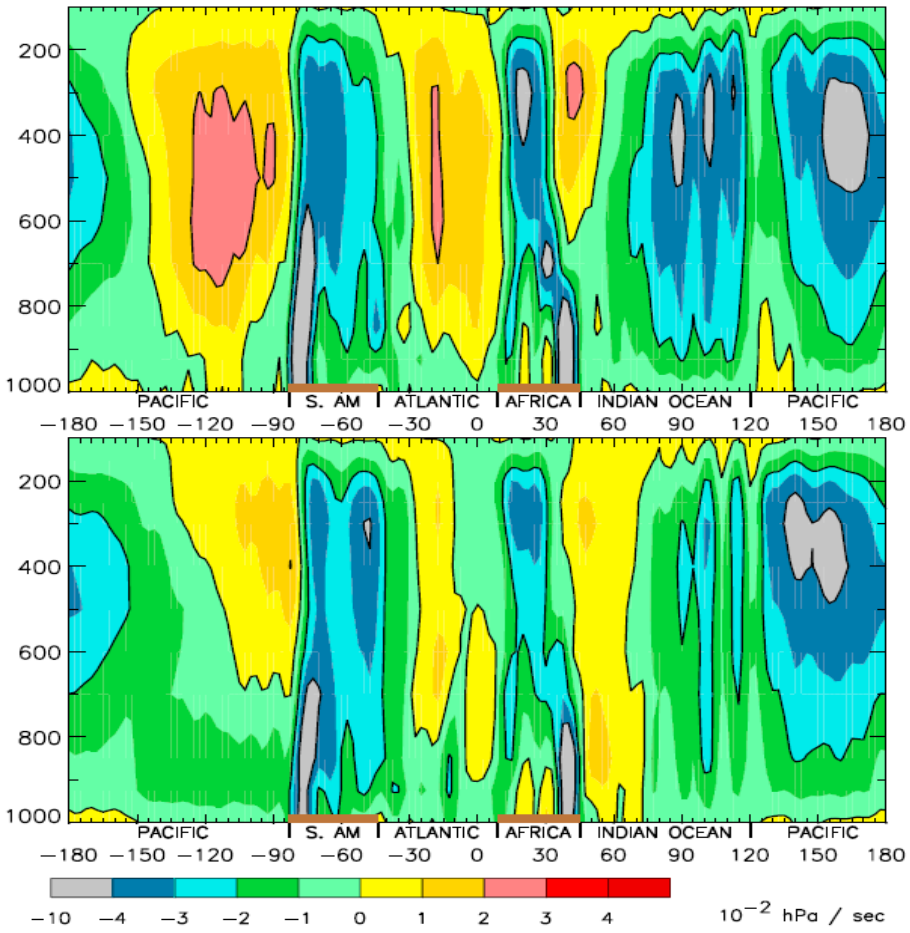

Figure 8: Vertical motion expressed by omega as a function of latitude averaged between 10° N- 10° S. Positive values represent subsidence and negative values ascent. Top diagram: October-November (short rainy season). Bottom diagram: March-April-May (long rainy season). Adapted from: Nicholson (2017).

4.1.2 El Niño-Southern Oscillation

The Walker circulation is altered by inter-annual fluctuations in the tropical sea surface temperature (SST). The El Niño-Southern Oscillation (ENSO) is the phenomenon of SST anomalies in the equatorial Pacific Ocean. During El Niño anomalous warm SSTs occur along the east-central equatorial Pacific (Figure 9). Warm surface water now appears farther east and is spread over a broader area. This causes ascent of air over the Pacific Ocean. The result is disturbance of the normal Walker circulation with displacement or even reversion of descending and ascending branches. Easterly flow over the Indian Ocean and westerly flow over the African continent is increased. This and the presence of a relatively strong ascending branch enhances rainfall over East Africa. During La Niña anomalous cool SSTs occur along the east-central equatorial Pacific. This reinforces the pressure difference between the eastern and western Pacific, which strengthens the Walker circulation. It results in increased subsidence over East Africa, increased Indian Ocean westerlies and equatorial continent easterlies, reducing rainfall in East Africa. An El Niño or La Niña event typically last 9-12 months. In June-August they often begin to form, reaching peak strength in December-April. During May-August they fade away. The events have an irregular periodicity but happen every 3-4 years on average (Schreck & Semazzi, 2004; Kijazi & Reason, 2005; Hoell et al., 2014; NOAA, 2014). Multiple indices are available characterizing the ENSO. They used different locations and time scales to define the phase and strength of the ENSO (NOAA, 2020).

Kijazi & Reason (2005) studied the influence of the ENSO on short rainy season (October-December) rainfall over North Tanzania. During El Niño events rainfall increases. The season starts earlier, fewer dry spells occur, and rainfall is more intense during El Niño events compared to long-term averages. During La Niña the opposite occurs. Bowden & Semazzi (2007) also found increased rainfall during El Niño in October-December, but strong intra-seasonal fluctuation is present. During La Niña rainfall is below normal but wet and dry spells occur within the season. However, the increase/decrease in October-December rainfall during El Niño/ La Niña is not evident during all events. During the short rainy season from 1901 to 1991 rainfall was anomalously high in 12 of 20 El Niño events, and anomalously low in 12 of 17 La Niña events (Nicholson & Kim, 1997; Nicholson & Selato, 2000). The links between the ENSO and (October-December) rainfall in East Africa furthermore varies on regional basis and depends on temporal scale (Omondi et al., 2012). Observations also show that the impact of the ENSO can vary per event, depending on the occurrence of warming or cooling of the equatorial Indian and Atlantic Oceans during the event (Nicholson et al., 2001).

The net impact of the ENSO on the long rainy season tends to be insignificant as the anomalies switch sign in the middle of the season (Nicholson & Kim, 1997). Hoell et al. (2014) showed that La Niña can increase as well as decrease rainfall during the long rainy season depending on the characteristics of the event. Various types of La Niña can produce different patterns of subsidence and convergence over East Africa. The contrast between the high correlation between months of the short rainy season and the uncorrelated months of the long rainy season could be due to impact of the ENSO. The ENSO is large and of the same sign during boreal autumn, but weak and inconsistent during boreal spring (Camberlin & Wairoto, 1997; Indeje et al., 2000). Mutai & Ward (2000) found little relationship between the Southern Oscillation Index and March/April rainfall, and some relationship with May rainfall. Gebrechorkos et al. (2020) only found insignificant correlations between 1981-2016 rainfall in Tanzania and the Niño 3.4 index for all seasons (October-December, January-February, March-May and June-September).

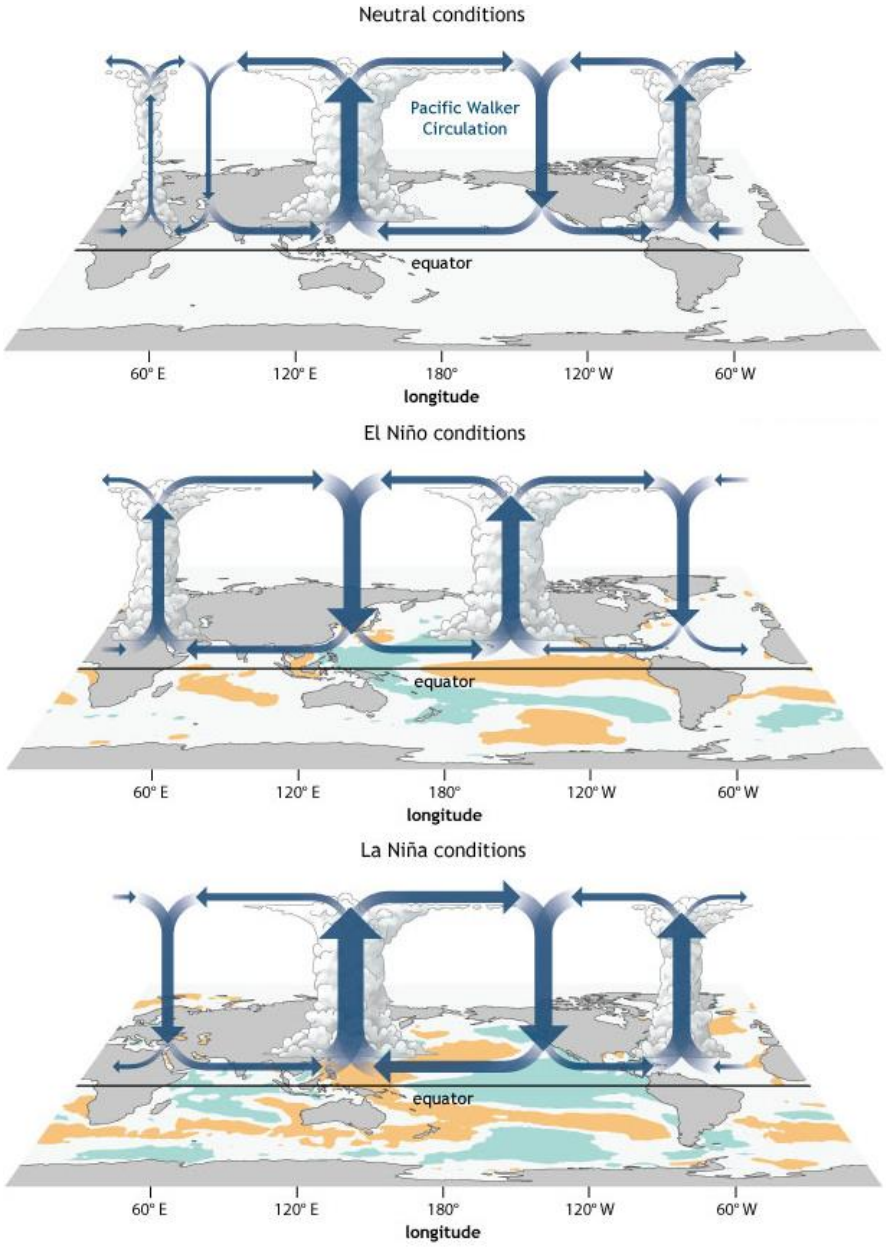

Figure 9: Generalized Walker circulation (Dec-Feb) during ENSO-neutral conditions (upper), El Niño (middle) and La Niña (lower). Colours indicate anomalous ocean cooling (blue/green) and warming (orange). Adapted from: NOAA (2014).

4.1.3 Indian Ocean Dipole

Changes in Indian Ocean SSTs also influence the Walker circulation. The Indian Ocean Dipole (IOD) is a zonal dipole in the tropical Indian Ocean SST varying on the inter-annual timescale. During a positive IOD event anomalous cooling of SST occurs in the south eastern equatorial Indian Ocean and anomalous warming of SST occurs in the western equatorial Indian Ocean (Figure 10). Westerly equatorial winds weaken. This results in a shift of warm water to the west and upwelling of cool water in the east. The temperature gradient causes the motion of air of the zonal cell over the Indian Ocean to reverse in direction. The increased convection over the western Indian Ocean causes more rainfall in East Africa. During a negative IOD, westerly equatorial winds intensify over the Indian Ocean. This results in higher SST in the east and lower SST in het west, due to accumulation of warm water and upwelling respectively (Figure 10). As a result of the temperature gradient, the zonal cell increases. This reinforces subduction over the eastern Indian Ocean, causing less rainfall in East Africa (Saji et al., 1999; Webster et al., 1999; JAMSTEC, 2012).

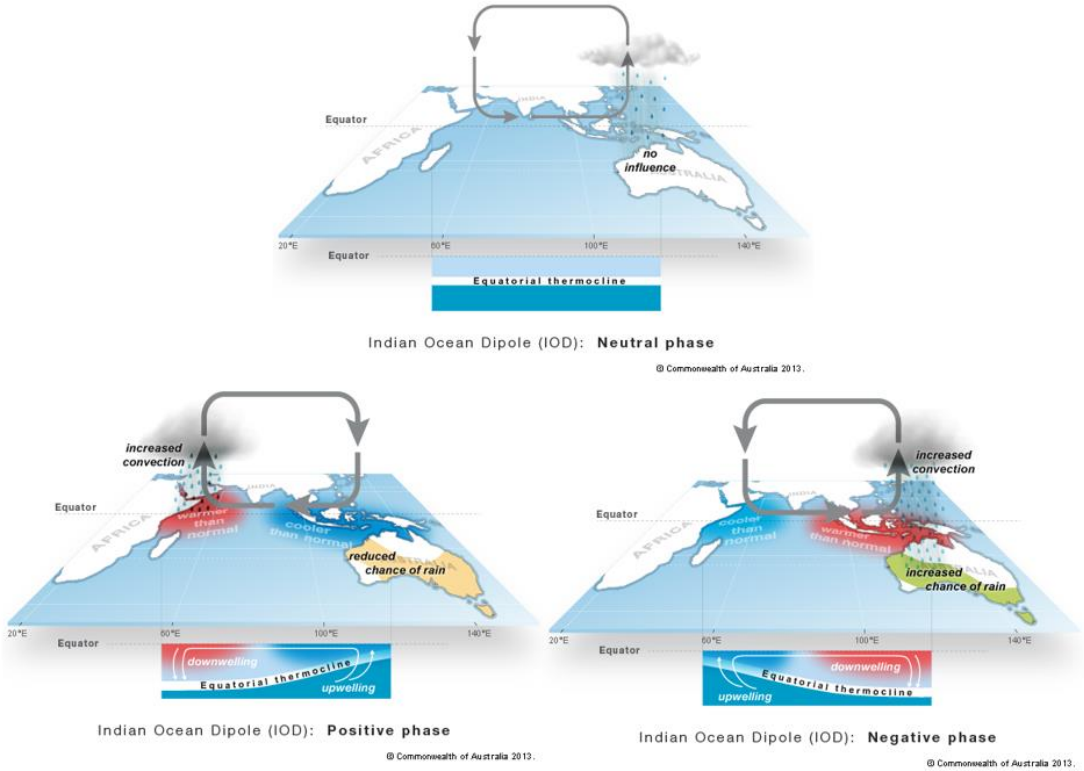

Figure 10: Circulation pattern, equatorial thermocline and SST anomalies across the equatorial Indian Ocean during a neutral, positive and negative IOD phase. Adapted from: Commonwealth of Australia (2013).

Events typically last about 6 months. They often begin in May or June, reaching peak strength in August-October, and decaying rapidly in November-December. The events have an irregular periodicity. The strength and phase of the IOD is commonly defined by an index taking the difference between SST anomalies between a region in the east and a region in the west of the tropical Indian Ocean (Commonwealth of Australia, 2013).

The ENSO was believed to be the primary driver of interannual rainfall variability until the discovery of the IOD in ±1999. The importance of the IOD in modulating East African rainfall, especially during the short rainy season, has since been described by many papers (Saji & Yamagata, 2003; Black, 2005; Slingo et al., 2005; Behera et al., 2006; Ummenhofer et al., 2009; Nakamura et al., 2011; Nicholson, 2015). The correlation between October-December rainfall and the IOD was 0.61 for 1874-2012 (Nicholson, 2015). Liebmann et al. (2014) found a correlation of 0.8 for 1979-2012. Gebrechorkos et al. (2020) showed correlations between the IOD and rainfall in Tanzania for the period 1981-2016 to be 0.63 for October-December, 0.37 for January-February, -0.14 for March-May and 0.28 for June-September. October-December and January-February correlations were significant (α=0.05). Studies comparing the influences of the ENSO and IOD on short rainy season rainfall have generally concluded that the Indian Ocean has more overall influence on both interannual and interdecadal timescales (Omondi et al., 2013; Nicholson, 2017).

4.1.4 Madden-Julian Oscillation

The Walker circulation is affected on intra-seasonal timescales by the Madden-Julian Oscillation (MJO). The MJO causes fluctuation in tropical weather on weekly to monthly timescales. It is characterized as a west-to-east movement of tropical convective anomalies and associated circulation anomalies (Figure 11). In the first phases of the MJO, enhanced convection develops over Africa and the western Indian Ocean, which then moves eastward over the Indian ocean. In phase 4 and 5 it has reached Indonesia and West Pacific. Then it moves further eastward and dies

out in the central Pacific. The total cycle occurs every 30-60 days. Following and preceding the convective region are regions of suppressed convection (Madden & Julian, 1972; Madden, 2014). Two (daily) indices defining the MJO are commonly used. The index of CPC defines the strength of the MJO at different longitudes. The other by Wheeler and Hendon displays the strength and phase (Figure 11) of the convective centre of the MJO per day (NOAA, 2020).

Several studies show that intra-seasonal variability over East Africa is not random, but concentrated on specific time scales (Nicholson, 2017). This is at the time scales of the MJO, with rainfall having strong coherence with the amplitude of the MJO (DeMott et al., 2015). According to Pohl et al. (2005) the MJO is the dominant factor controlling intra-seasonal variability over East Africa during both rainy seasons. The long rainy season has an earlier onset, more wet spells and enhanced daily rainfall during March and April when the MJO is very strong. The MJO overall explained 44% of the interannual variability of the long rains between 1979 and 1995 (Pohl & Camberlin, 2006).

The MJO has a larger influence on rainfall during the long rainy season than during the short rainy season (Berhane & Zaitchik; 2014). In general, the Indian Ocean cell of the Walker circulation is much weaker (Pohl & Camberlin; 2011) or almost absent (Hastenrath, 2000) throughout the long rainy season compared to the short rainy season (Figure 8). The subsidence over East Africa is therefore much weaker in April and May than in October and November (Nicholson, 2017). Consequently, the MJO can have a more distinct influence on rainfall in the long rainy season. The overall influence of the MJO is strongest early (March) and late (May) in the long rainy season and in the middle of the short rains (November). This is suggested to be the result of zonal shifts in the MJO convective centre and adjective zones.

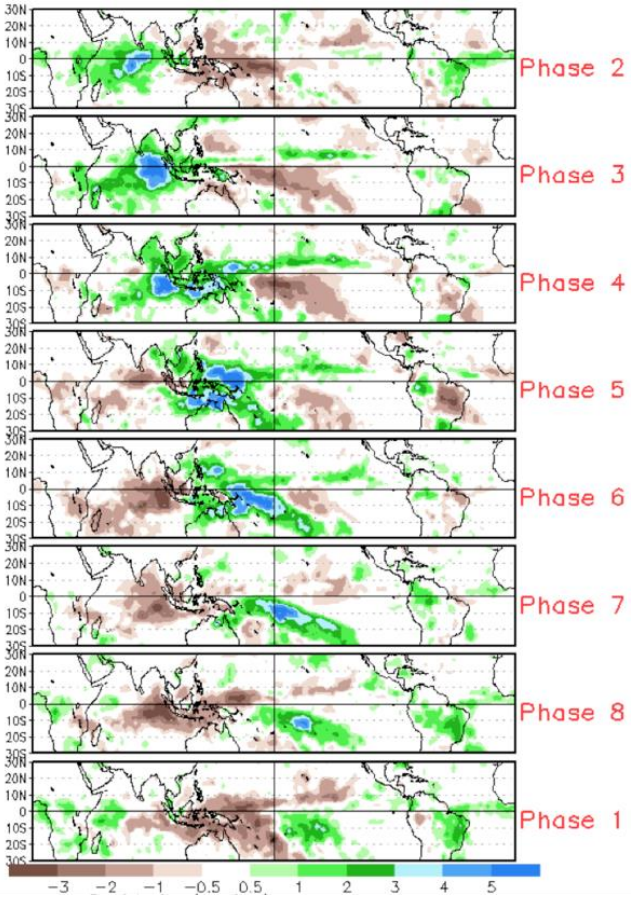

Figure 11: Rainfall anomalies for all 1979-2012 November-March MJO events. The phases represent the grouped geographically based stages of the convection zone. Green shaded areas show above average rainfall (enhanced convection), while brown shaded areas show below-average rainfall (suppressed convection). The eastward movement of the shaded areas can be seen in each successive phase from top to bottom. Adapted from: Gottschalck (2014).

4.1.5 Southern Annular Mode

Climate anomalies stretched over the tropics can be connected to atmospheric anomalies in the extratropics. These anomalies are called annular modes and are caused by internal atmospheric dynamics in the extratropical circulation (Thompson & Lorenz, 2004). The Southern Annular Mode (SAM) or Antarctic Oscillation is an annular mode present in the southern hemisphere. It is the north-south movement of strong westerly winds blowing in the mid- to high-latitudes. The SAM has 3 phases: positive, negative and neutral (Figure 12). During the positive phase, anomalous low pressure occurs over Antarctica, and high pressure over the mid-latitudes of the southern hemisphere. The belt of westerly winds surrounding Antarctica moves south and becomes stronger. The opposite happens during negative events. The effect of the SAM on rainfall depends on both region and season. The events last for at least one or two weeks, with a week to a few months between positive and negative events (Commonwealth of Australia, 2019). It shows its most fluctuations in the 30-60 day range (Pohl et al., 2010). In recent decades there has been a trend towards more positive events (Jones & Widmann, 2004). According to Thompson & Solomon (2002) and Arblaster & Meehl (2006) this can only be explained by taking into account ozone depletion and increased atmospheric greenhouse gasses.

East African rainfall during the short rainy season (October-December) can be influenced by the SAM (Figure 13). A positive SAM strengthens the Mascarene High (MH), the subtropical high-pressure system in the southern Indian Ocean (Xue et al., 2004). The SAM is probably also the cause of the westward shift of the MH during its strengthening (Manatsa et al., 2014). This movement and the increase in strength of the MH increases the strength of the relatively cool and dry southeast trade winds. A positive SAM thus strengthens the southeast trade winds through the MH. During a negative SAM, the opposite happens and the trade winds weaken. During the rainy seasons, rainfall is associated with the intensity and location of the ITCZ. At the ITCZ humid air from the South Atlantic converges with southeast trade winds from the Indian Ocean. Stronger southeast trade winds can thus shift the meridional ITCZ westward, resulting in decreased rainfall in East Africa. The increased supply of dry and cool air can furthermore induce cold SSTs, suppressing convection over the western equatorial Indian Ocean and reducing East African rainfall. A positive event thus reduces East African rainfall. During a negative event, the opposite occurs and East African rainfall is increased. The strength and phase of both the SAM and MH can be defined by indices. These indices use sea level pressure differences and geopotential heights respectively, which indicates the state of the relevant pressure areas seen in Figure 12 (Marshall, 2003; NOAA, 2020).

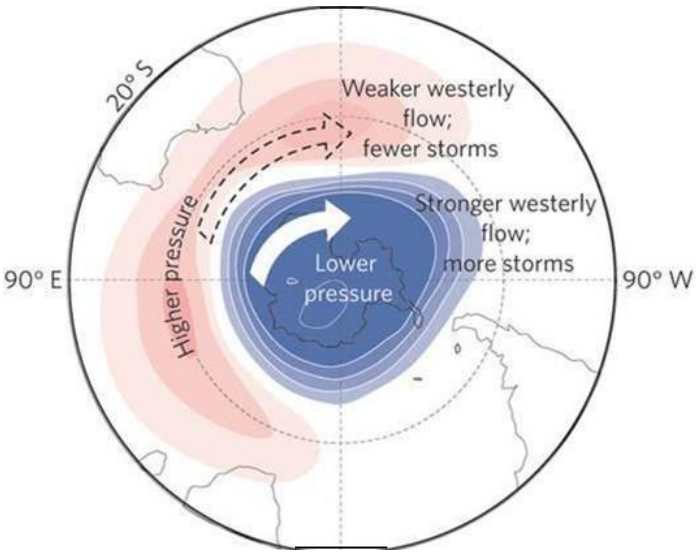

Figure 12: Changes around Antarctica during a positive SAM. Adapted from: Government of Western Australia (2019).

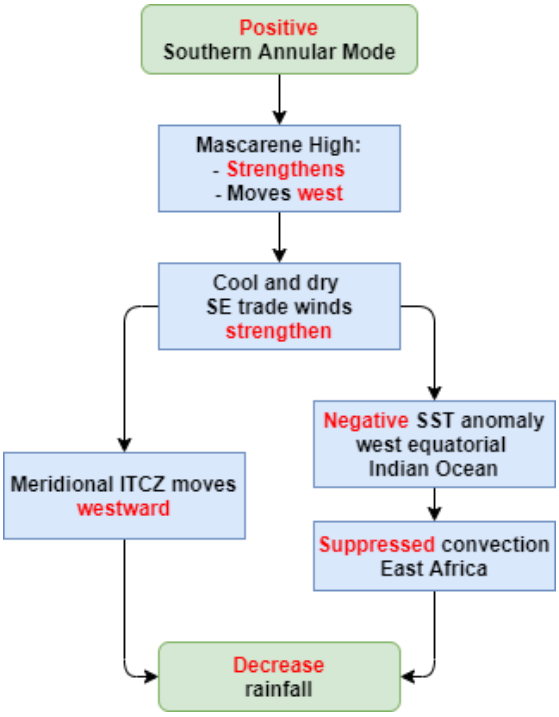

Figure 13: Mechanism of the influence of a positive SAM on October-December rainfall in East Africa. Replacing the red words with the antonym gives the mechanism of a negative SAM.

Many studies investigated the influence of the MH on October-December rainfall in East Africa. The strengthening and zonal displacement of the MH are believed to be related to the SAM (Xue et al., 2004; Manatsa et al., 2014). Sun et al. (1999) linked a weakened MH to an early onset of the short rainy season over Tanzania due to the ITCZ shifting further south. Weaker MH also caused wet years due to eastward shift of the meridional ITCZ. McHugh & Rogers (2001) discovered anomalous south-easterly flow off the Indian Ocean during dry summers in south-eastern Africa. Ogwang et al. (2015) related East African October-December rainfall with the MH. During dry years, the MH was observed to be intensified and align itself in a southeast-northwest orientation towards the continent. During wet years, the MH was weak and shifted to the east in a zonal orientation. Nkurunziza et al., (2019) obtained similar conclusions investigating the influence of the MH on October-December rainfall in Rwanda. Gillett et al. (2006) investigated the impact of positive SAM on rainfall in the southern hemisphere. They produced regression coefficients of monthly precipitation on the SAM index for one standard deviation positive SAM anomaly. One meteorological station in Tanzania showed a small but significant decrease in rainfall (-0.2 mm/day) with a positive SAM. The few other data points in East Africa showed no significance. No research concerning the influence of the SAM on other seasons was found. Funk et al. (2008) linked the decline of the long rains in recent decades with warming in the south-central Indian Ocean, with more dry air sent toward East Africa. This might be related to the trend in the SAM.

4.1.6 North Atlantic Oscillation

The North Atlantic Oscillation (NAO) refers to the fluctuations in the north-south pressure difference across the northern Atlantic Ocean. This pressure difference determines the strength of the westerly winds across the Atlantic Ocean, especially during boreal winter (Met Office UK, 2020). During a positive NAO, the pressure difference is large, with stronger westerly winds across the Atlantic. During a negative NAO the difference is small, with weaker westerly winds (McHugh & Rogers, 2001). Fluctuations in the NAO exist on a wide range of timescales (day-to-day to long-term). It can be positive or negative for prolonged periods (several months). Extent and sign of impacts can differ per season and per region (Met Office UK, 2020). The index for the NAO is defined as the normalized pressure difference between a station on Iceland and a station in the south: Azores, Lisbon or Gibraltar (CRU, 2000).

The influence of the NAO on East African rainfall appears to occur in the upper troposphere (300-hPa). Here, NAO variability is linked to five statistically significant alternating bands of zonal wind strength (Figure 14). These bands extend south-eastward from the north Atlantic Ocean, with south-eastern Africa being the most equatorward zonal wind anomaly cell. The anomalous current extends down to the 850-hPa (surface) level although with a lower statistical significance. Figure 15 shows how the NAO can influence (boreal winter) rainfall. During a positive NAO, the band produces prevailing easterly currents. These currents bring dry air towards Eastern Africa from the Indian Ocean, producing a decrease in boreal winter rainfall (McHugh & Rogers, 2001). The stronger easterlies over East Africa could also cause a westward movement of the meridional ITCZ. This decreases rainfall in boreal winter. During a negative NAO, the opposite occurs. Moist air is supplied from the Atlantic Ocean and the ITCZ shifts eastward, causing an increase in rainfall. Information on the effect of the NAO on rainfall in East Africa during other seasons than boreal winter was not found.

McHugh & Rogers (2001) correlated December-February rainfall in East Africa with the NAO and found a significant (α=0.05) negative correlation in the LMC region (Monduli station r=-0.51). During 1898-1989 December-February rainfall and the NAO had a significant (α=0.01) correlation of -0.48. Meehl & van Loon (1979) showed that the air temperature seesaw between Greenland and northern Europe was linked to latitudinal shifts in January rainfall associated with the ITCZ. Rainfall in January was higher north of 15°S (compared to south) when the temperatures in Greenland were above average, while those of northern Europe were below average. This would indicate a negative NAO. The opposite was also observed. They implied that the ITCZ shifts northward when the North Atlantic westerlies are unusually weak indicating a negative NAO. The ITCZ would shift southward when a positive NAO occurs. However, this is controversial as McHugh & Rogers (2001) explained the difference between north and south of 15°S to be caused by different teleconnections influencing rainfall variability in the regions.

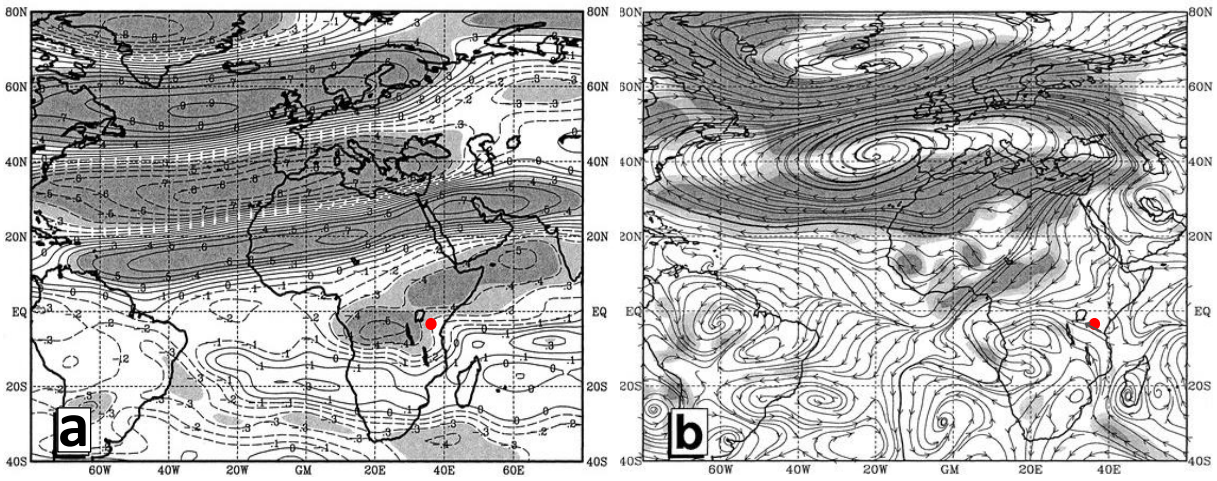

Figure 14: Influence of the NAO on East African wind fields. Lighter and darker grey zones represent statistical significance at the 95% and 99% confidence intervals. The red dot indicates the location of the LMC. A) Location of the five alternating bands of zonal wind strength. Values represent 300-hPa u-component wind velocity standardized regression coefficients associated with the NAO index. Negative isolines are broken. B) 850-hPa streamlines associated with a positive NAO index. Adapted from: McHugh & Rogers (2001).

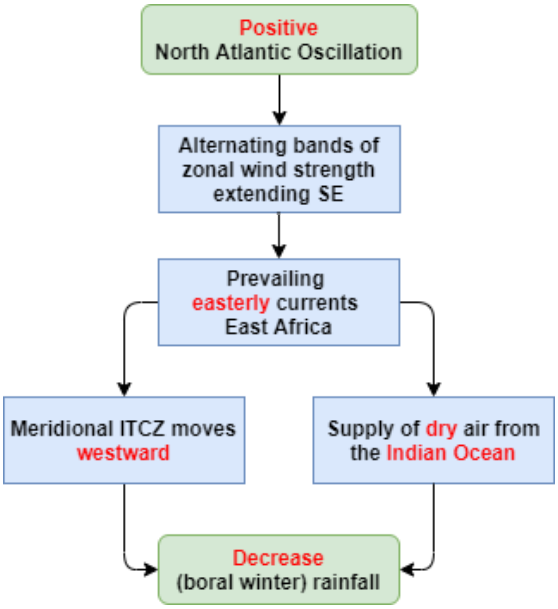

Figure 15: Mechanism of the influence of a positive NAO on boreal winter rainfall in East Africa. Replacing the red words with the antonym, and Indian Ocean with Atlantic Ocean, gives the mechanism of a negative NAO.

4.1.7 Nonstationary relationship teleconnections and East African rainfall

Discrepancies between studies can arise due to non-stationarity of relationships between teleconnections and rainfall. Therefore, results can vary depending on time periods chosen for correlation.

Nicholson (2015) examined the relationships between the ENSO (Niño 3.4 index), the IOD and October-November rainfall in East Africa throughout 1874-2012 using 20-year sliding correlations (Figure 16). She did not include December rainfall as this made the season less homogenous in some regions. The relations show major shifts in 1918, 1961, 1983 and 1994-1997. The shifts occur at times identified as major regime shifts in the tropics (Clark et al., 2003; Ihara et al., 2008; Manatsa et al., 2012; Manatsa & Behera, 2014).

Before 1918 rainfall is more linked to the IOD (Figure 16). Between 1918 and 1960 it is more linked to the ENSO, but the overall coupling is much weaker. The Walker cell over the Indian Ocean was extremely weak during these decades (Figure 17). The relation between the IOD and rainfall is not significant (α=0.05). Furthermore, total October-November rainfall is very low during this period. In the decades after 1961 October-November rainfall increased. This shift coincides with intensification of the Indian Ocean Walker cell and the IOD taking over control again. After 1982 the Pacific cell weakened and Indian Ocean cell further intensified. The Atlantic cell became progressively stronger from 1948 to 1996, reaching maximum intensity from 1983 to 1997 (Nicholson, 2015). During the latter period, correlation between the ENSO, IOD and rainfall decreased. Furthermore, rainfall was sometimes anomalously high despite ENSO and IOD events implying a reduction of rainfall. At these times, low-level convergence was anomalously strong and subsidence at higher levels weak (Smoleroff, 2015). This could be due to the strong Atlantic Walker cell, increasing westerlies over the continent and enhancing convergence over East Africa. After 1997 the increasing trend in strength of the Atlantic cell was reversed. The correlations with the IOD and ENSO increased again.

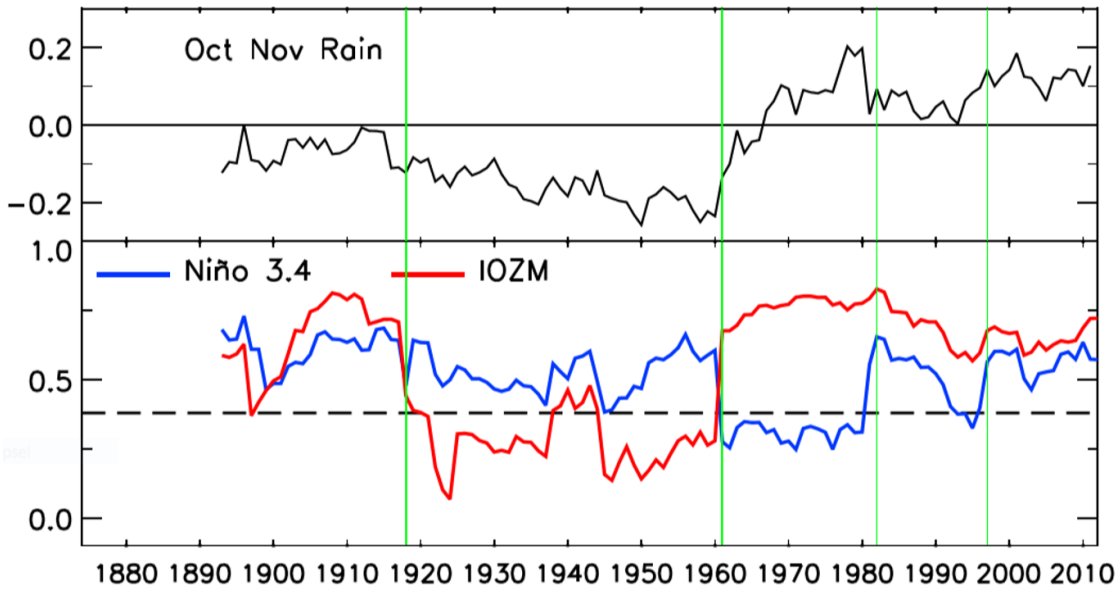

Figure 16: Upper: 20-year mean October-November rainfall. Bottom: Sliding 20-year correlation between October-November rainfall and the IOD/Niño 3.4 index. Values are plotted at the final year of the 20-year interval. Vertical lines indicate regime shifts. Values exceeding ±0.38 are significant (α=0.05). Adopted from: Nicholson (2015).

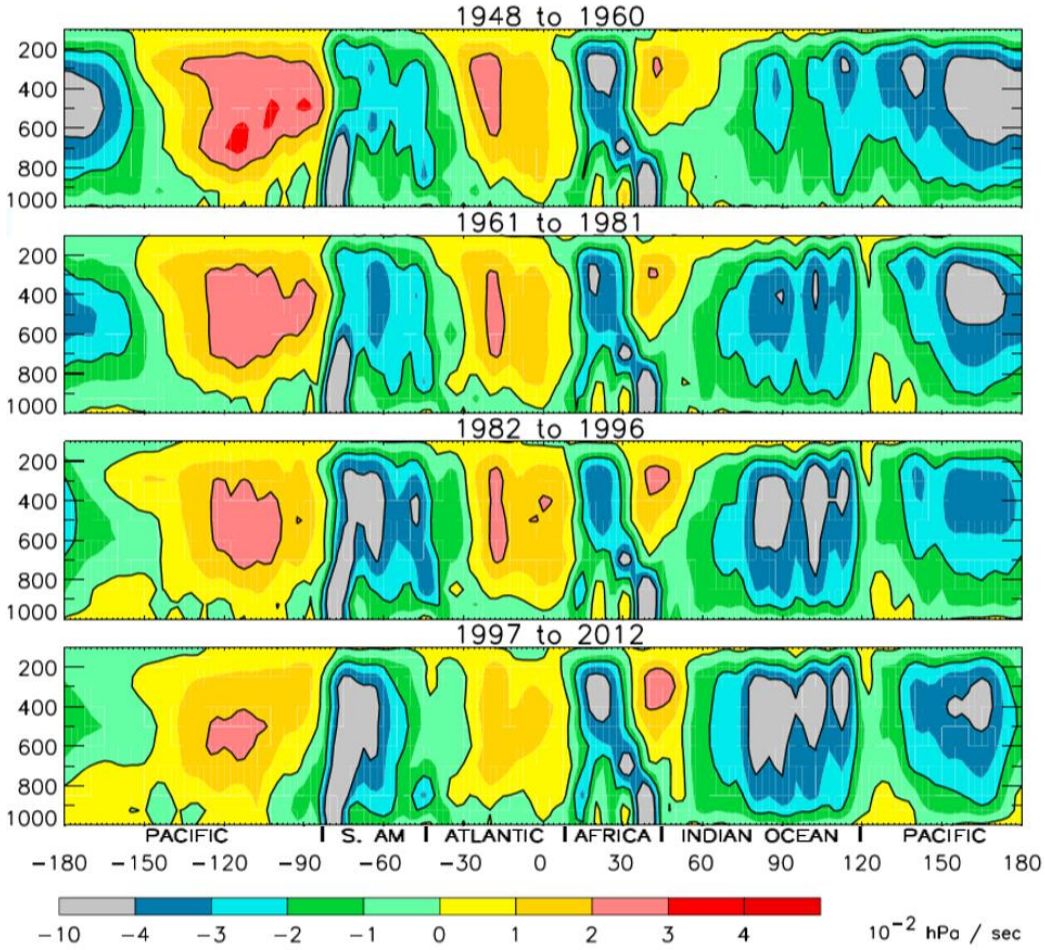

Figure 17: Vertical motion expressed by omega as a function of latitude averaged between 10° N- 10° S over four time periods. Adapted from: Nicholson (2015).

Major shifts in control could thus be linked to the strength of the different Walker circulation cells (Camberlin & Philippon, 2001; Nicholson, 2015). Furthermore, the shift in 1917 coincides with abrupt greenhouse gas increases. The shifts in 1961 and 1997 can be linked to stratospheric ozone level changes (Manatsa et al., 2016). Furthermore, the 1961, 1982 and 1997 shifts were marked by high rainfall events and extremely positive IOD. The last two shifts also show a positive ENSO event (Nicholson, 2015). Inclusion/exclusion of these extreme years influences in the apparent strength of the teleconnections (Camberlin & Philippon, 2001). The regime shifts are nonetheless only investigated for the short rainy season.

Regime shifts occurring in the SAM (1917,1961 and 1997) coincide with those in total October-December rainfall. The 31-year running correlation between the SAM and October-December rainfall by Manatsa et al. (2016) is shown in Figure 18. Before 1961 a significant (=0.10) correlation exists. This is also visible after 1997, with all years except one showing significant correlation. Between 1961 and 1997 the significant correlation is absent. According to Manatsa et al. (2016) the SAM creates a meridional dipole in sea level pressure in the Indian Ocean, with one pole over the tropics and the other over the extratropics (MH). During 1961-1997 this dipole was weakly developed, decoupling the SAM from East African rainfall. The IOD takes over control in this period (Figure 16), showing an increased correlation. The IOD shows significant and high correlation with October-December rainfall between 1961 and ±1984 and after 1997. Manatsa et al. (2016) also concluded that the ENSO is not the dominant modulator of epochal change in October-December rainfall as it does not show large resemblance with the rainfall shifts according to their research.

The correlation between the NAO and rainfall is also non-stationary. McHugh & Rogers (2001) found a correlation of -0.28 for 1889-1922, -0.42 for 1923-1959 and -0.70 for 1958-1989. This increase might be due to long-term changes in position of the pressure areas. Rogers (1997) indicated an eastward migration and intensification in the subtropical high-pressure area. This may have sharpened the NAO's impact on regions farther east and south.

The short rainy season thus shows strong evidence for control by both Indian, Pacific and Atlantic Ocean (Onyutha & Willems, 2015). The relative importance of these oceans in driving the variability and providing forecast skill is a controversial point. The major control shifts over time, making it harder to pin down the mechanisms causing rainfall variability.

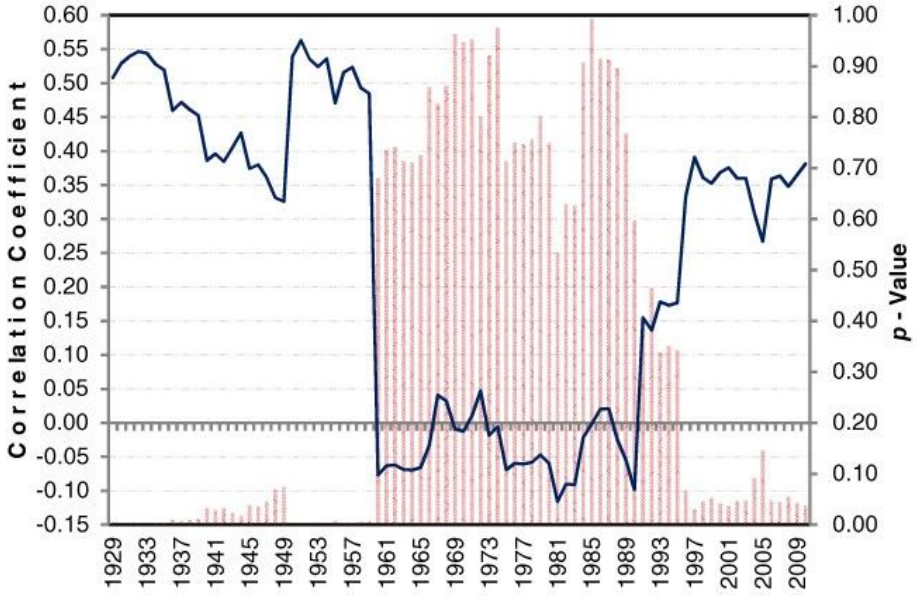

Figure 18: 31-year running correlation between the SAM and East African October-December rainfall. Blue line represents the correlation values. Bars show the p-values. Adapted from Manatsa et al. (2016).

4.1.8 Interrelations teleconnections

Due to interrelations of teleconnections, the effect of each phenomenon on East African rainfall is controversial. As teleconnections influence atmospheric conditions across the globe, they might also influence each other. The ENSO for instance also influences atmospheric flow over the Indian Ocean. Therefore, the ENSO is speculated to influence or even cause the IOD (e.g. Black, 2005; Yuan & Li, 2008; Manatsa et al., 2011; Yang et al., 2015; Kajtar et al., 2017). Others however argue that the IOD is an independent event (e.g. Saji et al., 1999; Webster et al., 1999; Ashok et al., 2003; Behera et al., 2006). It is possible that some connection to the ENSO is due to synchronous occurrence with the IOD or links between the phenomena (Black, 2005; Wenhaji Ndomeni, 2018). Nevertheless, all agree that coinciding ENSO and IOD events can have a much larger impact on East African rainfall compared to one event by itself.

The ENSO has also been linked to other teleconnections. The ENSO and the NAO showed the same departure sign in 47 of 70 boreal winters between 1921 and 1990. The correlation is +0.23. Excluding a major ENSO event in the winter of 1982/1983 improves the correlation to a significant +0.32. A positive NAO increases rainfall in East Africa, while a positive ENSO decreases rainfall. As the circulation patterns of the NAO and ENSO are acting in close proximity, adjacent areas could thus show negative and positive rainfall anomalies depending on which phenomena has most influence (McHugh & Rogers, 2001). During boreal winter the ENSO also shows a significant link with the SAM at interannual timescales. In this way the events would reinforce each their influence on rainfall (Pohl et al., 2010).

The IOD is believed to be able to overshadow the influence of the SAM (Manatsa et al., 2016). This might have happened from 1961 to 1997, when the SAM showed a decrease influence on October-December rainfall. Manatsa et al. (2016) blamed the co-occurrence of positive IOD and ENSO events during this period, which created the strongest teleconnections during the century. This deprived the SAM any significant contribution to rainfall variability.

The MJO might influence the duration of IOD events. Normally, the IOD events terminate around December. The end of an IOD event is almost always preceded by strong 30-60 day oscillations in zonal equatorial winds (the MJO). In 1997 this did not occur, and the IOD event sustained until February 1998 (Rao et al., 2007; Behera et al., 2013). The MJO is also shown to significantly influence NAO variability (Lin et al., 2009).

The interrelations of teleconnections should also be considered when correlating rainfall to a teleconnection (index). For instance, Pohl et al. (2010) correlated the SAM to boreal winter rainfall in southern Africa. At the interannual time scale, rainfall shows statistically significant (α=0.05) correlations with the SAM. However, once the influence of the ENSO is removed using partial correlation, the correlation becomes very weak and barely significant (α=0.05). The apparent correlation was thus due to the dependency between the SAM and ENSO. At intra-seasonal time scales the SAM affected rainfall significantly, also without interference of other teleconnections. Behera et al. (2005) showed the relation between the ENSO and East African October-December rainfall to become insignificant when removing the IOD effect. Ashok et al. (2003) also pressed the use of partial correlation to isolate the IOD impact on climate phenomena without contamination by the ENSO.

4.1.9 Conclusion

The rainy seasons in East Africa coincide with the occurrence of low-level convergence over east Africa, with subsidence at higher levels. The low-level convergence shows to be affected by the strength of the Indian Ocean Walker cell and equatorial westerlies over the African continent. Atmospheric teleconnections can influence the Walker circulation. Normally, subsidence occurs over East Africa. The El Niño-Southern Oscillation (ENSO) is the phenomenon of SST anomalies in the equatorial Pacific Ocean. During El Niño, the positive phase of ENSO, this subsidence is

reversed. This would result in an increase of rainfall in East Africa. During La Niña, the negative phase of ENSO, the opposite occurs. The net impact of the ENSO on the long rainy season tends to be less pronounced, compared to the short rainy season, as ENSO anomalies switch sign in the middle of the season. The Indian Ocean Dipole (IOD) is a zonal dipole in the SST of the tropical Indian Ocean which alters the Walker circulation. During the positive phase, the Indian Ocean Walker cell is reversed in direction, causing an increase in rainfall. During the negative phase the cell is strengthened, increasing rainfall in East Africa. Whether the ENSO by itself has a significant impact on rainfall in East Africa or if its influence is established through the IOD is not unambiguous. The Madden-Julian Oscillation (MJO) is characterized as a west-to-east movement of tropical convective anomalies and associated circulation anomalies. The MJO controls intra-seasonal rainfall variability during both rainy seasons. The effect on the long rainy season is larger, probably due to weaker subsidence over East Africa during this season. The location of the ITCZ also plays a role, with the location of the meridional ITCZ affecting rainfall. The SAM and NAO can influence this location, by increasing south eastern trade winds and easterly winds respectively during positive phases. The meridional ITCZ will shift west causing less rainfall over East Africa. Winds are decreased during negative events, causing eastward shift of the ITCZ which increases rainfall over East Africa. The increase or decrease in supply of cool and dry air from the Indian Ocean reinforces the impact of the SAM and NAO on rainfall.

The correlations between teleconnections and East African (October-December) rainfall are nonstationary. The control of teleconnections on rainfall shifts over time, making it harder to pin down the mechanisms causing rainfall variability. Major shifts in control occur in 1917, 1961, 1982 and 1997. Changes in the position of pressure areas and the strength of the Walker circulation cell might be the cause of the changing correlations between teleconnections and rainfall. Furthermore, the interrelation of the above discussed teleconnections is not unambiguous. Papers correlating the ENSO & SAM/ ENSO & IOD with rainfall in East Africa advice the use of partial correlation, removing the influence of the other teleconnections.

4.2 Drought analysis

4.2.1 Precipitation and temperature

Before looking at the drought indices, the used precipitation and mean temperature datasets are shown and examined here. Total long rainy season (Figure 19), short rainy season (Figure 20) and annual (Figure 21) rainfall all show large interannual variability according to both dataset. For the In-situ dataset precipitation values are higher and more extreme compared to the Reanalysis dataset. The long rainy season overall shows a decreasing trend. This trend is significant according to the Reanalysis dataset (α=0.05) and In-situ dataset (α=0.10). Overall rainfall decreased from the 1900s to 2019 with 1.8 mm/decade according to the Reanalysis dataset, and with 10 mm/decade according to the In-situ dataset. Average rainfall of the long rainy season (Reanalysis dataset: 326 mm, In-situ dataset: 435 mm) is larger than average rainfall of the short rainy season (Reanalysis dataset: 181 mm, In-situ dataset: 214 mm). A general increase in rainfall of the short rainy season is visible during the research period. The Reanalysis dataset indicates an increase of 1.3 mm/decade and the In-situ dataset an increase of 4.8 mm. This increase is thus smaller than the decrease of rainfall of the long rainy season according to both datasets.

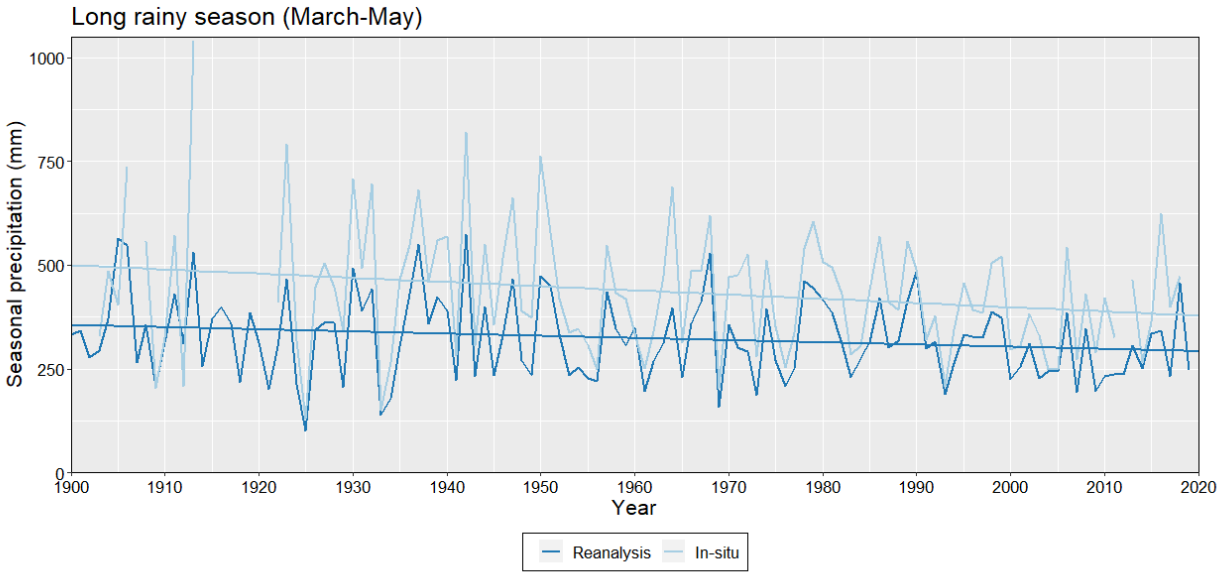

Figure 19: Total rainfall of the long rainy season (March-May) from 1900 up to and including 2018 according to the In-situ and Reanalysis datasets. A linear trend line is presented for both datasets.

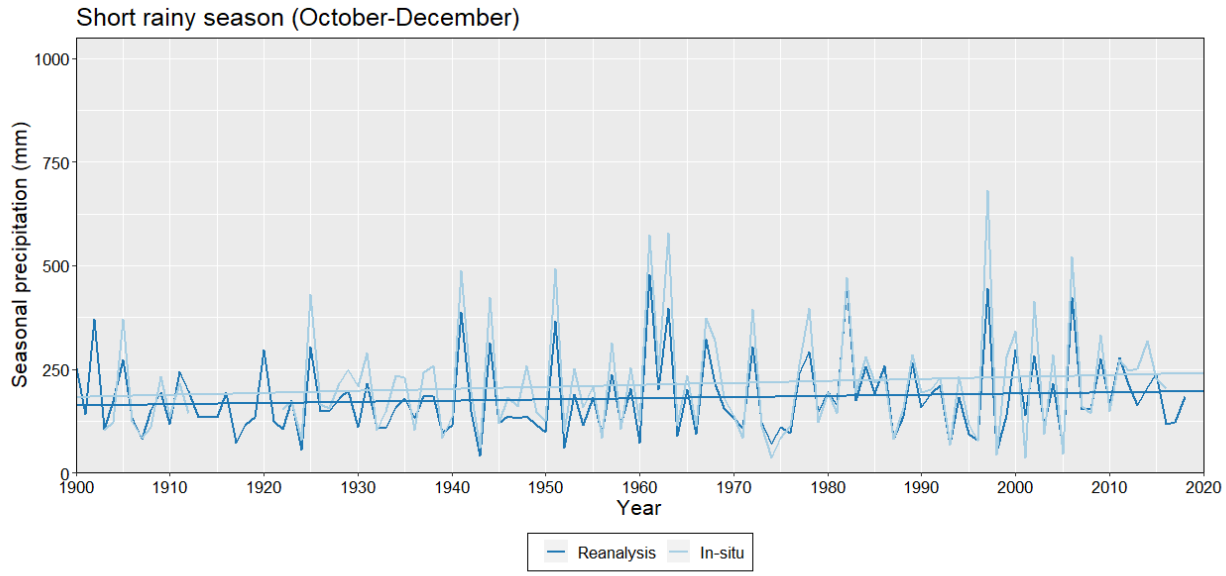

Figure 20: Total rainfall of the short rainy season (October-December) from 1900 up to and including 2018 according to the In-situ and Reanalysis datasets. A linear trend line is presented for both datasets.

Annual rainfall values show a decreasing trend during the research period. For the Reanalysis this trend is significant (α=0.10) and annual rainfall decreased with 5.2 mm/decade. The In-situ dataset shows an (insignificant) decrease in annual rainfall of 6.5 mm/decade. Average annual rainfall is 720 mm for the Reanalysis dataset and 850 for the In-situ dataset.

In Figure 22 the significant (α=0.05) increase in mean temperature from 1930 to 2019 can be observed. The period ±1922-1929 stands out a relatively warm period. This can be due to an error in the CRU model or observations the model uses. It could also have a physical cause. Annual rainfall is also relatively low during this period. The seasonality in mean temperature is also visible throughout the research period. The increasing trend starting in the 1930s is visible for both the periods with relatively high mean temperature and the periods with relatively low mean temperature.

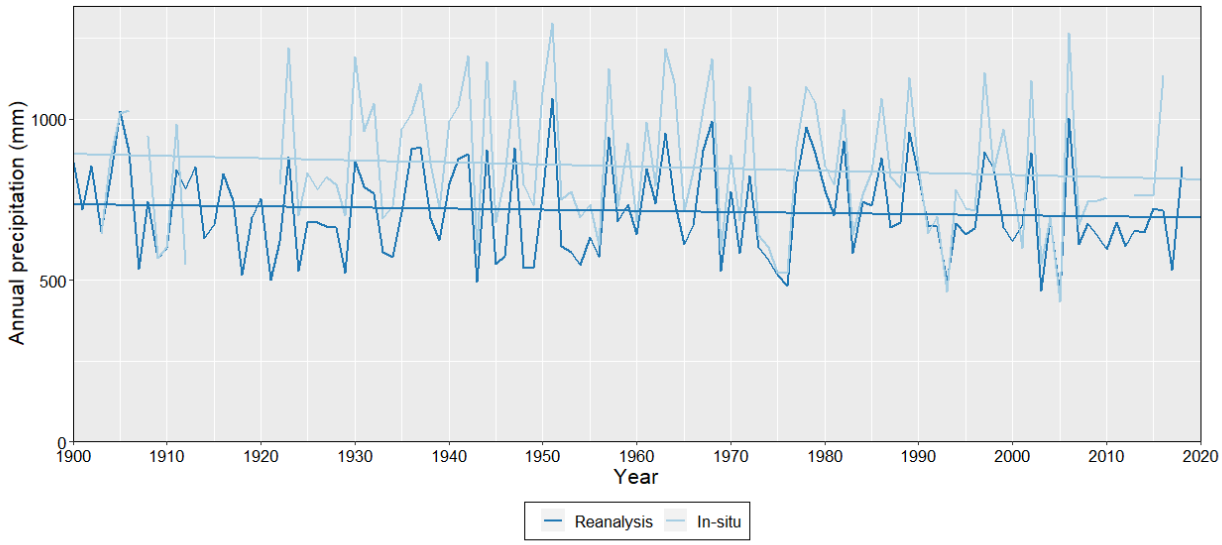

Figure 21: Annual rainfall from 1900 up to and including 2018 according to the In-situ and Reanalysis datasets. A linear trend line is presented for both datasets.

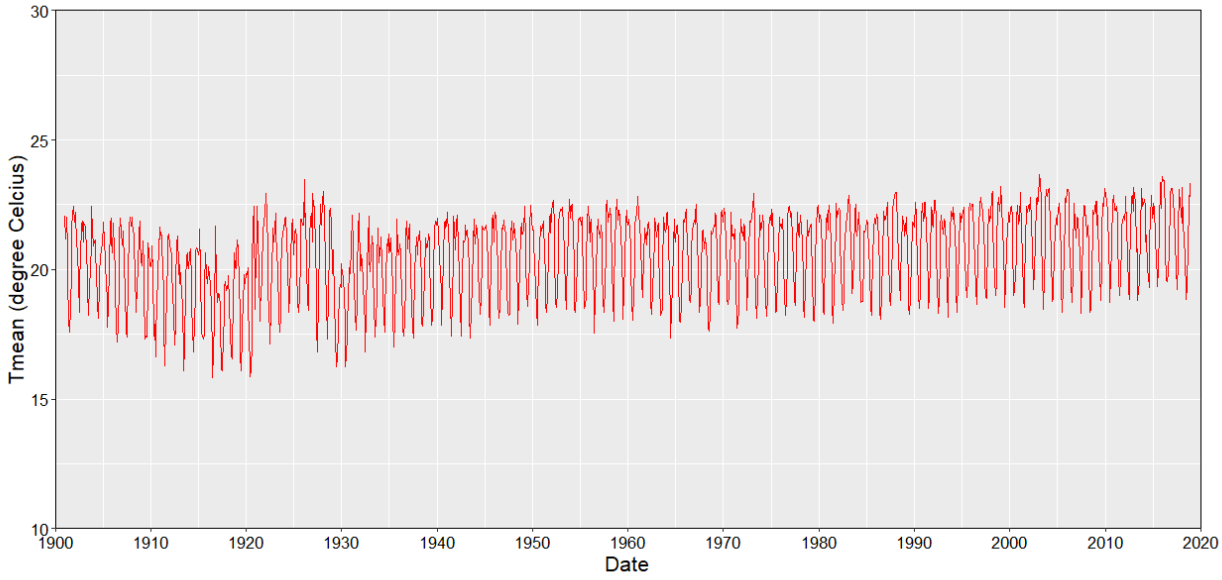

Figure 22: CRU monthly mean temperature of the region 3-6° S, 35-37° E from 1901 up to and including 2018.

4.2.2 SPI and SPEI

The SPI and SPEI were calculated for periods of interest of 3 months (short-term droughts/floods) and 12 months (long-term droughts/floods) for both the In-situ and Reanalysis dataset. Figure 23 shows the 3-month SPI and SPEI time-series for both datasets. Variation exists between the values, but overall they generate the same pattern. Both relatively wet (e.g. 1930-1940) and dry (e.g. 1990-1997) periods can be observed, with respectively many positive and negative SPI and SPEI values in general. Furthermore, both periods with long duration of events (e.g. 1961-1970, 1996-1999) or rapid alteration of SPI/SPEI values and wet/dry circumstances (e.g. 1938-1942, 1984-1990) are visible. In recent decades the area below zero (dry) is relatively large compared to the area above zero (wet) and relative to previous decades.

Figure 24 shows the 12-month SPI and SPEI. These represent long-term drought as here the cumulative rainfall of 12 months is used. In comparison with the 3-month SPI and SPEI time-series, there are less events visible. Multiple smaller events now form one event. This is known as pooling. The length of each event also increases, as it represents long-term droughts/floods. Here, dominantly wet or dry periods are visible as well. From 1930 to 1953 wet circumstances dominate. This is followed by a period of alternating wet and dry events. From 1973-1977 a long drought occurs. Then a relatively wet period ensues until 1991. Hereafter dry conditions are dominant, with the exception of two wet events in 1998 and 2007. The 12-month SPI and SPEI time-series of both datasets follow the same pattern in general. However, differences are visible especially in peak values.

When zooming in to the period 1990-2010 for the 3-month SPI and SPEI (Figure 25), the differences between the datasets and SPI/SPEI can be observed more clearly for these time-series. Sometimes, the drought indices and datasets give almost the same SPI/ SPEI values for the drought, as in 1993. This indicates little influence of evapotranspiration and low differences between the measurements of the datasets. SPI and SPEI values differ due to the inclusion of evapotranspiration. In Figure 25, the droughts at the end of 1995 and 2007 are an example. During these events the SPEI values are more negative than the SPI values. Thus, including evapotranspiration indicates dryer circumstances. However, this is not always the case, as can be seen during boreal summers of 1992 and 1993. Here the SPI values of the In-situ dataset are more negative than the SPEI values. Figure 26 shows the differences between the SPEI and SPI values for both datasets and periods of interest for the whole research period. The pattern follows in general the opposite shape of the temperature data (Figure 26). When mean monthly temperature is relatively high, PET is also relatively high. This causes a relatively low input value (P-PET) for the SPEI, resulting in a lower SPEI value. Relatively high temperature can thus cause the SPEI to be more negative than SPI, indicating dryer circumstances. Relatively low mean monthly temperature gives higher SPEI values. In this way the SPEI could become higher/less negative than SPI, showing wetter conditions. This happens between ±1910-1920 and around ±1930. From the year ±2000 to present SPEI values are lower than SPI values, indicating dryer conditions due to relatively high temperatures. This shows the marked effect of the inclusion of evapotranspiration on the appearance of the meteorological droughts. During other periods the SPEI and SPI are in general equal. The 3-month SPEI and SPI values show most scatter around the general pattern as individual observations have more influence here.

The effect of differences in precipitation observations between the datasets can also be seen in Figure 25. Around the year 2000 the Reanalysis dataset indicates a much lower SPI and SPEI values than the In-situ dataset. The opposite occurs in e.g. 1991 and 1996. Figure 27 shows the differences in index values between the datasets for the whole research period. The pattern can be explained partly due to differences in precipitation values between that datasets (e.g. around the year 2000). It is also due to the computation of the SPEI and SPI with some differences between observations of the datasets being more pronounced than others.

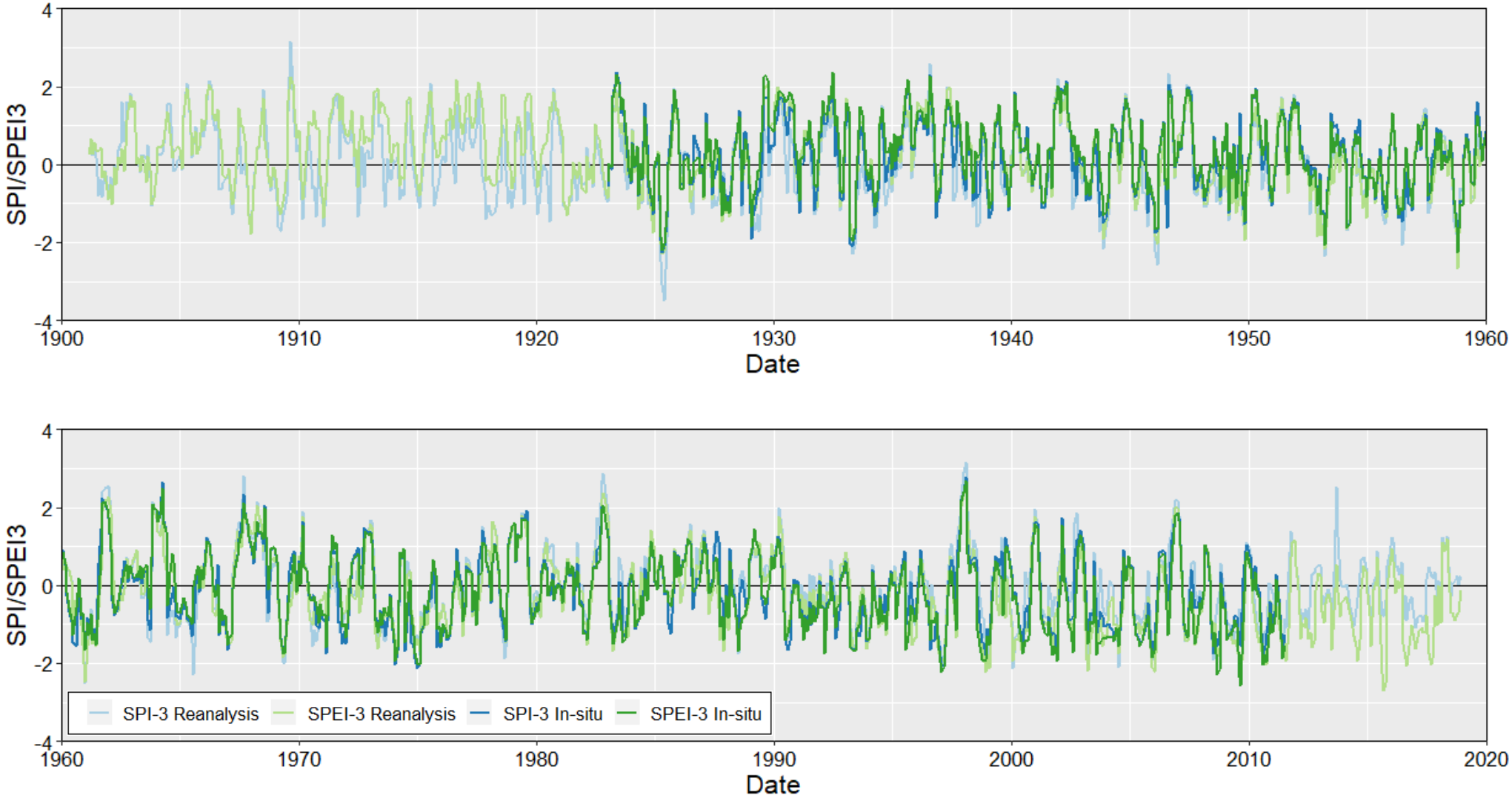

Figure 23: 3-month SPI and SPEI values through time for the In-situ and Reanalysis datasets.

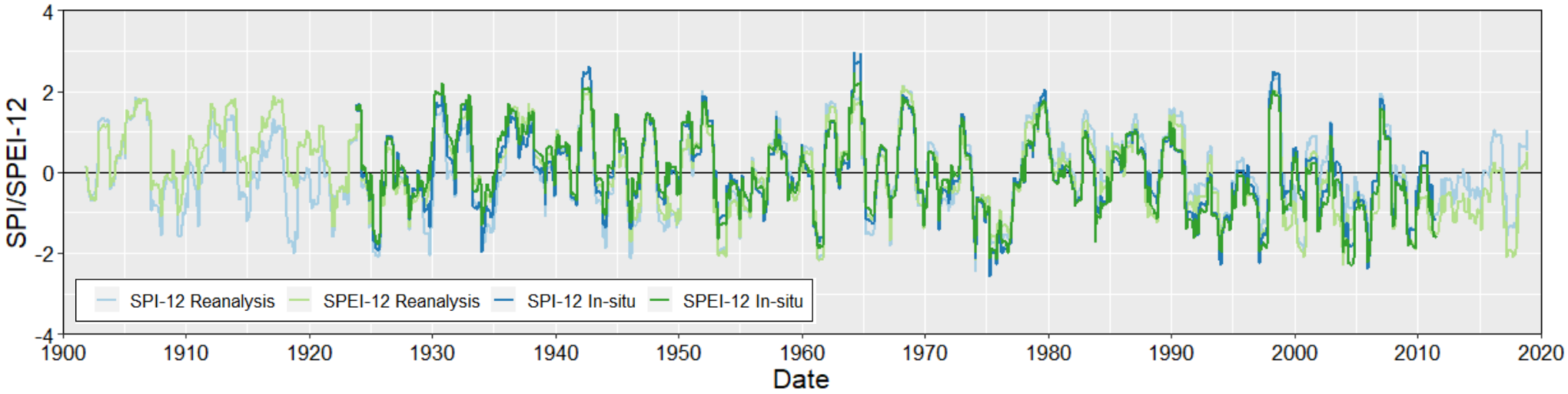

Figure 24: 12-month SPI and SPEI values through time for the In-situ and Reanalysis datasets.

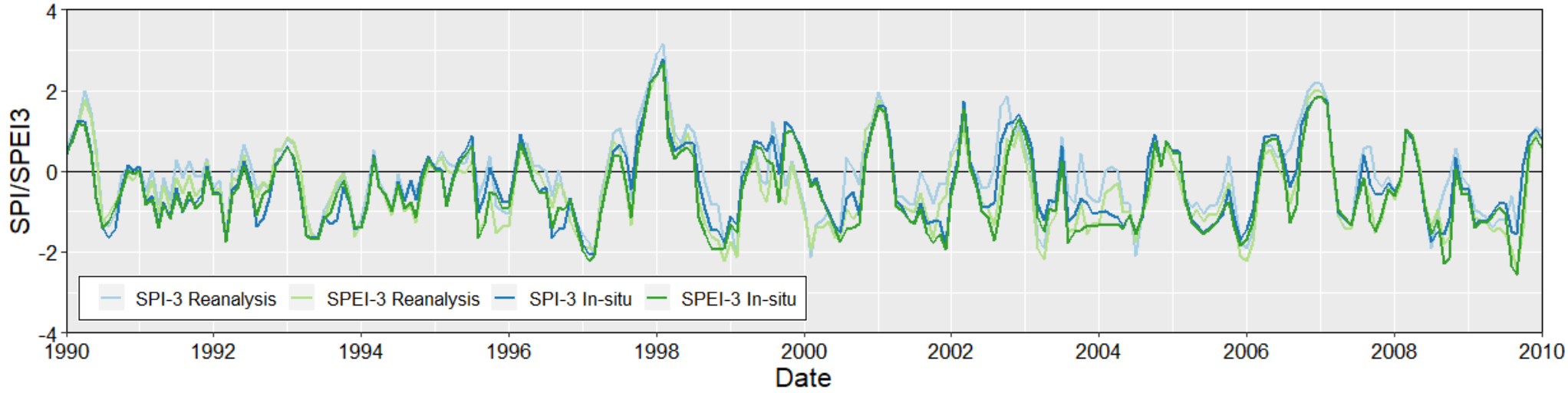

Figure 25: 3-month SPI and SPEI values from 1990 to 2010.

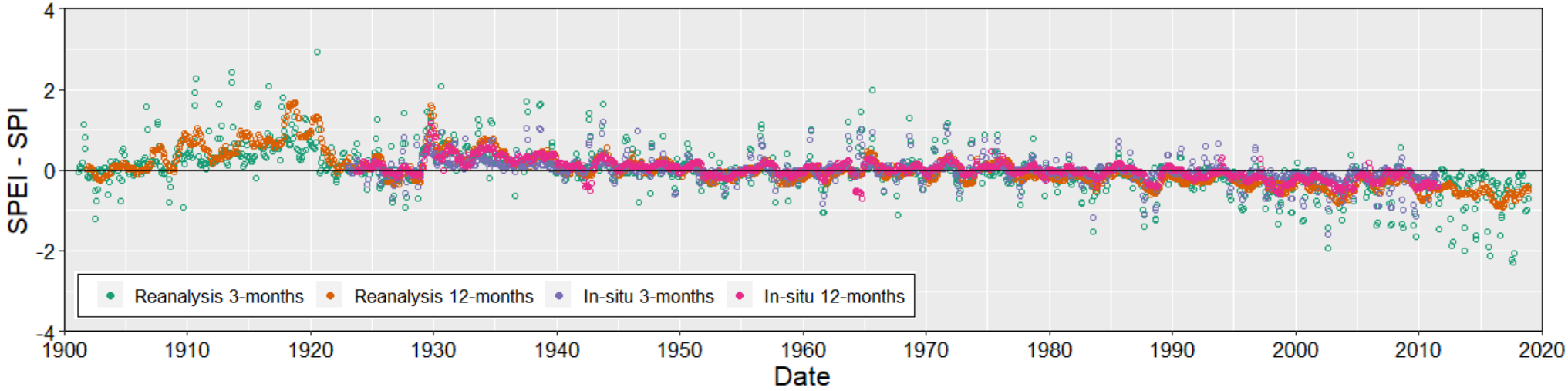

Figure 26: Differences between SPEI and SPI values for both 3- and 12-months period of interest and the In-situ and Reanalysis datasets.

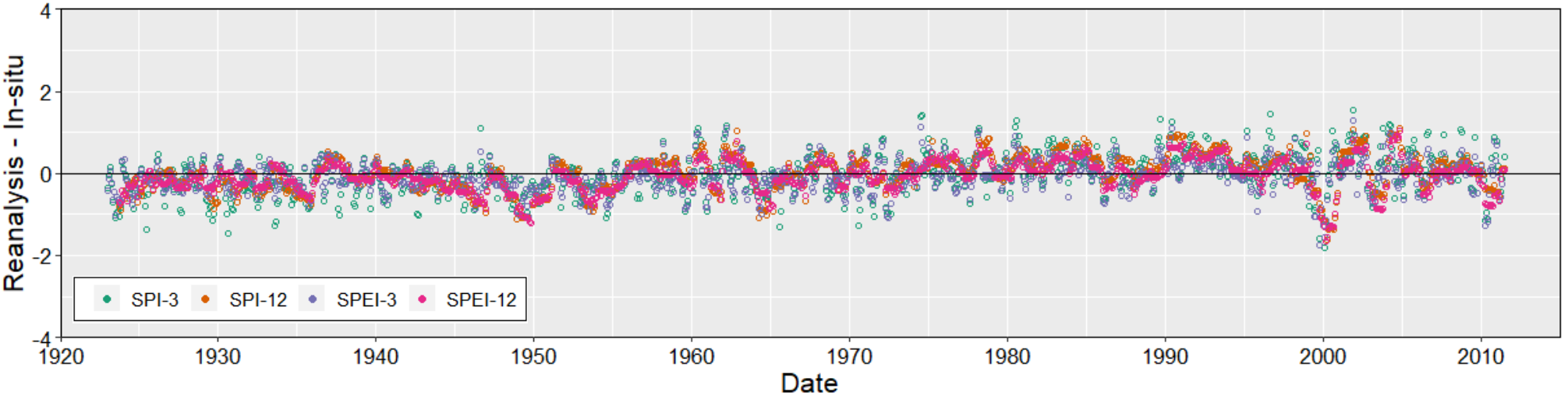

Figure 27: Differences between the In-situ and Reanalysis datasets in SPI-3, SPI-12, SPEI-3 and SPEI-12 values.

Sometimes, both differences in observations and the inclusion of evapotranspiration seems to play a role in the appearance of a drought. For example, around 2004 in Figure 25. In boreal autumn 2003, the SPEI values of both datasets are lower than both SPI values, meaning a large role of evapotranspiration. From 2004 the difference in observations seems more important, as both the SPI and SPEI values of the In-situ dataset are more negative than the SPI and SPEI values of the Reanalysis dataset. So both the use of dataset and inclusion of evapotranspiration can play a role in how meteorological droughts are observed. It influences the number of droughts that are observed and their characteristics.

Considering the whole research period, the SPEI and SPI time-series for both datasets and periods of interest show a significant decreasing trend (Table 5). This means that in general a drying trend is present in the LMC. Regarding seasonal drought, the 3-month SPI and SPEIs can be consulted. For example, May represents the March-May (MAM) trend, as it used cumulative rainfall of these months. SPEI shows significant decreasing trends for more months than the SPI. This is due to the inclusion of evapotranspiration, enhancing the drying trend as the temperature data shows a significant upward trend (Figure 22). Furthermore, the SPI-3 timeseries of the In-situ dataset shows more months with a (significant) trend than the Reanalysis data. This can be caused by the more local signal of the In-situ data, compared to the average and therefore less extreme catchment data of the Reanalysis dataset (Figure 19, 20 and 21). The short rainy (OND) and short dry (±DJF) seasons do not show a significant trend. The boreal summer dry season (JJA/JAS) and the long rainy season (MAM) however do show a significant drying trend according to nearly all SPI and SPEIs. Only the SPI of the Reanalysis dataset shows no significant trend for MAM and JAS. Graphs of the SPI/SPEI-3 values of the rainy seasons through the years can be viewed in Appendix C.

*Table 5: Results of Mann-Kendall Trend test applied to SPI and SPEI values of individual months for all 3-month SPI/SPEI and applied to all values (overall) for both 3- and 12-month SPI/SPEI. Plus indicates a positive trend. Minus indicates a negative trend. Significant trend (α=0.05) indicated by *.*

	Periods (months)	**SPI – 3 In-situ**	**SPI – 3 Reanalysis**	**SPEI – 3 In-situ**	**SPEI – 3 Reanalysis**	**SPI – 12 In-situ**	**SPI – 12 Reanalysis**	**SPEI – 12 In-situ**	**SPEI – 12 Reanalysis**
Jan	**NDJ**	**+**	**+**	**-**	**-**				
Feb	**DJF**	**-**	**+**	**-**	**-**				
Mar	**JFM**	**-**	**-**	**-**	**-**				
Apr	**FMA**	**-**	**-**	**-***	**-***				
May	**MAM**	**-***	**-**	**-***	**-***				
Jun	**AMJ**	**-***	**-***	**-***	**-***				
Jul	**MJJ**	**-***	**-***	**-***	**-***				
Aug	**JJA**	**-***	**-***	**-***	**-***				
Sep	**JAS**	**-***	**-**	**-***	**-***				
Oct	**ASO**	**-***	**+**	**-***	**-***				
Nov	**SON**	**-**	**+**	**-**	**-**				
Dec	**OND**	**-**	**+**	**-**	**-**				
Overall		**-***	**-***	**-***	**-***	**-***	**-***	**-***	**-***

4.2.3 Drought characteristics

The decadal variation in total drought duration (TDD), total drought severity (TDS) and average drought intensity (ADI) is shown in Figure 28. For each SPI and SPEI time-series, approximately the same trends in TDD and TDS decadal changes can be seen. In decades with relatively many months of drought occurrence, the total severity of droughts is also high. The general pattern throughout the decades is similar for both long-term and short-term droughts, SPI and SPEI, and both the Reanalysis and In-situ datasets. From the 1920s to the 1930s a decline is visible. Hereafter, TDD and TDS generally increase, with a little wobble round the 1950s and 1960s. The increase is present until the 1980s. The 1980s stand out as a sharp decrease in TDD and TDS occurs. From 1990 to 2010 the TDD and TDS are high again, even higher than before the 1980s according to the 3- and 12-months SPEI. For the SPEI the trends are more pronounced due to evapotranspiration and thus the increasing trend in temperature being taken into account. Not all observed trends are significant though (Table 6). All short-term trends in TDD and TDS are significant except for the Reanalysis SPI-3 time-series. This time series contains data from the 1910s and 1920s, which have quite high TDD and TDS values. Therefore, it does not show a significant positive trend regarding all decades. Concerning long-term droughts, the SPI's do not show significant trends in TDD or TDS. The SPEIs do, except the TDD for the Reanalysis dataset, which shows a high value for the 1920s. The ADI shows that short-term droughts were on average most intense during the 1920s, 1960s and 2000s according to both SPI and SPEI. For the long-term droughts the datasets disagree on the most intense decades. The In-situ dataset indicates the 1990s and 2000s as the decades with highest ADI for both SPI and SPEI. The Reanalysis dataset indicates the 1940s and 1960 as most intense. The trends in ADI are all positive, except for the Reanalysis SPI-12, which shows no positive nor negative trend (Table 6). The In-situ SPI-12 and SPEI-12 ADI trends are furthermore significant. There is no significant decadal trend in short-term drought ADI.

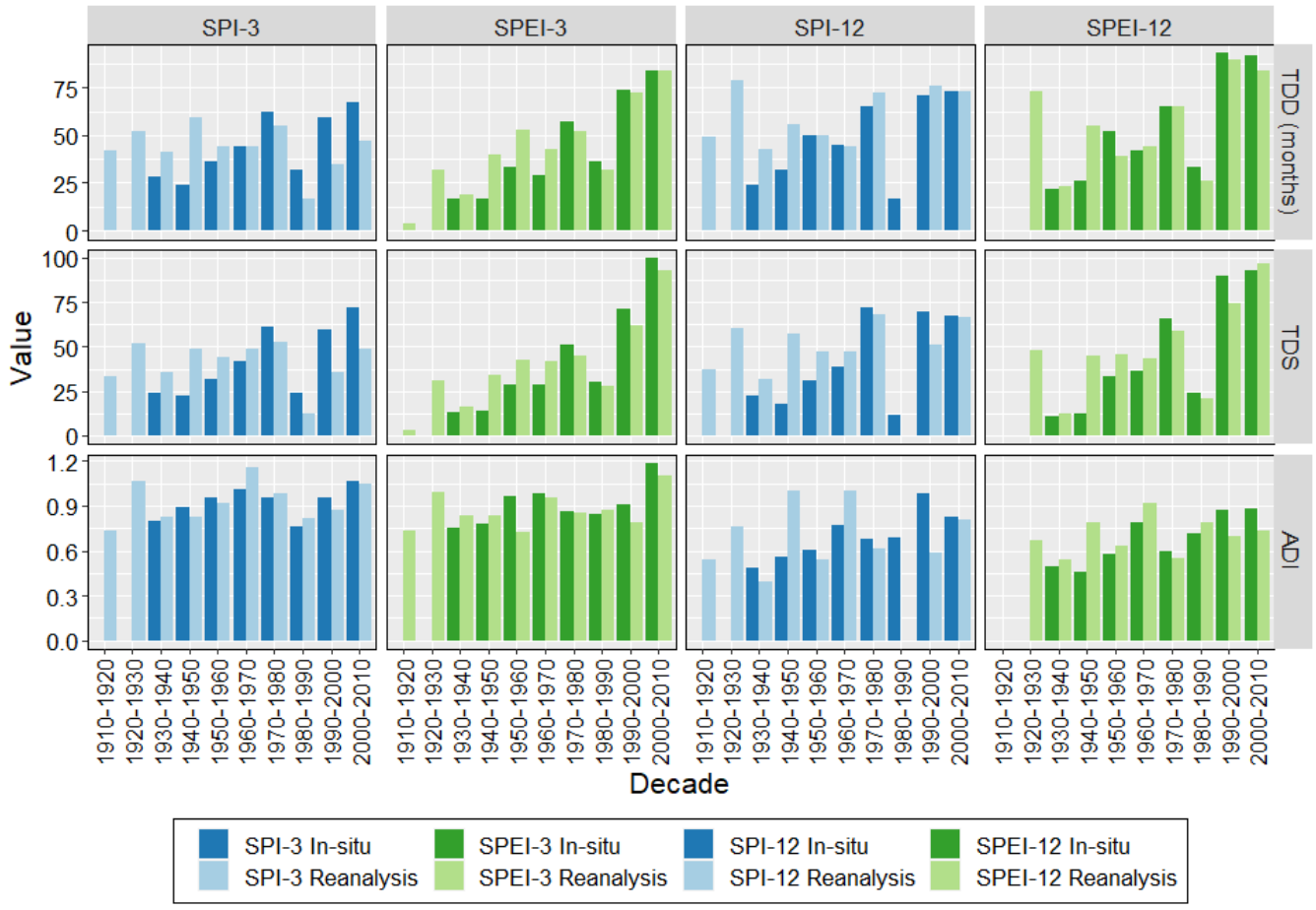

Figure 28: Total drought duration (TDD), total drought severity (TDS) and average drought intensity (ADI) per decade for both SPI and SPEI, periods of interest and datasets.

In Figure 29 the types of droughts are presented per decade. Large differences in number and types of droughts are present among the datasets and between the indices. The large differences in drought types are caused by differences in peak SPI/SPEI values between the time-series during a drought, which defines the type. Furthermore, the number of droughts can vary as an event ends when a SPI/SPEI value befalls just above zero or continues when it remains just below zero. Long-term droughts show less droughts per decade as multiple smaller events may now form one event. Almost all timeseries show an increasing trend in total drought frequency (DF; Table 6). Only the Reanalysis SPI-3 shows a negative trend due to high DF in 1910-1930, where the In-situ dataset has no observations. Which types of droughts occur also varies, but no clear general trend among the time-series can be observed. The frequency of moderate droughts shows a neutral or negative trend. Both the frequency of short-term and long-term severe and extreme droughts increase according to the SPEIs, with the trend in severe short-term droughts being significant. The SPIs agree with this trend, except for the In-situ SPI-3. The long-term SPIs show large disagreement on the types of drought occurring during the decades.

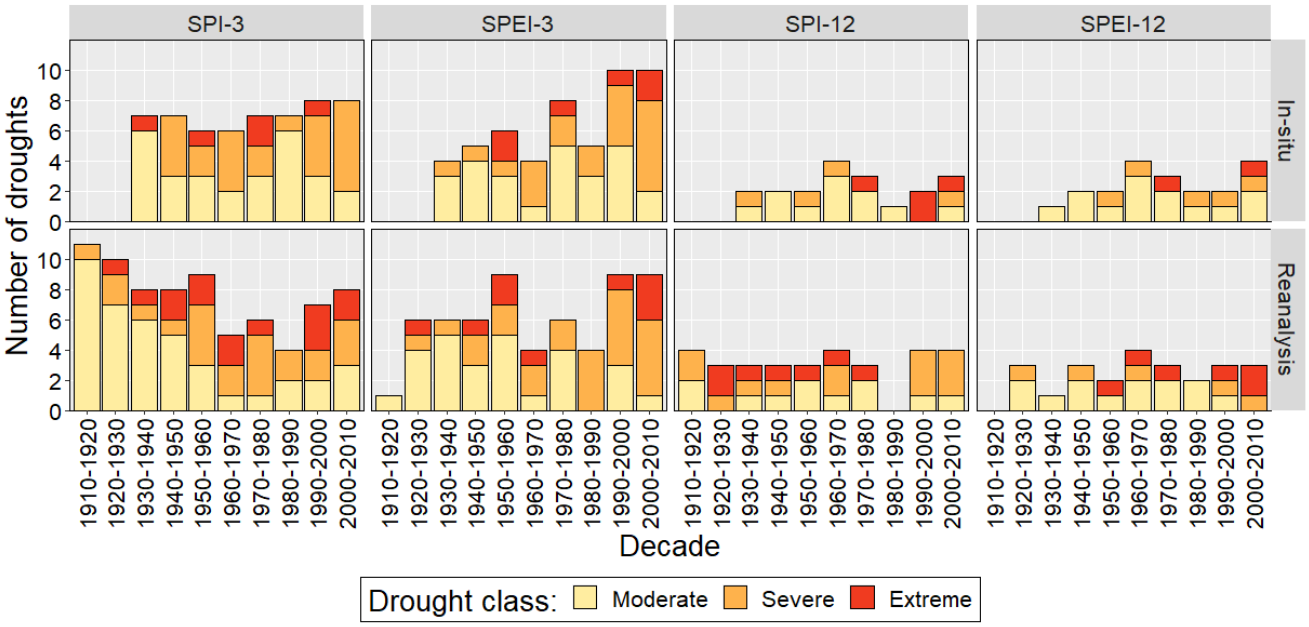

Figure 29: Total number of moderate, severe and extreme droughts per decade for each SPI and SPEI time-series.

*Table 6: Results of Mann-Kendall Trend test applied to decadal drought characteristics. Plus means an increasing trend of the variable through the decades (1910/1930-2010), minus indicates a decreasing trend. Zero indicates no positive nor negative trend. Significant trend (α=0.05) indicated by *.*

	SPI – 3 In-situ	**SPI – 3** Reanalysis	**SPEI – 3** In-situ	**SPEI – 3** Reanalysis	**SPI – 12** In-situ	**SPI – 12** Reanalysis	**SPEI – 12** In-situ	**SPEI – 12** Reanalysis
TDD	+*	-	+*	+*	+	+	+*	+
TDS	+*	+	+*	+*	+	+	+*	+*
ADI	+	+	+	+	+*	0	+*	+
DF Total	+	-	+*	+	+	+	+	+
DF Moderate	-	-*	0	-	-	-	0	0
DF Severe	+	+	+*	+*	-	+	+	+
DF Extreme	-	+	+	+	+	-	+	+

4.3 Influence of atmospheric teleconnections on LMC rainfall

In this section monthly and seasonal rainfall is correlated with the teleconnections mentioned in the literature study. These are the ENSO, IOD, MJO, SAM and NAO. The literature study provided information about how each teleconnection would influence rainfall in the LMC, at least for the short rainy season (October-December). Given these results and how the teleconnection indices are defined, a negative relation is expected between almost every teleconnection index and rainfall. Only the IOD would be expected to show a positive relation with rainfall. Besides standard correlation (with a lead-lag effect), sliding and partial correlation was also applied.

4.3.1 Monthly correlation

Precipitation was first correlated with each teleconnection for each month of the year separately. Both Pearson's and Kendall's correlation were computed. To determine the influence of teleconnections in advance of rainfall, the correlations with a maximum lead of 6 months were also calculated. The result for each month of the rainy seasons is shown in Figure 30. The results for the other months are presented in Appendix D.

The first thing standing out in Figure 30 is the stronger links of rainfall in October, November and December with teleconnections compared to March, April and May. The datasets and correlation methods agree in general about the relations, but differences in correlation values exist. During October, November and December, rainfall shows significant (α=0.05) correlations with the IOD and ENSO at multiple months lead. Nevertheless, in October the MJO shows the strongest relationship with rainfall, followed by the IOD and ENSO. For the Reanalysis dataset Pearson's r at a 0-months lead are -0.52 for the MJO, 0.42 for the IOD and -0.27 for the ENSO. Highest correlations are found at 0- or 1-months lead. In November and December, the relation with the MJO is less strong and only significant at a lead or not at all depending on the dataset and correlation test. The ENSO and IOD show higher correlations with rainfall than the MJO during these months. In November, the influence of the ENSO and IOD on LMC rainfall is almost as large. Pearson's r for the Reanalysis dataset at 1-month lead is -0.42 for the ENSO and 0.44 for the IOD. For the ENSO maximum correlation occurs at a lead of one month. In December the correlation with the ENSO decreases in strength but stays significant. The SAM and NAO show relatively little to no influence in October, November and December.

For March, April and May rainfall relations with teleconnections are less distinctive and weaker. In March the MJO at 0-months lead is significantly correlated with rainfall (Reanalysis r=0.33). The Reanalysis dataset also shows weak but significant correlation between March rainfall and the IOD (r= -0.22 at 0-months lead) and SAM (r= -0.25 at 0-months lead). April rainfall only shows significant weak correlation with the IOD (Reanalysis r= -0.27 at 0-months lead). For May the Reanalysis dataset shows significant relation with the ENSO at 0-months lead (r=-0.21), the IOD at 1-month lead (r=-0.20), the MJO at 5-months lead (r=0.33) and the SAM at 6-months lead (π=-0.17). The In-situ dataset only shows significant correlation with the SAM at 6-months lead (r=-0.33). Overall, the months of the long rainy season show weak correlations between rainfall and teleconnections.

Rainfall in the months of the long dry season (June-September) did not show strong significant relations with the teleconnections (Appendix D). For the short dry season (January-February), January rainfall did show some influence of the IOD at a 1-month lead (Reanalysis r=0.34). The In-situ dataset also showed influence of the MJO (r=-0.34 at 1-month lead) and SAM (r=0.34 at 2-months lead). February shows significant relations with all teleconnections, though for some only at a lead. For the Reanalysis dataset highest significant Pearson's r is for ENSO -0.27 at 5-months lead, for the IOD -0.23 at 0-months lead, for the MJO -0.41 at 1-month lead, for the SAM -0.28 at 2-months lead and for the NAO -0.24 at 1-month lead.

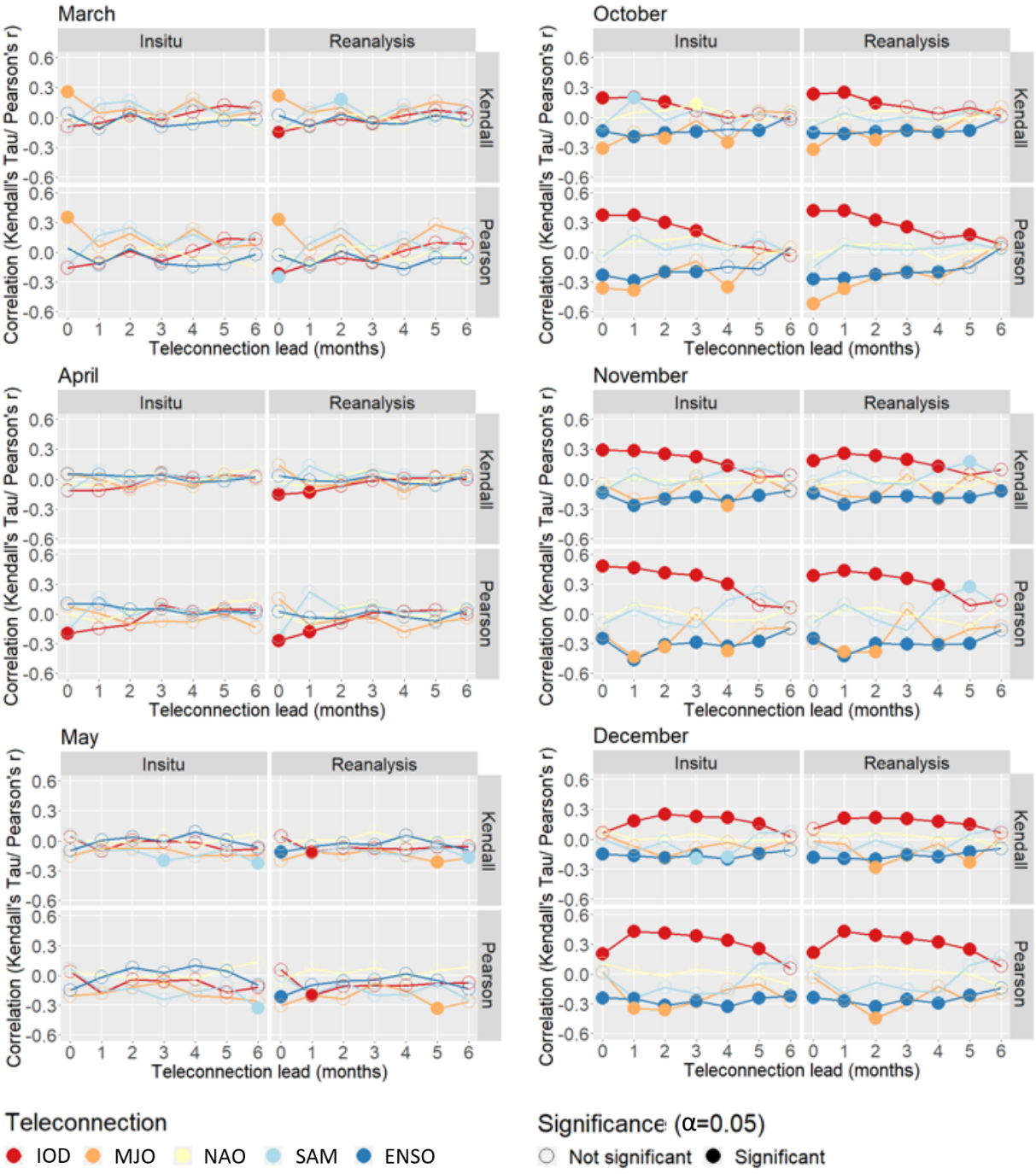

Figure 30: Correlations between rainfall and teleconnection indices with a maximum lead of 6 months for the separate months of the rainy seasons. Both Kendall and Pearson's correlations are shown for the In-situ and Reanalysis datasets. These figures for the other months can be found in Appendix D.

4.3.2 Seasonal correlation

SPI-3 values of May and December, representing the long (March-May) and short (October-December) rainy season respectively, were also correlated with the teleconnection indices. The teleconnections are represented by their respective index and the cumulative of the 3 months of the season is used for the correlation. In this way the influence of teleconnections on seasonal precipitation can be determined. The SPI timeseries are normally distributed so only Pearson correlations is calculated. In Figure 31 the seasonal correlations are shown.

As with the monthly correlations, the short rainy season shows a stronger relation with teleconnections. The seasonal correlations are higher than the monthly correlations. The ENSO, IOD and MJO show the strongest significant correlations with October-December rainfall at multiple months lead. The highest values are (In-situ/ Reanalysis): for ENSO -0.42/-0.41 (moderate) at 2-month lead, for IOD 0.55/0.53 (strong) at 1-month lead and for MJO -0.49/-0.47 (moderate) at 1-month lead. The SAM and NAO do not show significant correlations.

The long rainy season only shows a significant correlation with the IOD at 0 and 1-month leads. The correlation values at 0 months lead are -0.25 for the In-situ dataset and -0.30 for the Reanalysis dataset. All other teleconnections do not show a significant relation with March-May rainfall. Redefining the long rainy season as February-April or April-June did not improve correlations.

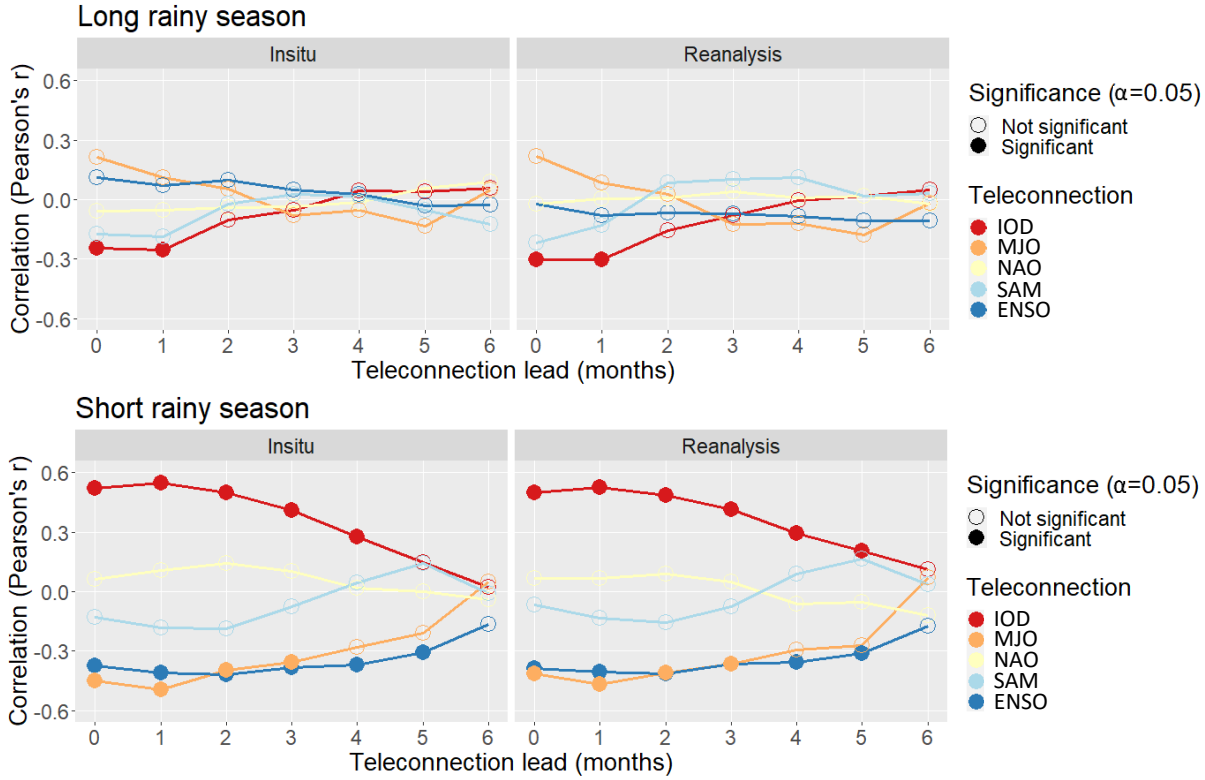

Figure 31: Correlations between rainfall and teleconnection indices with a maximum lead of 6 months for the long (March-May) and short (October-December) rainy season. Pearson's correlations are shown for the In-situ and Reanalysis datasets.

4.3.2 Sliding correlation

To see whether the relations between LMC rainfall and teleconnections changed through time, sliding correlations were established using a 20-year window. The relation through time is explored for seasonal rainfall (March-May and October-December) as this showed highest and most clear correlations with teleconnections. The teleconnections are defined by their respective index and the cumulative of the 3 months of the corresponding season is used to correlate with seasonal rainfall. The seasonal rainfall is again represented by the SPI-3. No lag/lead is applied. Due to data availability, sliding correlations of the SAM and MJO through time can be only presented after 1978 and 1997 respectively.

The long rainy season already showed barely significant and mostly weak relations between rainfall and teleconnections. This is also evident through time (Figure 32). Roughly five periods can be distinguished: 1921-1961, 1961-1984, 1984-2000, 2000-2010 and 2010-2019. At first the IOD is most important, even showing a significant negative relation during the 1930s and begin 1940s. After 1944 this relation weakens until even zero relation in 1961 or 1972 according to In-situ or Reanalysis data respectively. Up to this point the ENSO and NAO barely show influence. The NAO shows maximum negative correlation for 1961. Between 1961 and 1984 the coupling between teleconnections and rainfall appears to be very weak. From 1984 to 2010 the ENSO and NAO show positive relations. The ENSO reaches a maximum and significant correlation in 1996, after which it decreases and becomes insignificant again. The NAO reaches a high around 2000-2004, but the relation stays insignificant. Meanwhile the IOD and SAM show negative correlations. In 2010 correlations of the MJO, SAM and NAO with March-May rainfall switch sign (positive relations become negative and vice versa) according to both rainfall datasets. According to the Reanalysis dataset the ENSO relation also switches sign. The IOD relation however remains negative. From the year 2010 only the Reanalysis dataset provides information, showing the correlations to first increase in strength and becoming around zero again in 2019. The IOD relation stays ± -0.40 during this period. From what is visible, the MJO follows approximately the same pattern in correlation values as the NAO.

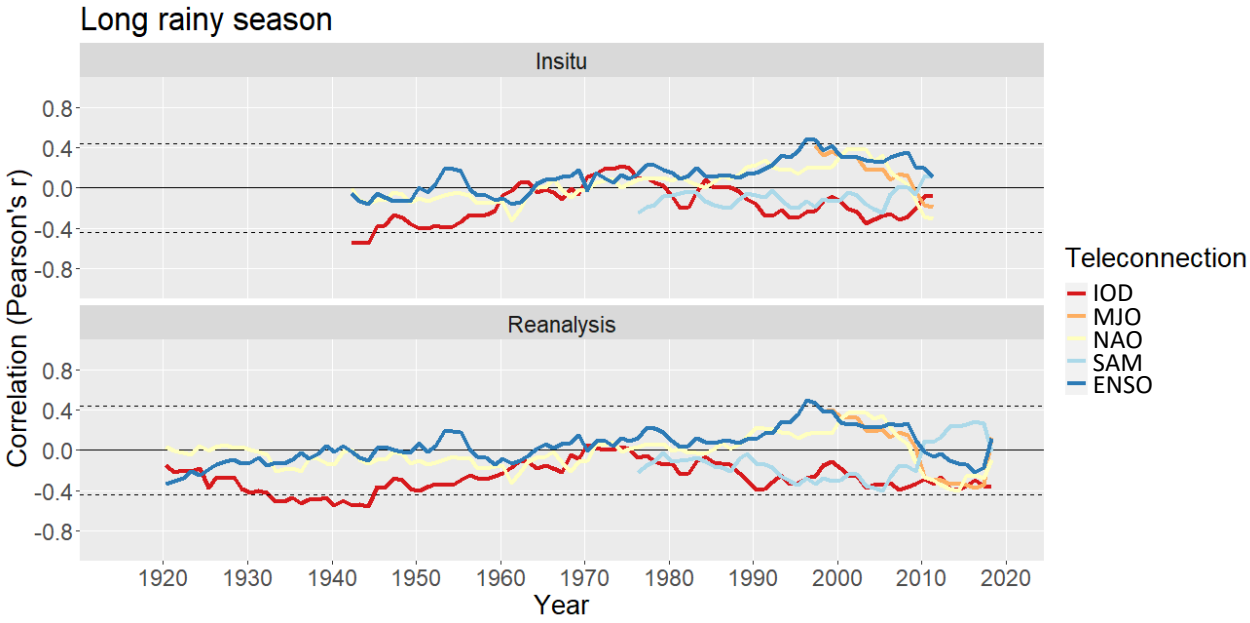

Figure 32: Sliding 20-year correlations between March-May rainfall and the teleconnections IOD, MJO, NAO, SAM and ENSO. Values are plotted at the final year of the 20-year interval. The sliding correlations are calculated for both the In-

The short rainy season (Figure 33) also shows the non-stationarity of the relation between teleconnections and rainfall in the LMC. Overall, the ENSO and MJO show a negative relation with rainfall during the whole research period and the IOD shows a positive relation. The SAM and NAO relations in the meantime switch sign. Furthermore, the SAM and NAO, which did not show a significant or high correlation overall, do show higher and significant correlations during specific periods in time. Here, also roughly four periods can be distinguished: 1921-1961, 1961-1982/1984, 1982/1984-1996/1998 and 1996/1998-2019. Prior to 1930 the relation between rainfall and the ENSO was the strongest and only significant relation. Hereafter the influence of the ENSO decreased, and no relation is significant until the IOD becomes significant. After 1961 this positive relation becomes even stronger and correlations of ± 0.78 are reached from 1964. Furthermore, after 1961 the correlation between the NAO and LMC rainfall becomes negative and increases. During 1982-1984 the regime seems to change again. The NAO relation changes sign and becomes positive. The dominant IOD relation starts to decrease in strength. The ENSO relation suddenly increases in strength. The relation with the SAM is also visible now and a plunge from significant positive correlation values to zero correlation in 1982-1984 is evident. From 1982-1984 to 1998 the NAO and IOD seem to show opposite patterns. While the NAO correlation increases up to a significant value in 1996, the IOD correlation decreases to zero in 1996. Hereafter the IOD correlation increases and NAO relation decreases. Meanwhile the influence of the ENSO decreases. The negative relation between October-December rainfall and the SAM increases, becoming significant. Furthermore, the negative significant relation with the MJO is now visible. The relation with the MJO follows approximately the same pattern as the relation with the ENSO. From 1998 to 2019, the ENSO, MJO and SAM correlations become weaker and insignificant. In the meantime, the coupling between LMC rainfall and the IOD becomes stronger, significant and dominant. The last two years show a decrease in influence of all teleconnections on rainfall of the short rainy season.

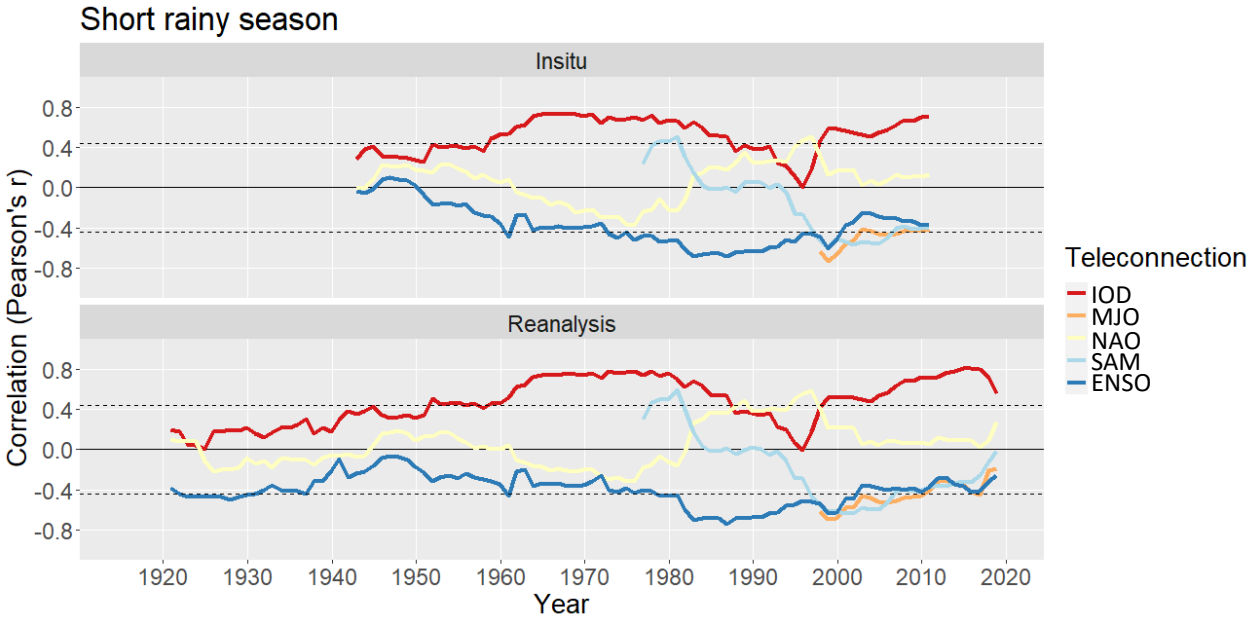

Figure 33: Sliding 20-year correlations between October-December rainfall and the teleconnections IOD, MJO, NAO, SAM and ENSO. Values are plotted at the final year of the 20-year interval. The sliding correlations are calculated for both the In-situ and Reanalysis dataset. Values exceeding ±0.44 (indicated by dotted lines) are significant (α=0.05).

4.3.3 Partial correlation

Partial correlation was applied to see whether the other teleconnections influence the relation between one teleconnection and rainfall in the LMC. Partial correlation was calculated between seasonal teleconnection values and rainfall of the rainy season using the Pearson method. Seasonal rainfall is again represented by the SPI-3. Data from 1978 to 2010 was used as during this period all teleconnections indices were available. In Table 7 and 8 the results using this data are presented.

Table 7 shows the differences between ordinary correlation and partial correlation for the long rainy season (March-May). Here the significant influence of the IOD according to the Reanalysis dataset is also visible. This correlation value does not change much using partial correlation, indicating little influence of the other teleconnections on the apparent relation. Some relations between other teleconnections and rainfall, e.g. the ENSO, do show changing correlation values and therefore interference of other teleconnections. However, this is not of much importance as the influence on March-May rainfall is already weak.

The results for the short rainy season (October-December) are visible in Table 8. Here interrelations of teleconnections are more evident. The ENSO, IOD, MJO and SAM all showed significant correlation with short rainy season rainfall during 1978-2010. However, partial correlation shows most of these relations become insignificant when removing the influence of other teleconnections. The IOD relation is the only one to stay significant, although it becomes weaker. Thus, the teleconnections have an effect on each other's apparent influence on October-December rainfall. This indicates joint influence of the teleconnections on rainfall during the short rainy season.

*Table 7: Correlation values between March-May rainfall and teleconnections for the period 1978-2010. Both partial and standard Pearson correlation values were calculated for comparison. Significance of the relation: * significant at α=0.10, ** significant at α=0.05.*

Long rainy season	**In-situ SPI**		**Reanalysis SPI**	
Teleconnection	Standard correlation	Partial correlation	Standard correlation	Partial correlation
ENSO	0.19	0.07	0.08	-0.11
IOD	-0.28	-0.26	-0.42**	-0.41**
MJO	0.21	0.12	0.22	0.27
SAM	-0.12	-0.08	-0.25	-0.15
NAO	-0.01	-0.01	-0.01	-0.07

*Table 8: Correlation values between October-December rainfall and teleconnections for the period 1978-2010. Both partial and standard Pearson correlation values were calculated for comparison. Significance of the relation: * significant at α=0.10, ** significant at α=0.05.*

Short rainy season	**In-situ SPI**		**Reanalysis SPI**	
Teleconnection	Standard correlation	Partial correlation	Standard correlation	Partial correlation
ENSO	-0.40**	-0.09	-0.46**	-0.15
IOD	0.52**	0.38**	0.51**	0.35*
MJO	-0.45**	0.06	-0.48**	0.06
SAM	-0.40**	-0.22	-0.41**	-0.21
NAO	0.21	0.15	0.23	0.15

4.4 Drought occurrence and Lake Manyara fluctuations

In this part influence of drought on the size of Lake Manyara is explored. 83 images of the Surface Water Dataset from the Joint Research Centre (JRC) were used to provide the surface area of Lake Manyara. Exact months, values and a boxplot showing the distribution of values can be found in Appendix B. The number of observations for the same month vary from 13 (January and December) to 1 (April and May). The size of the Lake Manyara varies strongly. It does not depend on the time of year whether the surface area is particularly large or small. The surface area values were transformed to volume using the method described in section 3.2.3.

Several variables were tested to see if they influence the water volume of the lake. These are the monthly SPI-3, SPI-12, SPEI-3, SPEI-12, P and P-PET. At first this was done using both the In-situ and Reanalysis datasets. However, due to missing precipitation values, the In-situ dataset has less matches to use for correlation. The In-situ data has for example only SPI/SPEI values up to 2011 and thus less values (32 instead of 83) to compare with the lake volume data. Furthermore, correlations with the In-situ dataset showed lower correlation values than the Reanalysis dataset. Therefore, the In-situ dataset was not used in this analysis. The SPI-3, SPI-12, SPEI-3, SPEI-12, P and P-PET used below are all from the Reanalysis dataset. Correlations were performed using both Kendall and Pearson's correlation to account for the non-normality of the surface area data.

Looking at the volume of Lake Manyara and the different variables through time (Figure 34), a couple of things stand out. The first is the large increase in volume at the end of 2002. This coincides with both a short (SPI/SPEI-3) and long (SPI/SPEI-12) wet period, high P and positive P-PET. The same can be observed in boreal spring 2018. However, an increase also occurs when there is only high P and positive P-PET and no relatively wet period as in spring 2013. The volume can furthermore be relatively large after a short drought (end of 2001) or long drought (end of 2000). In September 2000 the lake is still relatively large after short- and long-droughts and months of low P and negative P-PET. In 2010/2011, 2011/2012, 2012/2013, 2015/2016 and 2017/2018 a rough pattern can be observed during boreal autumn and winter. After the long dry season, the lake is relatively small. When precipitation falls again in the short rainy season the volume of the lake increases. This is not always the case as for example can be seen in 2013/2014. Here, the lake is quite big and even increases in volume at the end of the long dry season. This increase coincides with a short wet period. Then it decreases in volume during the short rainy season, even though P is high and P-PET is positive. Lastly the sudden increase and decrease in volume of Lake Manyara between November 2016 and January 2017 stands out. Only P indicates rainfall which could cause the increase, but P-PET is negative and the SPI and SPEIs indicate no relatively wet period.

To determine which variable has most influence on the volume of Lake Manyara several correlations were computed. First it was attempted to find a connection between the size of Lake Manyara in a certain month and variable of this month or the prior months. For SPI-12 and SPEI-12 correlations are highest with no lead (Figure 35). The SPI-3 shows highest correlation value with the surface area at a lead of 6 months. Correlation with the SPEI-3 (short droughts) is slightly higher at a lead of 1 month, but is also significant (α=0.05) with no lead. Though some correlations are significant, all correlations with SPI or SPEI are fairly weak (<~0.3). In Figure 36 the SPI-3, SPI-12, SPEI-3 and SPEI-12 were plotted against the size of Lake Manyara of the same month. Here it is evident that even though there has been a long or short drought (-2), the lake can still be large (~0.22 km^3). Droughts do thus not show much (linear) relation with the monthly total volume of Lake Manyara.

Figure 34: Monthly SPI-3, SPEI-3, SPI-12, SPEI-12, P, P-PET and the volume of Lake Manyara plotted from 2000 to 2019.

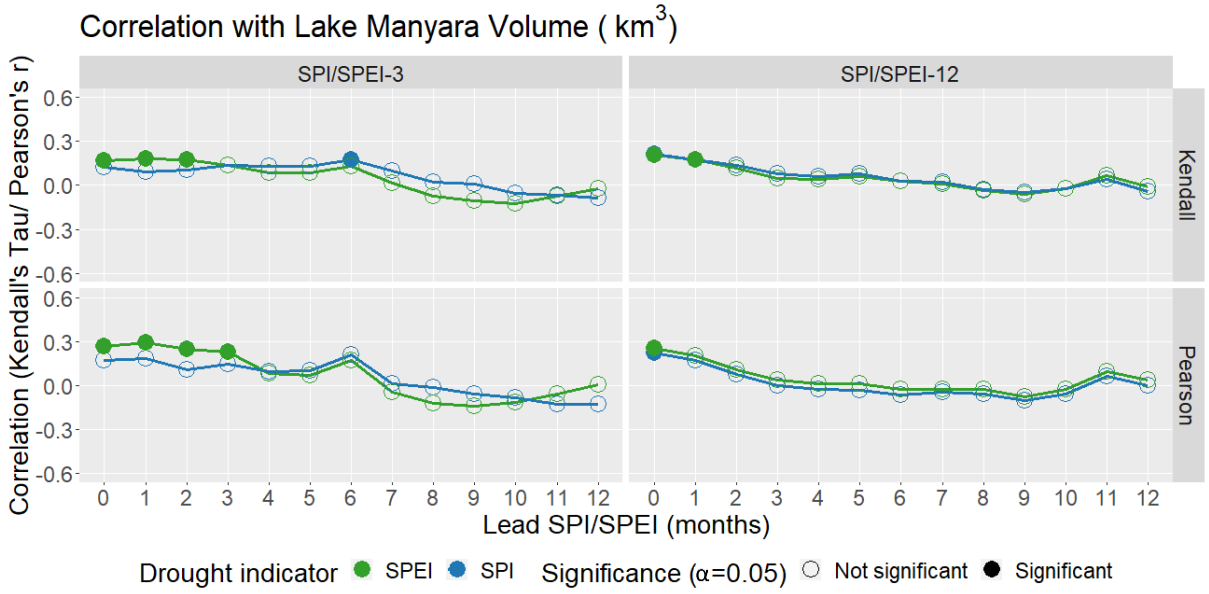

Figure 35: Correlations between the volume of Lake Manyara and drought indicators with a maximum lead of 12 months. Both Kendall and Pearson's correlations are shown.

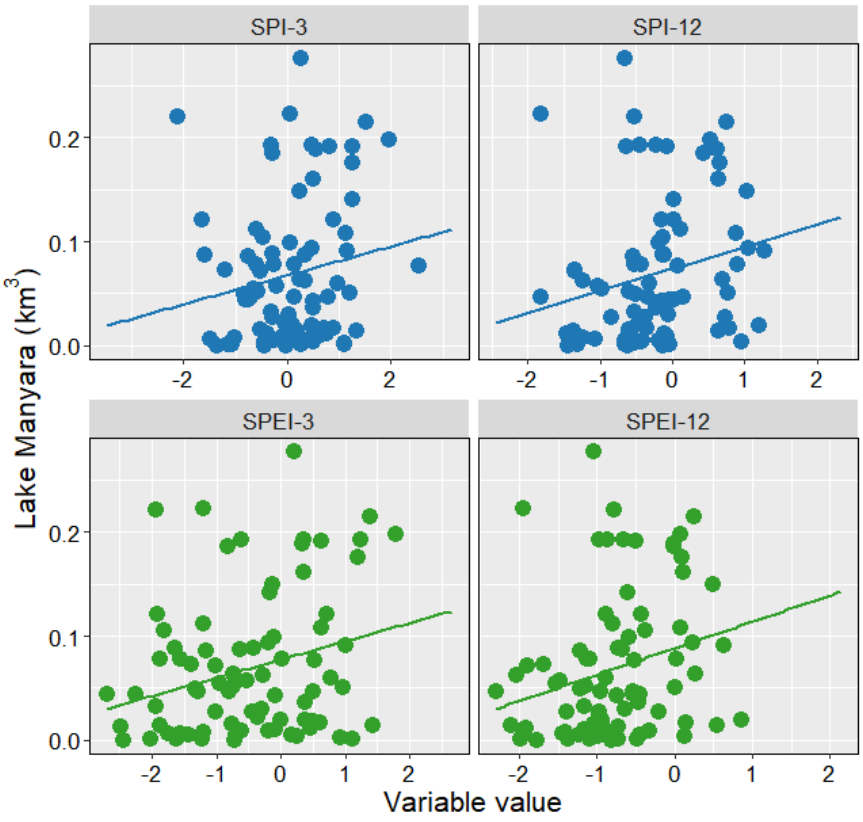

Figure 36: Volume of Lake Manyara plotted against SPI-3, SPEI-3, SPI-12, SPEI-12 values of the same month. Blue indicates evapotranspiration is not taken into account. Green indicates evapotranspiration is taken into account. Linear trend lines are also shown. R^2 of this line is the squared of Pearson's r in Table 9.

P and P-PET of the same month, the month before and the cumulative of 3, 6 and 12 months before the observations were also correlated to the surface area of Lake Manyara (Table 9). P and P-PET do not show much difference in correlation values. Cumulative P and P-PET 3 months prior to the observation show highest correlation with the volume of the lake. P and P-PET show overall weak correlations.

To investigate the effect of seasonal differences ideally correlations would be executed for each month. However, many months have even less than 10 observations. To study the effect of correlating monthly values and thus accounting for seasonal differences, the 13 observations of January were used. This month was chosen as, together with December, it has the highest number of observations. January was chosen over December so the whole short rainy season had passed. Though caution should be taken as it comprises only 13 values, the correlations using only January observations paint a different picture than when using all observations. The relation between January lake volume and short droughts is strong and significant (Table 9). This indicates the impact of a relatively dry/wet short rainy season on January lake volume. Correlation with P and P-PET of the same month are much higher and significant. The higher correlations when including variables of the month January itself indicates that recent events have a large impact on lake volume. However, whether the observations were taken after large events during this month is not known.

The link between the change in volume of Lake Manyara and several variables was also studied. Every time the change in volume between two consecutive observations was compared with the cumulative of a variable from the first observation to the second. Variables were again the P, P-PET, SPI-3, SPI-12, SPEI-3 and SPEI-12. Of the 82 matches between change in lake volume and variables, four were taken out as they created outliers having a pronounced effect on the correlations. These had overall large cumulative values of the variables due to at least 2 years elapsing between observations of the lake. Taking them out gave stronger relations, which are visible in Figures 37 and 38 and Table 10.

*Table 9: Correlations values between several variables and the volume of Lake Manyara. No lag/lead applied. Significance: * significant at α=0.10, ** significant at α=0.05.*

		Correlation with volume all observations		**Correlation with volume January**	
Variable		Kendall	Pearson	Kendall	Pearson
SPI	-3	0.12	0.17	0.46**	0.59**
	-12	0.22**	0.22**	-0.15	0.26
SPEI	-3	0.17**	0.27**	0.51**	0.60**
	-12	0.20**	0.25**	0.26	0.25
P	Same month	0.08	0.12	0.44**	0.53*
	1 month prior	0.16**	0.26**	0.31	0.44
	Cum 3 months prior	0.23**	0.30**	0.33	0.43
	Cum 6 months prior	0.13*	0.21*	0.28	0.43
	Cum 12 months prior	0.18**	0.18*	-0.12	0.17
P-PET	Same month	0.12	0.17	0.46**	0.55*
	1 month prior	0.16**	0.28**	0.31	0.46
	Cum 3 months prior	0.19**	0.32**	0.26	0.45
	Cum 6 months prior	0.12	0.22**	0.28	0.48
	Cum 12 months prior	0.17**	0.21*	-0.08	0.18

As is visible in the scatterplots, negative drought indicators or P-PET does not always mean shrinkage of the lake. Among the drought indicators, SPEI-3 showed the strongest relation with changes in the size of Lake Manyara. The rest of the correlations with drought indicators is weak. Furthermore, it is clear that including evapotranspiration gives higher correlation values. This can also be seen comparing the P and P-PET correlations. P shows weak and insignificant relations with the change in lake volume. The linear relation is even negative, and as can be seen in Figure 38. With high cumulative P (e.g. 841 mm) the lake can still shrink (-0.45 km^3). This shows the importance of including evapotranspiration. P-PET provides the strongest link with changes in the volume of Lake Manyara. According to Kendall's and Pearson's correlation this relation is moderate or strong respectively.

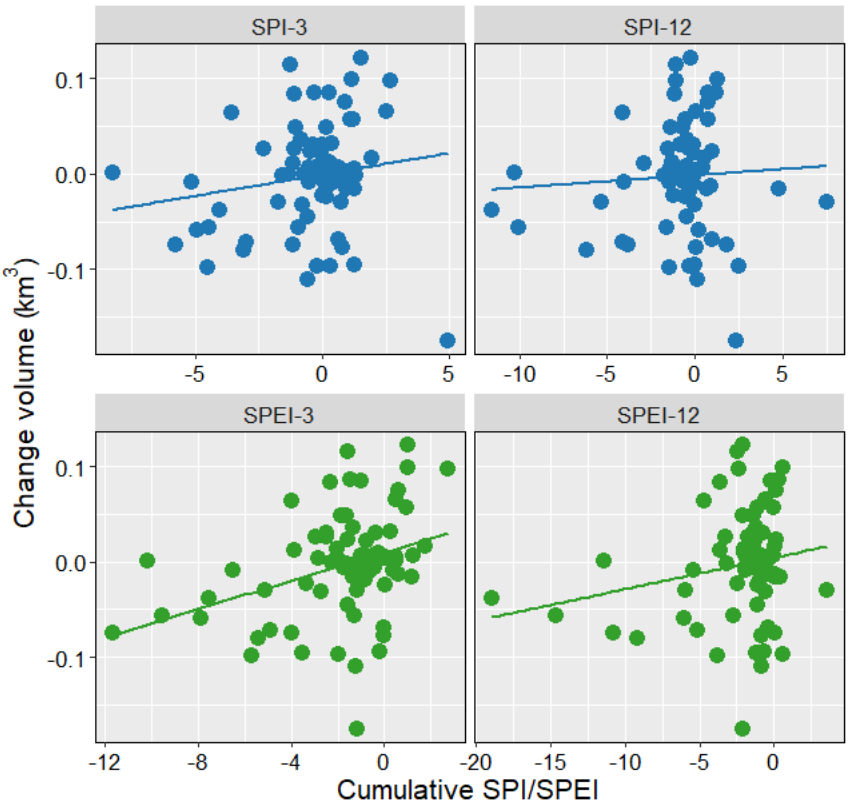

Figure 37: Change in volume of Lake Manyara plotted against cumulative SPI-3, SPEI-3, SPI-12, SPEI-12 values between the observations. Blue indicates evapotranspiration is not taken into account. Green indicates evapotranspiration is taken into account. Linear trend lines are also shown. R^2 of this line is the squared of Pearson's r in Table 10.

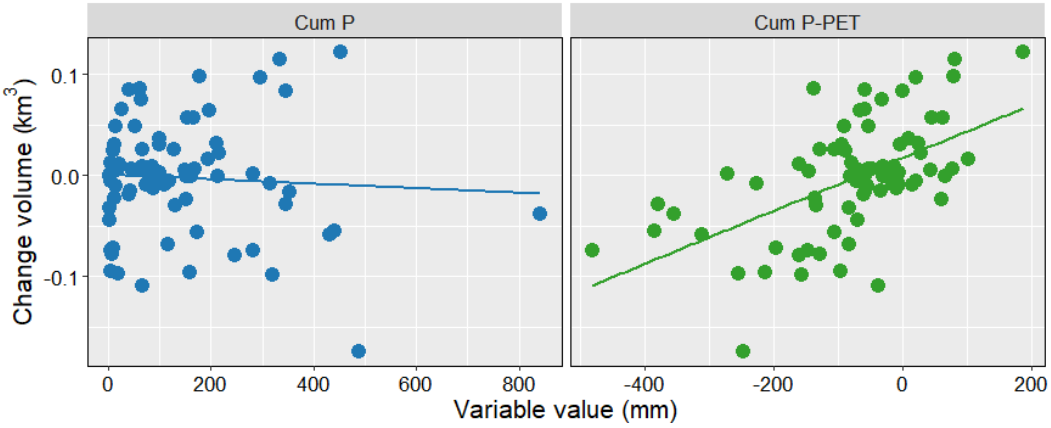

Figure 38: Change in volume of Lake Manyara plotted against cumulative P and P-PET values between the observations. Blue indicates evapotranspiration is not taken into account. Green indicates evapotranspiration is taken into account. Linear trend lines are also shown. R^2 of this line is the squared of Pearson's r in Table 10.

*Table 10: Correlations values between several variables and the change in volume of Lake Manyara. Significance: * significant at α=0.10, ** significant at α=0.05.*

		Correlation with change in volume	
Variable		Kendall	Pearson
SPI	-3	0.12	0.17
	-12	-0.01	0.06
SPEI	-3	0.21**	0.36**
	-12	0.05	0.20*
P		0.02	-0.06
P-PET		0.37**	0.56**

5. Discussion

5.1 Data limitations and method implications

Methodological choices in this study were constrained by data limitations. Reanalysis products were considered because in-situ precipitation data showed many missing values. Comparison of precipitation products with in-situ data shows their accuracy for the region of interest (Gebrechorkos et al., 2020). In this way, precipitation products which were not accurate could be excluded. The average of available stations (In-situ dataset) and the average of precipitation products (Reanalysis dataset) were used to come as close to the true value as possible. In this way the difference between the use of data types could also be studied. The In-situ and Reanalysis datasets were quite similar (R^2=0.87). The In-situ dataset showed higher values in general. This can be explained by the location of the stations at relatively high elevations within the LMC. In general the created In-situ and Reanalysis datasets produced similar results regarding answers to the research questions, showing they can both produce valuable results but with different absolute (SPI/SPEI/correlation) values. Therefore, the use of only the Reanalysis dataset for comparison with lake fluctuation is considered valid.

Data limitations also delimit the drought analysis to meteorological drought. The analysis of hydrological drought would also have been interesting to apply to Lake Manyara because this type of drought is concerned with the amount of water in water bodies. However, this research still gives useful insights (e.g. on the predictability of lake volume) as the influence of the total amount of water entering the catchment on Lake Manyara is considered. Furthermore, the influence of (potential) evapotranspiration on drought was investigated. Because of data availability, potential evapotranspiration was calculated using only monthly mean temperature. Although actual evapotranspiration could not be calculated, evapotranspiration shows to be water-limited through most of the year (P-PET<0). In this case average actual evapotranspiration is nearly equal to the average precipitation, meaning net input of precipitation is zero. When it is energy-limited (P-PET>0), actual average evapotranspiration is essentially equal to average potential evapotranspiration (Dingman, 2015). In water-limited situations it is still important to take into account negative P-PET values. Although in theory all precipitation is evaporated, the evaporation of the water of Lake Manyara continues.

The use of the average monthly precipitation over the LMC to compare with Lake Manyara fluctuations required some assumptions. The first one is equal contribution throughout the catchment to the volume of Lake Manyara. In reality, the amount of rainfall, net runoff created, stream water abstractions and the travelling time of water to the lake can differ within the catchment. Furthermore, using P-PET, precipitation is assumed to be evenly affected by PET throughout the month. However, daily gauge station data from 2006 to 2010 from TMA (2019) shows that rainfall is not always evenly distributed throughout the month. If intense rainfall events occur, the influence of PET will be relatively smaller. Monthly P-PET is in that case an underestimation.

The correlation of the available monthly/seasonal data with teleconnections as the MJO and SAM can be less accurate as these operate on weekly to monthly scales. Furthermore, these teleconnections had indices which did not cover the entire research period. This affects the overall correlations and hampered the study of changing impact on LMC rainfall of the MJO and SAM.

Lastly, data regarding the fluctuations of Lake Manyara was limited. Obtained surface area observations were mainly from after the year 2000, obstructing studying lake fluctuations throughout the entire research period. Furthermore, gaps existed between the observations and cumulatively each of the 12 months of the year had very few observations (max. 13). Therefore, it was not possible to study seasonal effects and differences regarding used variables affecting lake volume. The conversion from lake surface area to volume is also imperfect as it is based on the relation between surface area and depth, which was not fully linear though an R^2 of 0.975 was

reached (Figure 4). This can lead to a bit over- or underestimation of the volume. Additionally, the map that was used to obtain the relation between depth and surface area was manually digitized and was created using bathymetric data of 2010. Sedimentation of Lake Manyara was not taken into account. Wynants et al. (2020) show increasing sedimentation rates into the lake from ±2002, reaching peak value in 2010 after which they decrease again. The exact effect on the relation between lake surface area and volume is however not known and therefore not taken into account in this study.

The analysis of the impact of variables on fluctuations in lake volume is also not ideal. Factors as intense rainfall events or catchment characteristics and their influence on the amount of water reaching the lake are not addressed. This would require daily data and a hydrological model. Nonetheless, the aim in this study was to investigate the general influence of (meteorological) drought on the size of Lake Manyara. The used analysis achieves this goal.

5.2 Drought analysis

The first research objective of this study was to analyse meteorological drought occurrence (duration, severity and frequency) in the Lake Manyara region from 1900 up to and including 2019. Both the inclusion/exclusion of evapotranspiration and the used data (In-situ vs. Reanalysis) influence the appearance of drought. However, in general the same patterns were obtained. The SPEI, which includes potential evapotranspiration, shows more negative (dryer) values than SPI in the most recent decades. This is due to the relatively high temperatures during these decades compared to the whole research period. The increasing trend in temperature throughout the research period also causes the studied trends to be more pronounced for the SPEI relative to the SPI.

Throughout the research period the SPI and SPEI time-series for both the In-situ and Reanalysis datasets for short- and long-term droughts show a significantly decreasing trend in values. So in general a drying trend is present in the LMC over the last century. Furthermore, the results indicate drying trends for the long rainy season and long dry season. The short rainy season and short dry season do not show a clear or significant trend. The drying trend of the long rainy season is in line with other studies observing this trend among the larger Horn of Africa (Funk et al., 2008; Williams & Funk, 2011; Lyon & Dewitt, 2012; Liebmann et al., 2014; Yang et al., 2014; Rowell et al., 2015; Conway et al., 2017a). Possible causes for this trend are discussed in section 5.3. In contrast to the results of this study, which did not show a clear or significant trend for the short rainy season, Nicholson et al. (2018) and Liebmann et al. (2014) did find a weak wetting trend. They blame the weakness on interannual variability.

Throughout the decades, changes in drought characteristics occurred. Overall total drought duration, severity, intensity and frequency increased throughout the decades since the 1930s for both short- and long-term droughts (Table 6). The only exception is the 1980s, which stands out as a relatively wet decade with sharp decreases in total drought duration and total drought severity. The overall drying trend of the long rainy season and long dry season in combination with the large interannual variability of the short rainy season could be the cause of the changes and trends in drought characteristics. Due to the drying of the seasons, droughts can prolong multiple seasons (increasing in duration) and be more severe. Local people stated that it is drier and warmer nowadays and reported more frequent periods of drought now compared to 10-20 years ago (van den Bergh, 2016). The results of this study confirm these perceptions. The 1980s were relatively wet compared to the previous and following decades. Nicholson (1993) also found this decade to be anomalously wet in Eastern Africa in general compared to 1901-1991. On the contrary, the rest of Africa was anomalously dry during this decade. Potential causes for this divergent decade are the apparent change in teleconnections around 1980 (further discussed in 5.3) or a change in the zonal rainfall gradient existing between east and west zones during the short rainy season (Nicholson et al., 2018).

Differences between the results of this study and other studies can be due to variations in study design: timescales, dataset, research periods or study area (Nicholson, 2017). The importance of the latter is underlined by e.g. Gebrechorkos et al. (2020) who found trends in precipitation and temperature between 1980 and 2010 to vary largely among the Greater Horn of Africa. Furthermore, Nicholson et al. (2018) showed that decadal rainfall anomalies varied within East Africa. Trends present in the LMC could thus be local, emphasizing the importance of the catchment taken as the study area in this research. This is also evident looking at future projections.

Conway et al. (2017a, b) analysed the results of 34 climate models simulating future precipitation and temperature in Tanzania. They give contrasting results whether precipitation will increase or decrease in the future. Furthermore, the models show wide variations within Tanzania. The average of the models shows an increase in precipitation of the long rainy season for the LMC: 4-7% for 2040 and 9% for 2090 compared to 1976-2005. The observed drying trend of the long rainy season compared to the increase in rainfall projected by climate models is known as the East African climate paradox. Rowell et al. (2015) explored multiple hypotheses for this paradox and concluded two possible explanations. The first suggests that the mechanisms on which the models base the precipitation change are flawed (e.g. the representation of aerosol-climate interactions or SST-rainfall teleconnections) and therefore unreliable. The second comprises a genuine physical reason for the contrast in trends e.g. the changing balance between competing drivers as aerosol emissions and carbon dioxide. For the short rainy season, the change in rainfall within the catchment is predicted as -3 to 3% for 2040 and 0-9% for 2090. Overall annual rainfall is predicted to increase (1-3% for 2040 and 1-7% for 2090). The models do agree that the number of rainy days will decrease and the intensity of events will increase. This suggest more variable rainfall with a higher chance of droughts or floods in the future. In contrast to rainfall, the climate models do show consensus about temperature. They project warming between 0.8 and 1.8°C for 2040 and 1.6 and 5.0°C for 2090. The change is evenly distributed across Tanzania. So while future changes in precipitation are uncertain, it can be stated that temperatures will continue to rise.

5.3 Influence of atmospheric teleconnections on LMC rainfall

The second objective was to analyse the influence of atmospheric teleconnections on rainfall in the Lake Manyara catchment. For the short rainy season, the seasonal correlations are higher than the monthly correlations. Overall the IOD has the strongest influence on this season (Reanalysis r=0.53 at 1-month lead), followed by the MJO (Reanalysis r= -0.47 at 1-month lead) and the ENSO (Reanalysis r=-0.41 at 2-month lead). The SAM and NAO did not show significant correlations. Furthermore, partial correlation showed that the teleconnections do influence each other's impact on LMC rainfall during the short rainy season. The IOD is the only teleconnection that remains a significant relation with rainfall when the influence of other teleconnections is removed. This is also shown by Bahaga et al. (2019), concluding that the ENSO influence is mediated by the co-occurrence of in-phase IOD events. Though correlations are quite strong, the relations between rainfall and teleconnections changed through time. Therefore, differences between results of overall correlations of this study and others (as mentioned in the literature study) is partly due to variations in time periods used. The SAM and NAO, which did not show a significant or high correlation overall, do show higher correlation during specific periods in time.

The correlations between teleconnections and LMC rainfall of the short rainy season shows the same shifts as Nicholson (2015) found: 1961, 1982-1984 and 1997. These match with major regime shifts in the tropics (Clark et al., 2003; Ihara et al., 2008; Manatsa et al., 2012; Manatsa & Behera, 2014). Changes in the correlations can be linked to changes in the Walker circulation, human interference e.g. through stratospheric ozone level changes in 1961 and 1997, and the occurrence of extreme events (for example high rainfall events in 1961, 1982 and 1997). These events may largely increase the correlation with one teleconnection, but decrease the correlation with another (Camberlin & Philippon, 2001; Manatsa et al., 2016). For example, high rainfall in

1961 coincided with positive IOD (increasing the correlation), but a positive ENSO event was absent (decreasing the correlation). Overall changes in correlations for the short rainy season showed the same patterns as Nicholson (2015) and Manatsa et al. (2016) found, discussed in 4.1.7. Absolute values can differ due to differences in study area or indices used. Changes in relations between teleconnections and rainfall in the short rainy season correspond with changes in the strength of Walker circulation cells of the Indian, Pacific and Atlantic Ocean (Figure 17).

What stands out is the unexpected positive correlation of the NAO between 1982 and 1997. This would imply an increase of rainfall, instead of a decrease, by the enhanced (dry and cool) easterly winds. It could be due to changes in the position of the pressure areas and/or the alternating bands of zonal wind strength caused by the NAO. In this way enhanced westerlies instead of easterlies might be present over East Africa during a positive NAO and vice versa (McHugh & Rogers; 2001). Another explanation is the position of the ITCZ or low-level convergence. Through 1982-1997 the Atlantic Ocean Walker cell was relatively strong. This strengthened the (south-) westerlies over the continent which influences the position of the ITCZ, pushing it more north- and eastward. The positive NAO easterly winds in this case might have kept the ITCZ more southward and westward, extending the season and causing more rainfall (Meehl & van Loon, 1979). A third option is apparent higher correlation while the NAO did not actually have an influence. The strength of the Atlantic Walker cell creating low-level convection and other teleconnections may have caused high/low rainfall events, while the NAO coincidently had a positive/negative sign, resulting in an apparent correlation.

Concerning the long rainy season, Camberlin & Philippon (2002) and Nicholson (2017) advised using monthly correlations due to non-coherence of the long rainy seasons. The causes of rainfall anomalies during this season would be less clear when using seasonal anomalies. The season as a whole showed a significant correlation with the IOD (Reanalysis r=-0.30). The monthly correlations only showed this a significant correlation with the IOD in April (Reanalysis r=-0.27) and a significant correlation with the MJO in March (Reanalysis r=0.33). The use of monthly correlations did not show clearer links as suggested by Camberlin & Philippon (2002) and Nicholson (2017). In addition, partial correlations showed no large changes in correlation values, thus the teleconnections do not show large influence on each other's impact on LMC rainfall.

Through time the same years of shifts can be recognized as for the long rainy season plus an additional shift in 2010. However, the long rainy season shows less connection between changes in influences of teleconnections and changes in the strength of Walker circulation cells. This may be due to the difference in strength of the Walker circulation between the seasons. During the short rainy season, it is relatively strong. During the long rainy season, it is weaker or it can even be absent (Pohl & Camberlin, 2011). For instance, the weak link between rainfall and SST anomalies in 1961-1982 can be due to absence of the Walker circulation cells in the long rainy season during this period. Though some correlations are significant, it can be concluded that rainfall during the long rainy season is only relatively weakly linked to atmospheric teleconnections. This was also found by multiple studies (Camberlin & Philippon, 2002; Liebmann et al., 2014; Nicholson, 2017; Bahaga et al., 2019). The reason could be that rainfall during this season is the net result of various influences acting on different timescales. It would therefore not be constrained by teleconnections on interannual time scales. Therefore, it would not be showing a distinct relation with the teleconnections (Pohl & Camberlin, 2011; Omondi et al., 2013; Liebmann et al., 2014; Nicholson, 2017; Bahaga et al., 2019). Another reason can be the timing of teleconnection events. For instance, Nicholson & Kim (1997) state that the net impact of the ENSO on the long rainy season tends to be insignificant as the anomalies switch sign in the middle of the season. IOD events often die out in December and only start to develop in May or June. The MJO occurs at intra-seasonal timescales and could therefore have a more positive influence on rainfall

one year and negative the other year. NAO events show largest impact on winds during boreal winter (Met Office UK, 2020).

The uncertainty regarding the causes of rainfall variability of the long rainy season also makes it harder to pin down the cause of the drying trend of this season. So far studies have developed multiple hypotheses to explain the decline in rainfall. Lyon & Dewitt (2012) implicated tropical pacific warming (especially after 1999) as a cause of the decline, being part of a large-scale precipitation anomaly across the Indian and Pacific Oceans. Vigaud et al. (2017) suggested more frequent dry long rainy seasons are associated with earlier onset of the Indian Monsoon and Somali jet, reducing rainfall in May. Many papers provide evidence for the decline to be associated with a shift towards warming of the western tropical Pacific and cooling of the central and eastern tropical Pacific and multidecadal variability of the Pacific Ocean SSTs (Lyon & DeWitt, 2012; Lyon, 2014; Lyon et al., 2014; Yang et al., 2014; Vigaud et al., 2017). Anomalously warm SSTs over the western tropical Pacific and cooler SSTs in the central and eastern Pacific coincided with relatively dry long rainy seasons (Vigaud et al., 2017). These SST anomalies can induce a westward shift of the Walker circulation and increase subsidence over East Africa, reducing rainfall. Intensification of these anomalies through time could cause dryer conditions. So although teleconnections show little influence, the Walker circulation could still play a role in the variability of rainfall (Williams & Funk, 2011; Funk et al., 2014, Liebmann et al., 2014; Vigaud et al., 2017). Apart from natural variability, human-induced changes and anthropogenic aerosol emissions may have enhanced the trend (Rowell et al., 2015).

Regarding the wet 1980s decade, Nicholson et al. (2018) blamed changing teleconnection relations. Rainfall in the long dry season however did not show large influence of teleconnections. Though the ENSO influence is relatively strong and the IOD influence decreases for the short dry season during this decade, a logical explanation for the wet decade is the strong Atlantic Ocean Walker cell itself. This increases westerlies over the continent and enhances convergence over East Africa, decreasing the influence of subsidence over East Africa. What could furthermore have contributed is multidecadal variability of SSTs in the Pacific Ocean. Bahaga et al. (2019) show that the long rainy seasons in the Greater Horn of Africa in general were relatively dry during cold phases (1947-1976 and 1999-2019), while during warm phases they were wet (1924-1945 and 1977-1998). Though these periods do not apply fully to the LMC long rainy season (Appendix C), it could have been of influence to some extent during the 1980s.

5.4 Drought occurrence and Lake Manyara fluctuations

The aim of this study was to investigate the impact of drought on the size fluctuations of Lake Manyara. Using drought (represented by SPI and SPEI), P or P-PET as predictors of the overall Lake Manyara water volume did not show high correlations. Seasonal differences or initial state were not taken into account here. Correlations with the volume of Lake Manyara just in January showed more promising results. Short-term droughts and January P and P-PET show strong links with the size of the lake in January. This implies short-term/fast response of the lake to meteorological circumstances. However, these relations are based on only 13 observations. Seasonal differences could not be fully explored in this study due to lack of data regarding the size of Lake Manyara.

Initial state was taking into account when looking at the change in lake volume and the cumulative of variables between observations. P-PET shows a strong positive link with changing lake size. The importance of evaporation appears as P showed no relation. Overall growth or shrinkage of Lake Manyara does thus (for a substantial part) depend on both precipitation and evaporation. This makes sense because evaporation is the (only) output of the lake. That negative cumulative

P-PET can still result in growth of the lake can be due to local high-intensity rainfall events. The pronounced influence of climatological parameters on Lake Manyara fluctuations was also found by Deus & Gloaguen (2013). They investigated the impact of climate variability on interannual lake fluctuations of the long dry season. They showed that human activities are not the cause of lake shrinkage as this would result in shrinking of the lake at the same rate yearly without following trends of meteorological parameters.

From the drought indicators SPEI-3 showed the highest correlation (r=0.36) with change in lake volume, though it was much weaker than with monthly P-PET (r=0.56). This does not mean droughts are not important. After all, droughts define the negative deviation of the variables compared to normal. The differences in correlation values can be due to the computation of the drought indicator. This computation takes into account multiple months of P-PET, giving a different image than the monthly P-PET values when relating linearly. Furthermore, a drought in one season might be worse than another according to the indicators. This does not mean that P or P-PET is also lower in the former, as drought is taken relative to normal. This causes relative differences between cumulative SPI/SPEI and P/P-PET. The strong influence of P-PET on changing lake volume does however imply the impact of drought occurrence as this decreases the value of P and P-PET. Low P-PET by drought can cause shrinkage of Lake Manyara.

5.5 Recommendations

This study showed that the overall the size of Lake Manyara shows substantial influence of both precipitation and evapotranspiration. Evapotranspiration is expected to increase in the future due to increasing temperatures. This implies (long-term) shrinkage of the lake. Future change in P is uncertain due to the East African paradox. Though the long rainy season showed a decreasing trend during the last century, causes of fluctuations and the cause of the decrease is not fully clear. Better understanding of these causes could improve simulations by climate models, making them more accurate and precise. Suggestions are studying more local influences or looking at the state of the atmosphere in general instead of separate teleconnections (indices). Better understanding and improvement of the models simulating future precipitation of this season is also important as it is the most reliable season for agriculture, concerning the food production in the region (Camberlin et al., 2009). More reliable predictions are also important to estimate the magnitude of effort required to improve future water resource management.

Additionally, the share of influence of (changes in) meteorological variables and other factors as sedimentation, catchment characteristics or the subsurface on the size of Lake Manyara can be explored/modelled. In this way, the impact of (future) changes in one or more factors can be considered and the effect evaluated.

Lastly, it is recommended to take into account non-stationarity of the relations between atmospheric teleconnections and rainfall in further research. It should also be considered when comparing studies, as variations in time periods used can result in apparent differences in relations.

6. Conclusion

The aim of this study was to determine the impact of drought on the dynamics of Lake Manyara. The occurrence of drought over the past century in the Lake Manyara catchment (LMC), the influence of atmospheric teleconnections on LMC rainfall and the impact of drought on Lake Manyara were explored. Both the inclusion/exclusion of evapotranspiration and the used data (In-situ vs. Reanalysis) influenced the appearance of drought. In general, a drying trend was found in the LMC over the last century. Decadal drought characteristics (duration, severity, frequency) show a general increase from the 1930s to present, with the exception of the wet 1980s. The inclusion of evapotranspiration results in more pronounced drying trends due to the significant increasing trend of mean temperature in the past century.

The short rainy season does not show a clear drying or wetting trend. Precipitation of this season was found to be related to atmospheric teleconnections. Regarding the whole research period, the IOD has the strongest influence on short rainy season rainfall. Though correlations are quite strong, the relations between rainfall and teleconnections changed through time. This should be considered when comparing results of studies, as variations in time periods used can result in apparent differences in relations. Changes in the relations correspond with changes in the strength of Walker circulation cells of the Indian, Pacific and Atlantic Ocean. The long rainy season shows a drying trend. Rainfall during this season was found weakly linked to atmospheric teleconnections. Other papers relate the drying trend of the long rainy season to changes in strength and/or location of atmospheric branches of the Walker circulation and human-induced changes.

Using drought (represented by SPI and SPEI), P or P-PET as predictors of the overall Lake Manyara water volume did not show high correlations. Taking into account seasonal differences by looking only at January volume showed more promising results. Short-term droughts and January P and P-PET show strong links with the size of the lake in January. This implies short-term/fast response of the lake to meteorological circumstances. However, these relations are based on only 13 observations. Seasonal differences could not be fully explored in this study due to lack of data. Taking into account initial state showed much higher correlation than using predictors by themselves for lake volume throughout the year. Combined precipitation and evapotranspiration showed the largest impact on changes in the volume of Lake Manyara ($r=0.56$). Though the drought indicators did not show strong relations, the strong influence of P-PET on changing lake volume does imply the impact of drought occurrence. This would decrease the value of P and P-PET, which can cause shrinkage of Lake Manyara.

Global warming with increasing temperatures in East-Africa implies (long-term) shrinkage of the lake, due to enhanced evapotranspiration. However, future change in P is uncertain due to the East African paradox. Both were found to influence the overall the size of Lake Manyara substantially. Therefore, improvement of the models simulating future precipitation are important to estimate the magnitude of effort required to improve future water resource management in the Lake Manyara catchment.

References

Adler, R., Wang, J., Sapiano, M., Huffman, G., Chiu, L., Xie, P. P., Ferraro, R., Schneider, U., Becker, A., Bolvin, D., Nelkin, E., Gu, G. & NOAA CDR Program (2016). Global Precipitation Climatology Project (GPCP) Climate Data Record (CDR), Version 2.3 (Monthly). National Centers for Environmental Information [online]. Retrieved from doi:10.7289/V56971M6 [visited: 20-12-2019].

Arblaster, J. M., & Meehl, G. A. (2006). Contributions of external forcings to southern annular mode trends. *Journal of climate*, *19*(12), 2896-2905.

Arndt, C., Farmer, W., Strzepek, K., & Thurlow, J. (2012). Climate change, agriculture and food security in Tanzania. *The World Bank.*

Ashok, K., Guan, Z., & Yamagata, T. (2003). A look at the relationship between the ENSO and the Indian Ocean dipole. *Journal of the Meteorological Society of Japan. Ser. II*, *81*(1), 41-56.

Ashok, K., Guan, Z., Saji, N. H., & Yamagata, T. (2004). Individual and combined influences of ENSO and the Indian Ocean dipole on the Indian summer monsoon. *Journal of Climate*, *17*(16), 3141-3155.

AWF (African Wildlife Foundation) (2003). Lake Manyara Watershed Assessment. Progress Report, African Wildlife Foundation.

Bachofer, F., Quénéhervé, G. & Märker, M. (2014). The delineation of paleo-shorelines in the Lake Manyara basin using TerraSAR-X data. *Remote Sensing, 6*(3), 2195–2212.

Bahaga, T. K., Fink, A. H., & Knippertz, P. (2019). Revisiting interannual to decadal teleconnections influencing seasonal rainfall in the Greater Horn of Africa during the 20th century. *International Journal of Climatology*, *39*(5), 2765-2785.

Bayona, J.D.R. (2006). Oreochromis amphimelas. The IUCN Red List of Threatened Species 2006:e.T60629A12388607 [online]. Retrieved from http://dx.doi.org/10.2305/IUCN.UK.2006.RLTS.T60629A12388607.en. [visited: 20-11-2019].

Behera, S. K., Luo, J. J., Masson, S., Delecluse, P., Gualdi, S., Navarra, A., & Yamagata, T. (2005). Paramount impact of the Indian Ocean dipole on the East African short rains: A CGCM study. *Journal of Climate*, *18*(21), 4514-4530.

Behera, S. K., Luo, J. J., Masson, S., Rao, S. A., Sakuma, H., & Yamagata, T. (2006). A CGCM study on the interaction between IOD and ENSO. *Journal of Climate*, *19*(9), 1688-1705.

Behera, S., Brandt, P., & Reverdin, G. (2013). The tropical ocean circulation and dynamics. *International Geophysics,103*, 385-412.

Berhane, F., & Zaitchik, B. (2014). Modulation of daily precipitation over East Africa by the Madden–Julian oscillation. *Journal of climate*, *27*(15), 6016-6034.

BirdLife International (2019) Important Bird Areas factsheet: Lake Manyara [online]. Retrieved from http://www.birdlife.org [visited: 20-11-2019].

Birkett, C., Murtugudde, R., & Allan, T. (1999). Indian Ocean climate event brings floods to East Africa's lakes and the Sudd Marsh. *Geophysical Research Letters*, *26*(8), 1031-1034.

Black, E. (2005). The relationship between Indian Ocean sea–surface temperature and East African rainfall. *Philosophical Transactions of the Royal Society A: Mathematical, Physical and Engineering Sciences*, *363*(1826), 43-47.

Bowden, J. H., & Semazzi, F. H. (2007). Empirical analysis of intraseasonal climate variability over the Greater Horn of Africa. *Journal of Climate*, *20*(23), 5715-5731.

Busker, T., de Roo, A., Gelati, E., Schwatke, C., Adamovic, M., Bisselink, B., Pekel, J. F. & Cottam, A. (2019). A global lake and reservoir volume analysis using a surface water dataset and satellite altimetry. *Hydrology and Earth System Sciences*, *23*(2), 669-690.

Camberlin, P., & Philippon, N. (2001). The stationarity of lead-lag teleconnections with East Africa rainfall and its incidence on seasonal predictability. In *Detecting and modelling regional climate change* (pp. 291-307). Springer, Berlin, Heidelberg.

Camberlin, P., & Philippon, N. (2002). The East African March–May rainy season: Associated atmospheric dynamics and predictability over the 1968–97 period. *Journal of Climate*, *15*(9), 1002-1019.

Camberlin, P., & Wairoto, J. G. (1997). Intraseasonal wind anomalies related to wet and dry spells during the "long" and "short" rainy seasons in Kenya. *Theoretical and applied climatology*, *58*(1-2), 57-69.

Camberlin, P., Moron, V., Okoola, R., Philippon, N., & Gitau, W. (2009). Components of rainy seasons' variability in Equatorial East Africa: onset, cessation, rainfall frequency and intensity. *Theoretical and applied climatology*, *98*(3-4), 237-249.

Casanova, J. & Hillaire-Marcel, C. (1992). Chronology and Paleo-hydrology of late Quaternary High Lake levels in the Manyara basin (Tanzania) from isotopic data on fossil stromatolites. *Quaternary research, 38,* 205-226.

Choiński, A., & Ptak, M. (2009). Lake Infill as the Main Factor Leading to Lake's Disappearance. *Polish Journal of Environmental Studies*, *18*(3).

Clark, C. O., Webster, P. J., & Cole, J. E. (2003). Interdecadal variability of the relationship between the Indian Ocean zonal mode and East African coastal rainfall anomalies. *Journal of Climate*, *16*(3), 548-554.

Commonwealth of Australia (2013). Indian Ocean influences on Australian climate [online]. Retrieved from http://www.bom.gov.au/climate/iod/#tabs=Indian-Ocean-climate-drivers [visited: 30-10-2019].

Commonwealth of Australia (2019). Southern Annular Mode and the Australian climate [online]. Retrieved from http://www.bom.gov.au/climate/sam/#tabs=What-is-SAM%3F [visited:18-03-2020].

Conway, D., Mittal, N., & Vincent, K. (2017a). Country climate brief. Future climate projections for Tanzania: Cape Town: Future Climate for Africa [online]. Retrieved from https://media.africaportal.org/documents/fcfa_tanzania_climatebrief_web.pdf [visited: 10-06-2020].

Conway, D., Mittal, N., & Vincent, K. (2017b). Future climate projections for Tanzania (2017b). Annex: Future climate projections for Tanzania. Cape Town: Future Climate for Africa [online]. Retrieved from http://www.lse.ac.uk/GranthamInstitute/wp-content/uploads/2017/11/FCFA_Tanzania_Annex_Web.pdf [visited: 10-06-2020].

CRU (Climatic Research Unit) (2000). North Atlantic Oscillation [online]. Retrieved from http://www.cru.uea.ac.uk/documents/421974/1295957/Info+sheet+%2311.pdf/bc0835c5-da31-4b70-be72-1a7035e59be1 [visited: 21-05-2020].

Dee, D. P., Uppala, S. M., Simmons, A. J., Berrisford, P., Poli, P., Kobayashi, S., Andrae, U., Balmaseda, M. A., Balsamo, G., Bauer, P., Bechtold, P., Beljaars, A. C. M., van de Berg, L., Bidlot, J., Bormann, N., Delsol, C., Dragani, R., Fuentes, M., Geer, A. J., Haimberger, L., Healy, S. B., Hersbach, H., Hólm, E. V., Isaksen, L., Kållber, P., Köhler, M., Matricardi, M., McnNally, A. P., Monge-Sanz, B. M., Morcrette, J. J., Park, B. K., Peubey, C., de Rosnay, P., Tavolato, J. N., Thépaut, J. N. & Vitart, F. (2011). The ERA-Interim reanalysis: Configuration and performance of the data assimilation system. *Quarterly Journal of the royal meteorological society, 137*(656), 553-597.

DeMott, C. A., Klingaman, N. P., & Woolnough, S. J. (2015). Atmosphere-ocean coupled processes in the Madden-Julian oscillation. *Reviews of Geophysics*, *53*(4), 1099-1154.

Deus, D., & Gloaguen, R. (2013). Remote sensing analysis of lake dynamics in semi-arid regions: implication for water resource management. Lake Manyara, East African Rift, Northern Tanzania. *Water*, *5*(2), 698-727.

Deus, D., Gloaguen, R., & Krause, P. (2013). Water balance modelling in a semi-arid environment with limited in situ data using remote sensing in Lake Manyara, East African Rift, Tanzania. *Remote Sensing*, *5*(4), 1651-1680.

Dezfuli, A. K., & Nicholson, S. E. (2013). The relationship of rainfall variability in western equatorial Africa to the tropical oceans and atmospheric circulation. Part II: The boreal autumn. *Journal of climate*, *26*(1), 66-84.

Dhonneur, G. (1974). Nouvelle Approche des Réalités Météorologiques de l'Afrique Occidentale et Centrale. Vol. I. Agence pour la Sécurité de la Navigation Aérienne en Afrique et à Madagascar, Dakar, Senegal, 358 pp.

Dingman, S. L. (2015). *Physical hydrology.* Waveland press.

EDO (Copernicus European Drought Observatory) (2019). EDO indicator factsheet: Standardized Precipitation Index (SPI) [online]. Retrieved from https://edo.jrc.ec.europa.eu/documents/factsheets/factsheet_spi.pdf [visited: 20-12-2019].

Feldstein, S. B., & Franzke, C. L. (2017). Atmospheric teleconnection patterns. *Nonlinear and stochastic climate dynamics*, 54-104.

Funk, C., Dettinger, M. D., Michaelsen, J. C., Verdin, J. P., Brown, M. E., Barlow, M., & Hoell, A. (2008). Warming of the Indian Ocean threatens eastern and southern African food security but could be mitigated by agricultural development. *Proceedings of the national academy of sciences*, *105*(32), 11081-11086.

Funk, C., Hoell, A., Shukla, S., Blade, I., Liebmann, B., Roberts, J. B., Roberson, F. R. & Husak, G. (2014). Predicting East African spring droughts using Pacific and Indian Ocean sea surface temperature indices. *Hydrology and Earth System Sciences, 18(*12), 4965–4978.

Funk, C., Peterson, P., Landsfeld, M., Pedreros, D., Verdin, J., Shukla, S., Husak, G., Rowland, J., Harrison, L., Hoell, A. & Michaelsen, J. (2015). The climate hazards infrared precipitation with stations—a new environmental record for monitoring extremes. *Scientific data*, *2*(1), 1-21.

Gebrechorkos, S. H., Hülsmann, S., & Bernhofer, C. (2020). Analysis of climate variability and droughts in East Africa using high-resolution climate data products. *Global and Planetary Change*, *186*, 103130.

Gershunov, A., Schneider, N., & Barnett, T. (2001). Low-frequency modulation of the ENSO–Indian monsoon rainfall relationship: Signal or noise?. *Journal of Climate*, *14*(11), 2486-2492.

Gillett, N. P., Kell, T. D., & Jones, P. D. (2006). Regional climate impacts of the Southern Annular Mode. *Geophysical Research Letters*, *33*(23).

Goerner, A., Jolie, E., & Gloaguen, R. (2009). Non-climatic growth of the saline Lake Beseka, Main Ethiopian Rift. *Journal of arid Environments*, *73*(3), 287-295.

Gottschalck, J. (2014). What is the MJO, and why do we care? NOAA [online]. Retrieved from https://www.climate.gov/news-features/blogs/enso/what-mjo-and-why-do-we-care [visited: 30-10-2019].

Government of Western Australia. Department of Primary Industries and Regional Development: Agriculture and Food (2019). Climate drivers of the South West Land Division [online]. Retrieved from https://www.agric.wa.gov.au/climate-weather/climate-drivers-south-west-land-division [visited: 18-3-2020].

Harris, I., Jones, P.D., Osborn, T.J. & Lister, D.H. (2014). Updated high-resolution grids of monthly climatic observations – the CRU TS3.10 Dataset. *International Journal of Climatology, 34*(3), 623–642.

Hastenrath, S. (2000). Zonal circulations over the equatorial Indian Ocean. *Journal of Climate*, *13*(15), 2746-2756.

Heijenk, R. (2013). Prediction of seasonal rainfall in the West Usambara Mountains, Tanzania (Bachelor's Thesis). *Utrecht University.*

Henderson, J. P. (1949). Some Aspects of Climate in Uganda. East African Meteorological Department Memoirs, Vol. II, No. 5, East African Meteorological Department, 17 pp.

Hersbach, H., Bell, B., Berrisford, P., Horányi, A., Sabater, J. M., Nicolas, J., Radu, R., Schepers, D., Simmons, A., Soci, C. & Dee, D. (2019). Global reanalysis: goodbye ERA-Interim, hello ERA5. *ECMWF Newsletter*, *159*, 17-24.

Hoell, A., Funk, C., & Barlow, M. (2014). La Niña diversity and northwest Indian Ocean rim teleconnections. *Climate dynamics*, *43*(9-10), 2707-2724.

Ihara, C., Kushnir, Y., & Cane, M. A. (2008). Warming trend of the Indian Ocean SST and Indian Ocean dipole from 1880 to 2004. *Journal of Climate*, *21*(10), 2035-2046.

Ihucha, A. (2012). Tanzania national parks, wildlife under threat from global climate change. *The East African, 6 October 2012,* 16.

Indeje, M., Semazzi, F. H., & Ogallo, L. J. (2000). ENSO signals in East African rainfall seasons. *International Journal of Climatology: A Journal of the Royal Meteorological Society*, *20*(1), 19-46.

JAMSTEC (Japan Agency for Marine-earth Science and Technology) (2012). Indian Ocean Dipole [online]. Retrieved from http://www.jamstec.go.jp/aplinfo/sintexf/e/iod/about_iod.html [visited: 30-10-2019].

Jones, J. M., & Widmann, M. (2004). Early peak in Antarctic Oscillation index. *Nature*, *432*(7015), 290-291.

Jones, P. D., Jónsson, T., & Wheeler, D. (1997). Extension to the North Atlantic Oscillation using early instrumental pressure observations from Gibraltar and south-west Iceland. *International Journal of Climatology: A Journal of the Royal Meteorological Society*, *17*(13), 1433-1450.

Kajtar, J. B., Santoso, A., England, M. H., & Cai, W. (2017). Tropical climate variability: interactions across the Pacific, Indian, and Atlantic Oceans. *Climate Dynamics*, *48*(7-8), 2173-2190.

Karadimitriou, S.M. (2020). Correlation in R. Statstutor Community Project, University of Sheffield [online]. Retrieved from https://www.sheffield.ac.uk/polopoly_fs/1.536458!/file/MASH_Correlation_R.pdf [visited: 19-05-2020].

Karl, T. R., Melillo, J. M., Peterson, T. C., & Hassol, S. J. (Eds.). (2009). *Global climate change impacts in the United States*. Cambridge University Press.

Kendall, M. G. (1975). *Rank correlation methods. 2nd impression.* Charles Griffin and Company Ltd. London and High Wycombe.

Kijazi, A. L., & Reason, C. J. C. (2005). Relationships between intraseasonal rainfall variability of coastal Tanzania and ENSO. *Theoretical and applied climatology*, *82*(3-4), 153-176.

Kijazi, A. L., & Reason, C. J. C. (2009). Analysis of the 1998 to 2005 drought over the northeastern highlands of Tanzania. *Climate Research*, *38*(3), 209-223.

Lau, K. M., & Yang, S. (2003). Walker circulation. *Encyclopedia of atmospheric sciences*, 2505-2510.

Liebmann, B., Hoerling, M. P., Funk, C., Bladé, I., Dole, R. M., Allured, D., Quan, X., Pegion, P., & Eischeid, J. K. (2014). Understanding recent eastern Horn of Africa rainfall variability and change. *Journal of Climate*, *27*(23), 8630-8645.

Lin, H., Brunet, G., & Derome, J. (2009). An observed connection between the North Atlantic Oscillation and the Madden–Julian oscillation. *Journal of Climate*, *22*(2), 364-380.

Liu, Z., & Alexander, M. (2007). Atmospheric bridge, oceanic tunnel, and global climatic teleconnections. *Reviews of Geophysics*, *45*(2).

Lobell, D. B., Burke, M. B., Tebaldi, C., Mastrandrea, M. D., Falcon, W. P., & Naylor, R. L. (2008). Prioritizing climate change adaptation needs for food security in 2030. *Science*, *319*(5863), 607-610.

Lyon, B. (2014). Seasonal drought in the Greater Horn of Africa and its recent increase during the March–May long rains. *Journal of Climate*, *27*(21), 7953-7975.

Lyon, B., & DeWitt, D. G. (2012). A recent and abrupt decline in the East African long rains. *Geophysical Research Letters*, *39*(2).

Lyon, B., Barnston, A. G., & DeWitt, D. G. (2014). Tropical pacific forcing of a 1998–1999 climate shift: observational analysis and climate model results for the boreal spring season. *Climate dynamics*, *43*(3-4), 893-909.

Madden, R. A. (2014). Intraseasonal Oscillation (Madden-Julian Oscillation). *Encyclopedia of Atmospheric Sciences (Second Edition)*, 132-136.

Madden, R. A., & Julian, P. R. (1972). Description of global-scale circulation cells in the tropics with a 40–50 day period. *Journal of the atmospheric sciences*, *29*(6), 1109-1123.

Maerker, M., Quénéhervé, G., Bachofer, F., & Mori, S. (2015). A simple DEM assessment procedure for gully system analysis in the Lake Manyara area, northern Tanzania. *Natural Hazards*, *79*(1), 235-253.

Mafuru, K. B., & Guirong, T. (2018). Assessing prone areas to heavy rainfall and the impaction of the upper warm temperature anomaly during March–May rainfall season in Tanzania. *Advances in Meteorology*, *2018*.

Maggioni, V., & Massari, C. (Eds.). (2019). *Extreme Hydroclimatic Events and Multivariate Hazards in a Changing Environment: A Remote Sensing Approach*. Elsevier.

Manatsa, D., & Behera, S. K. (2014). On the major shifts in the IOD during the last century, the role of the Mascarene High displacements. *International journal of climatology*, *34*(6), 2033-2046.

Manatsa, D., Chingombe, W., & Matarira, C. H. (2008). The impact of the positive Indian Ocean dipole on Zimbabwe droughts. *International Journal of Climatology: A Journal of the Royal Meteorological Society*, *28*(15), 2011-2029.

Manatsa, D., Chipindu, B., & Behera, S. K. (2012). Shifts in IOD and their impacts on association with East Africa rainfall. *Theoretical and applied climatology*, *110*(1-2), 115-128.

Manatsa, D., Matarira, C. H., & Mukwada, G. (2011). Relative impacts of ENSO and Indian Ocean dipole/zonal mode on east SADC rainfall. *International Journal of Climatology*, *31*(4), 558-577.

Manatsa, D., Morioka, Y., Behera, S. K., Matarira, C. H., & Yamagata, T. (2014). Impact of Mascarene High variability on the East African 'short rains'. *Climate dynamics*, *42*(5-6), 1259-1274.

Manatsa, D., Mudavanhu, C., Mushore, T. D., & Mavhura, E. (2016). Linking major shifts in East Africa 'short rains' to the Southern Annular Mode. *International Journal of Climatology*, *36*(4), 1590-1599.

Mann, H. B. (1945). Nonparametric tests against trend. *Econometrica: Journal of the econometric society*, 245-259.

Marshall, G. J. (2003). Trends in the Southern Annular Mode from observations and reanalyses. *Journal of Climate*, *16*(24), 4134-4143.

Massoy, T. (2016). Policy context and scaling up CSA in Tanzania African Climate Smart Agriculture Alliance (ACSAA), *Tanzania Climate Smart Agriculture Workshop, 26th and 27th January, 2016, Colosseum Hotel, Oyster Bay, Dar-es Salaam.*

McHugh, M. J., & Rogers, J. C. (2001). North Atlantic oscillation influence on precipitation variability around the southeast African convergence zone. *Journal of Climate*, *14*(17), 3631-3642.

McKee, T. B., Doesken, N. J., & Kleist, J. (1993). The relationship of drought frequency and duration to time scales. *Proceedings of the 8th Conference on Applied Climatology*, 17(22), 179-183. Boston, MA: American Meteorological Society.

MDC (Monduli District Council) (2014). Monduli District Council (fact sheet). Retrieved via van den Bergh (2016). *Monduli District Council, Monduli, Tanzania*.

Meehl, G. A., & Van Loon, H. (1979). The seesaw in winter temperatures between Greenland and Northern Europe. Part III: Teleconnections with lower latitudes. *Monthly Weather Review*, *107*(9), 1095-1106.

Mercier, F., Cazenave, A., & Maheu, C. (2002). Interannual lake level fluctuations (1993–1999) in Africa from Topex/Poseidon: connections with ocean–atmosphere interactions over the Indian Ocean. *Global and Planetary Change*, *32*(2-3), 141-163.

Met Office UK, 2020. Climate modes [online]. Retrieved from https://www.metoffice.gov.uk/hadobs/monitoring/modes.html [visited: 19-03-2020].

Mishra, A. K., & Singh, V. P. (2010). A review of drought concepts. *Journal of hydrology*, *391*(1-2), 202-216.

Mölders, N., & Kramm, G. (2014). *Lectures in meteorology* (pp. 1-591). Cham/Heidelberg/New York/Dordrecht/London: Springer.

Msoffe, F. U., Kifugo, S. C., Said, M. Y., Neselle, M. O., Van Gardingen, P., Reid, R. S., Ogutu, J. O., Herero, M. & De Leeuw, J. (2011). Drivers and impacts of land-use change in the Maasai Steppe of northern Tanzania: an ecological, social and political analysis. *Journal of Land Use Science*, *6*(4), 261-281.

Munishi, L., Mtei, K., Bode, S., Dume, B., Navas, A., Nebiyu, A., Semmens, B., Smith, H., Stock, B., Boeckx, P. & Blake, W. (2017). Tackling soil degradation and environmental changes in Lake Manyara Basin, Tanzania to support sustainable landscape/ecosystem management. *EGU General Assembly Conference Abstracts*, *19*, 16640.

Mutai, C. C., & Ward, M. N. (2000). East African rainfall and the tropical circulation/convection on intraseasonal to interannual timescales. *Journal of Climate*, *13*(22), 3915-3939.

Mutai, C., Polzin, D., & Hastenrath, S. (2012). Diagnosing Kenya rainfall in boreal autumn: further exploration. *Journal of climate*, *25*(12), 4323-4329.

Mwalyosi, R. B. (1992). Land-use changes and resource degradation in south–west Masailand, Tanzania. *Environmental Conservation*, *19*(2), 145-152.

Nakamura, N., Kayanne, H., Iijima, H., McClanahan, T. R., Behera, S. K., & Yamagata, T. (2011). Footprints of IOD and ENSO in the Kenyan coral record. *Geophysical Research Letters*, *38*(24).

Ngana, J. O., Mwalyosi, R. B. B., Yanda, P., & Madulu, N. F. (2004). Strategic development plan for integrated water resources management in Lake Manyara sub-basin, North-Eastern Tanzania. *Physics and Chemistry of the Earth, Parts A/B/C*, *29*(15-18), 1219-1224.

Nicholson, S. E. (1993). An overview of African rainfall fluctuations of the last decade. *Journal of climate*, *6*(7), 1463-1466.

Nicholson, S. E. (2015). Long-term variability of the East African 'short rains' and its links to large-scale factors. *International Journal of Climatology*, *35*(13), 3979-3990.

Nicholson, S. E. (2017). Climate and climatic variability of rainfall over eastern Africa. *Reviews of Geophysics*, *55*(3), 590-635.

Nicholson, S. E. (2018). The ITCZ and the seasonal cycle over equatorial Africa. *Bulletin of the American Meteorological Society*, *99*(2), 337-348.

Nicholson, S. E., & Kim, J. (1997). The relationship of the El Niño–Southern oscillation to African rainfall. *International Journal of Climatology: A Journal of the Royal Meteorological Society*, *17*(2), 117-135.

Nicholson, S. E., & Selato, J. C. (2000). The influence of La Nina on African rainfall. *International Journal of Climatology: A Journal of the Royal Meteorological Society*, *20*(14), 1761-1776.

Nicholson, S. E., Funk, C., & Fink, A. H. (2018). Rainfall over the African continent from the 19th through the 21st century. *Global and planetary change*, *165*, 114-127.

Nicholson, S. E., Leposo, D., & Grist, J. (2001). The relationship between El Niño and drought over Botswana. *Journal of Climate*, *14*(3), 323-335.

Nkurunziza, I. F., Guirong, T., Ngarukiyimana, J. P., & Sindikubwabo, C. (2019). Influence of the Mascarene High on October-December Rainfall and their Associated Atmospheric Circulation Anomalies over Rwanda. *Journal of Environmental & Agricultural Sciences, 20,* 1-20.

NOAA (National Oceanic and Atmospheric Administration). (2014). The Walker Circulation: ENSO's atmospheric buddy [online]. Retrieved from https://www.climate.gov/news-features/blogs/enso/walker-circulation-ensos-atmospheric-buddy [visited: 30-10-2019].

NOAA (2019). Archive of MJO indices (1978-present) [online]. Retrieved from https://www.cpc.ncep.noaa.gov/products/precip/CWlink/daily_mjo_index/mjo_index.shtml [visited: 19-12-2019].

NOAA (2020). Climate Monitoring: Teleconnections [online]. Retrieved from: https://www.ncdc.noaa.gov/teleconnections/ [visited: 9-01-2020].

Nonga, H. E., Mdegela, R. H., Lie, E., Sandvik, M., & Skaare, J. U. (2010). Socio-economic values of wetland resources around lake Manyara, Tanzania: assessment of environmental threats and local community awareness on environmental degradation and their effects. *Journal of wetlands ecology*, *4*, 83-101.

Nonga, H. E., Mdegela, R. H., Lie, E., Sandvik, M., & Skaare, J. J. (2011). Assessment of farming practices and uses of agrochemicals in Lake Manyara basin, Tanzania. *African Journal of Agricultural Research 2011, Vol. 6(10):* 2216-2230*.*

Ogwang, B. A., Ongoma, V., Xing, L., & Ogou, K. F. (2015). Influence of Mascarene high and Indian Ocean dipole on East African extreme weather events. *Geographica Pannonica*, *19*(2), 64-72.

Omondi, P., Awange, J. L., Ogallo, L. A., Okoola, R. A., & Forootan, E. (2012). Decadal rainfall variability modes in observed rainfall records over East Africa and their relations to historical sea surface temperature changes. *Journal of Hydrology*, *464*, 140-156.

Omondi, P., Ogallo, L. A., Anyah, R., Muthama, J. M., & Ininda, J. (2013). Linkages between global sea surface temperatures and decadal rainfall variability over Eastern Africa region. *International Journal of Climatology*, *33*(8), 2082-2104.

Onyutha, C., & Willems, P. (2015). Spatial and temporal variability of rainfall in the Nile Basin. *Hydrology and Earth System Sciences*, *19*(5), 2227.

Pekel, J. F., Cottam, A., Gorelick, N., & Belward, A. S. (2016). High-resolution mapping of global surface water and its long-term changes. *Nature*, *540*(7633), 418.

Pohl, B., & Camberlin, P. (2006). Influence of the Madden–Julian oscillation on East African rainfall: II. March–May season extremes and interannual variability. *Quarterly Journal of the Royal Meteorological Society: A journal of the atmospheric sciences, applied meteorology and physical oceanography*, *132*(621), 2541-2558.

Pohl, B., & Camberlin, P. (2011). Intraseasonal and interannual zonal circulations over the equatorial Indian Ocean. *Theoretical and applied climatology*, *104*(1-2), 175-191.

Pohl, B., Camberlin, P., & Roucou, P. (2005). Typology of pentad circulation anomalies over the Eastern Africa–Western Indian Ocean region, and their relationship with rainfall. *Climate Research*, *29*(2), 111-127.

Pohl, B., Fauchereau, N., Reason, C. J. C., & Rouault, M. (2010). Relationships between the Antarctic Oscillation, the Madden–Julian Oscillation, and ENSO, and consequences for rainfall analysis. *Journal of Climate*, *23*(2), 238-254.

Prins, H. H. T. (1987). Nature conservation as an integral part of optimal land use in East Africa: the case of the Masai Ecosystem of northern Tanzania. *Biological Conservation, 40*(2), 141-161.

Quénéhervé, G., Bachofer, F., & Maerker, M. (2015). Experimental assessment of runoff generation processes on hillslope scale in a semiarid region in northern Tanzania. *Geografia Fisica e Dinamica Quaternaria, 38*(1), 55-66.

Rao, S. A., Masson, S., Luo, J. J., Behera, S. K., & Yamagata, T. (2007). Termination of Indian Ocean dipole events in a coupled general circulation model. *Journal of climate*, *20*(13), 3018-3035.

Rayner, N. A. A., Parker, D. E., Horton, E. B., Folland, C. K., Alexander, L. V., Rowell, D. P., Kent, E. C. & Kaplan, A. (2003). Global analyses of sea surface temperature, sea ice, and night marine air temperature since the late nineteenth century. *Journal of Geophysical Research: Atmospheres*, *108*(D14).

Rogers, J. C. (1997). North Atlantic storm track variability and its association to the North Atlantic Oscillation and climate variability of northern Europe. *Journal of Climate*, *10*(7), 1635-1647.

Rohde, R., & Hilhorst, T. (2001). A profile of environmental change in the Lake Manyara Basin, Tanzania. *International Institute for Environment and Development, Drylands Programme.*

Ropelewski, C.F. & Jones, P.D. (1987). An extension of the Tahiti-Darwin Southern Oscillation Index. *Monthly Weather Review, 115*(9), 2161-2165.

Rowell, D. P., Booth, B. B., Nicholson, S. E., & Good, P. (2015). Reconciling past and future rainfall trends over East Africa. *Journal of Climate*, *28*(24), 9768-9788.

Rwehumbiza, F. B. (2014). A Comprehensive Scoping and Assessment Study of Climate Smart Agriculture Policies in Tanzania. *Pretoria, South Africa: Food, Agriculture and Natural Resources Policy Analysis Network*.

Saji, N. H., & Yamagata, T. (2003). Possible impacts of Indian Ocean dipole mode events on global climate. *Climate Research*, *25*(2), 151-169.

Saji, N. H., Goswami, B. N., Vinayachandran, P. N., & Yamagata, T. (1999). A dipole mode in the tropical Indian Ocean. *Nature*, *401*(6751), 360.

Schneider, U., Becker, A., Finger, P., Meyer-Christoffer, A. & Ziese, M. (2018). GPCC Full Data Monthly Product Version 2018 at 1.0°: Monthly Land-Surface Precipitation from Rain-Gauges built on GTS-based and Historical Data. *Global Precipitation Climatology Centre, Deutscher Wetterdienst.*

Schreck III, C. J., & Semazzi, F. H. (2004). Variability of the recent climate of eastern Africa. *International Journal of Climatology: A Journal of the Royal Meteorological Society*, *24*(6), 681-701.

Schwabe, K., Albiac, J., Connor, J. D., Hassan, R. M., & González, L. M. (2013). *Drought in arid and semi-arid regions.* Springer.

Sechambo, F. (2001). Land use by people living around protected areas: the case of Lake Manyara National Park. *University of Dar es Salaam Journals UTAFITI Special Issue, 4,* 1998-2001: 105-116.

Simonsson, L. (2001). Applied Landscape Assessment in a Holistic Perspective. a case study from Babati District, north-central Tanzania. *Licentiate thesis, Uppsala University, Department of Earth Sciences. Geotryckeriet, Uppsala, Sweden*.

Slingo, J., Spencer, H., Hoskins, B., Berrisford, P., & Black, E. (2005). The meteorology of the Western Indian Ocean, and the influence of the East African Highlands. *Philosophical Transactions of the Royal Society A: Mathematical, Physical and Engineering Sciences*, *363*(1826), 25-42.

Smoleroff, K. (2015). Examining interannual variability of the short rains for different categories of wet and dry years (Master's thesis). *Florida State University.*

Somi, E.J. (1993). Palaeoenvironmental Change in Central and Coastal Tanzania during the Upper Cenozoic (Ph.D. Thesis). *University of Stockholm.*

Stan, C., Straus, D. M., Frederiksen, J. S., Lin, H., Maloney, E. D., & Schumacher, C. (2017). Review of tropical-extratropical teleconnections on intraseasonal time scales. *Reviews of Geophysics*, *55*(4), 902-937.

Sun, L., Semazzi, F. H., Giorgi, F., & Ogallo, L. (1999). Application of the NCAR regional climate model to eastern Africa: 2. Simulation of interannual variability of short rains. *Journal of Geophysical Research: Atmospheres*, *104*(D6), 6549-6562.

Tallaksen, L. M., & Van Lanen, H. A. (Eds.). (2004). *Hydrological drought: processes and estimation methods for streamflow and groundwater* (Vol. 48). Elsevier.

Thompson, D. W., & Lorenz, D. J. (2004). The signature of the annular modes in the tropical troposphere. *Journal of climate*, *17*(22), 4330-4342.

Thompson, D. W., & Solomon, S. (2002). Interpretation of recent Southern Hemisphere climate change. *Science*, *296*(5569), 895-899.

Thornthwaite, C. W. (1948). An approach toward a rational classification of climate. *Geographical review*, *38*(1), 55-94.

Tierney, J. E., Smerdon, J. E., Anchukaitis, K. J., & Seager, R. (2013). Multidecadal variability in East African hydroclimate controlled by the Indian Ocean. *Nature*, *493*(7432), 389.

TMA (Tanzania Meteorological Agency) (2019). Daily rainfall data, monthly rainfall data, monthly temperature data. Retrieved via Verhoeve (2019). Technical report, Tanzanian Meteorological Agency.

Ummenhofer, C. C., Sen Gupta, A., England, M. H., & Reason, C. J. (2009). Contributions of Indian Ocean sea surface temperatures to enhanced East African rainfall. *Journal of Climate*, *22*(4), 993-1013.

UNEP (United Nations Environment Programme). (2004). Odada, E.O., Olago, D., Kulindwa, K.A.A., Bugenyi, F., West, K., Ntiba, M., Wandiga, S. & Karimumuryango, J. East African Rift Valley Lakes, GIWA Regional assessment 47. *University of Kalmar, Kalmar, Sweden.*

United Republic of Tanzania (2007). National Adaptation Programme of Action (NAPA) under the United Nations Framework Convention on Climate change (UNFCCC). *United Republic of Tanzania, Vice President's Office Division of Environment*.

van den Bergh, H. A. J. (2016). The impacts of Maasai settlement on land cover, meteorological conditions and wind erosion risk in northern Tanzania (Master's thesis). *Utrecht University.*

Van Lanen, H. A. J., Wanders, N., Tallaksen, L. M., & Van Loon, A. F. (2013). Hydrological drought across the world: impact of climate and physical catchment structure. *Hydrology and Earth System Sciences*, *17*, 1715-1732.

van Loon, A. F. (2015). Hydrological drought explained. *WIREs Water*, *2*, 359–392.

van Mens, L. M. (2016). Unravelling the hydrological dynamics of Lake Manyara in Tanzania (Master's thesis). *Utrecht University.*

Verhoeve, S. L. (2019). Satellite based analysis of environmental changes in the Monduli and Longido districts, Tanzania (Master's thesis). *Utrecht University.*

Vicente-Serrano, S. M., Beguería, S., & López-Moreno, J. I. (2010). A multiscalar drought index sensitive to global warming: the standardized precipitation evapotranspiration index. *Journal of climate*, *23*(7), 1696-1718.

Vicente-Serrano, S. M., Beguería, S., Gimeno, L., Eklundh, L., Giuliani, G., Weston, D., El Kenawy, A., López-Moreno, J. I., Nieto, R., Ayenew, T., Konte, D., Ardö, J. & Pegram, G. G. S. (2012). Challenges for drought mitigation in Africa: The potential use of geospatial data and drought information systems. *Applied Geography*, *34*, 471-486.

Vigaud, N., Lyon, B., & Giannini, A. (2017). Sub-seasonal teleconnections between convection over the Indian Ocean, the East African long rains and tropical Pacific surface temperatures. *International Journal of Climatology*, *37*(3), 1167-1180.

Vörösmarty, C. J., McIntyre, P. B., Gessner, M. O., Dudgeon, D., Prusevich, A., Green, P., Glidden, S. Bunn, S. E., Sullivan, C. A., Reidy Liermann, C. & Davies, P. M. (2010). Global threats to human water security and river biodiversity. *Nature*, *467*(7315), 555.

Webster, P. J., Moore, A. M., Loschnigg, J. P., & Leben, R. R. (1999). Coupled ocean–atmosphere dynamics in the Indian Ocean during 1997–98. *Nature*, *401*(6751), 356.

Wenhaji Ndomeni, C., Cattani, E., Merino, A., & Levizzani, V. (2018). An observational study of the variability of East African rainfall with respect to sea surface temperature and soil moisture. *Quarterly Journal of the Royal Meteorological Society*, *144*, 384-404.

Williams, A. P., & Funk, C. (2011). A westward extension of the warm pool leads to a westward extension of the Walker circulation, drying eastern Africa. *Climate Dynamics*, *37*(11-12), 2417-2435.

Williams, C. A., & Hanan, N. P. (2011). ENSO and IOD teleconnections for African ecosystems: evidence of destructive interference between climate oscillations. *Biogeosciences*, *8*(1), 27-40.

Woodruff, S. D., Worley, S. J., Lubker, S. J., Ji, Z., Eric Freeman, J., Berry, D. I., Brohan, P., Kent, E. C., Reynolds, R. W., Smith, S. R. & Wilkinson, C. (2011). ICOADS Release 2.5: extensions and enhancements to the surface marine meteorological archive. *International journal of climatology*, *31*(7), 951-967.

World Bank (2017). Agriculture, forestry, and Fishing, value added (% of GDP) [online]. Retrieved from https://data.worldbank.org/indicator/NV.AGR.TOTL.ZS?end=2017&locations=TZ&start=1990 [visited: 12-09-2019].

WSDP (Water Sector Development Program) (2014). Daneshvar, S., Zttarzadeh, A. A., Kashaigili, J. & Dehghanipour, A. H. Consultancy Services for Preparation of Integrated Water Resources Management and Development Plan (IWRMDP) for Internal Drainage Basin (IDB) Vol. 2 Water Availability Part A – Surface Water. *United Republic of Tanzania, Ministry of Water.*

Wu, R., & Kinter III, J. L. (2009). Analysis of the relationship of US droughts with SST and soil moisture: Distinguishing the time scale of droughts. *Journal of Climate*, *22*(17), 4520-4538.

WWAP (World Water Assessment Programme) (United Nations), & UN-Water. (2009). *Water in a changing world* (Vol. 1). Earthscan.

Wynants, M., Millward, G., Patrick, A., Taylor, A., Munishi, L., Mtei, K., Brendonck, L., Gilvear, D., Boeckx, P., Ndakedemi, P. & Blake, W. H. (2020). Determining tributary sources of increased sedimentation in East-African Rift Lakes. *Science of The Total Environment*, *717*, 137266.

Wynants, M., Munishi, L., Solomon, H., Grenfell, M., Taylor, A., Millward, G., Boeckx, P. Ndakidemi, P., Gilvear, D. & Blake, W. (2017). The response of sediment source and transfer dynamics to land use (change) in the Lake Manyara catchment. *EGU General Assembly Conference Abstracts*, *19*, 5547.

Wynants, M., Solomon, H., Ndakidemi, P., & Blake, W. H. (2018). Pinpointing areas of increased soil erosion risk following land cover change in the Lake Manyara catchment, Tanzania. *International journal of applied earth observation and geoinformation*, *71,* 1-8.

Xue, F., Wang, H., & He, J. (2004). Interannual variability of Mascarene high and Australian high and their influences on East Asian summer monsoon. *Journal of the Meteorological Society of Japan. Ser. II*, *82*(4), 1173-1186.

Xue, Y., Higgins, W., & Kousky, V. (2002). Influences of the Madden Julian Oscillations on temperature and precipitation in North America during ENSO-neutral and weak ENSO winters. In *Proc. workshop on prospects for improved forecasts of weather and short-term climate variability on subseasonal (2 week to 2 month) time scales*. NASA/Goddard Space Flight Center.

Yanda, P. Z., & Madulu, N. F. (2005). Water resource management and biodiversity conservation in the Eastern Rift Valley Lakes, Northern Tanzania. *Physics and Chemistry of the Earth, Parts A/B/C*, *30*(11-16), 717-725.

Yang, W., Seager, R., Cane, M. A., & Lyon, B. (2014). The East African long rains in observations and models. *Journal of Climate*, *27*(19), 7185-7202.

Yang, Y., Xie, S. P., Wu, L., Kosaka, Y., Lau, N. C., & Vecchi, G. A. (2015). Seasonality and predictability of the Indian Ocean dipole mode: ENSO forcing and internal variability. *Journal of Climate*, *28*(20), 8021-8036.

Yevjevich, V. M. (1967). An objective approach to definitions and investigations of continental hydrologic droughts. *Hydrology Papers No*. *23*, Colorado State University, Fort Collins, 1967.

Yuan, Y., & Li, C. (2008). Decadal variability of the IOD-ENSO relationship. *Chinese Science Bulletin*, *53*(11), 1745-1752.

Zhang, Q., Qi, T., Singh, V. P., Chen, Y. D., & Xiao, M. (2015). Regional frequency analysis of droughts in China: a multivariate perspective. *Water Resources Management*, *29*(6), 1767-1787.

Appendices

Appendix A: Comparison precipitation datasets

The available precipitation datasets were compared to decide which ones to use for investigating drought in the LMC. The temporal period for comparison was chosen when the datasets overlap (1981-1994). Both differences in the seasonal cycle and annual precipitation were examined. Dataset inter-comparison is performed using the coefficient of determination (R^2), root-mean-square-error (RMSE) and t- and F-tests.

Comparison of the seasonal cycle and annual precipitation among the datasets

Monthly average precipitation values over the period 1981-1994 are shown in Figure A1 for all datasets. The in-situ datasets did have some missing observations during this period: April 1992 and all months of 1994 for Babati, June 1985-December 1986 and August 1992 for Karatu, June 1986 and June-July 1987 for Kondoa, September 1989 for Mbulu and October 1982 and September 1985 for Monduli. These missing values where not taken into account when calculating the mean of monthly precipitation.

Most datasets show the bimodal rainfall pattern present in the LMC (Figure A1). Highest monthly rainfall values are visible during the long rainy season, during with 8 of the 12 datasets experiencing peak precipitation values in April and 2 datasets in March. The value of this rainfall peak varies from 113 (ERA5) to 265 (Arusha). Only Kondoa and ERA-Interim (ERAI) show highest monthly rainfall in January. The long dry season (Jun-Sep) is visible in all datasets. From September rainfall increases in all datasets. A drop in rainfall values indicating the short dry season after a short rainy season is present in most datasets during February (9 of the 12) or January (ERA5). Kondoa and CRU do not show the presence of a short dry season nor a distinction between a long and short rainy season.

When comparing the in-situ datasets, the relatively high precipitation values of Arusha during the rainy seasons stand out. During the short rainy season Arusha values are lowest of all in-situ datasets. Annual precipitation values of Arusha are relatively high. Kondoa shows the opposite pattern, with high values during the short dry season and low values during the low rainy season. If fact, it barely shows the presence of the short rainy and short dry seasons. This contrast between Kondoa and Arusha could be due to location of the stations. Kondoa is by far the most southern

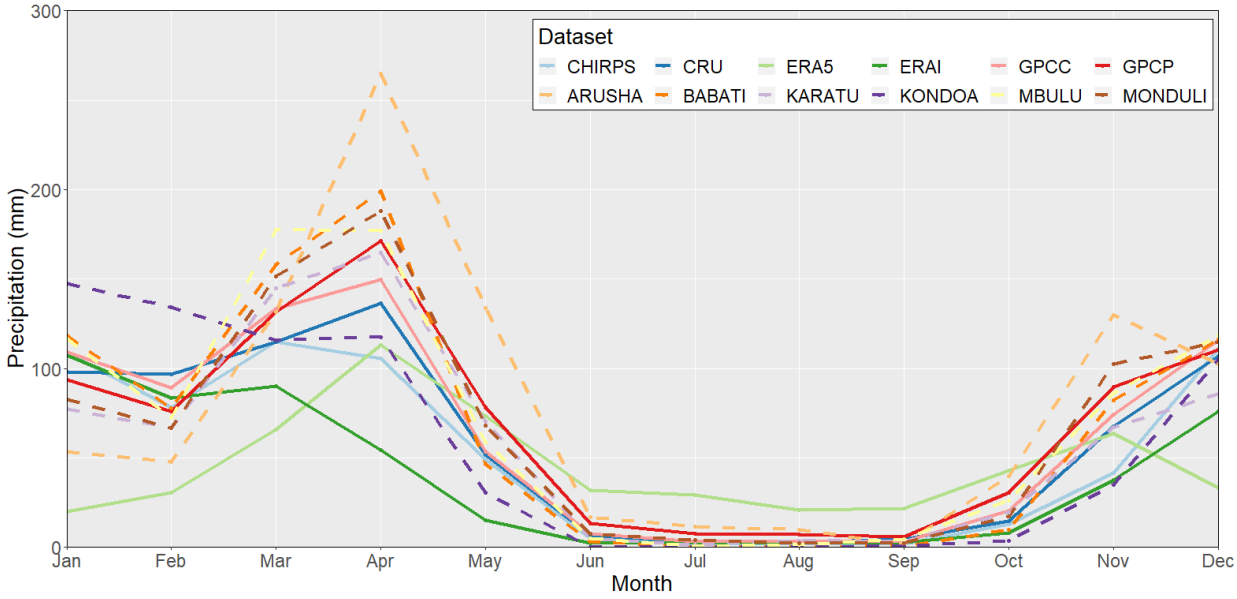

Figure A1: Monthly average precipitation (mm) from 1981 to 1994 for all datasets. In-situ datasets (Arusha, Babati, Karatu, Kondoa, Mbulu, Monduli) in dashed lines. Precipitation products (CHIRPS, CRU, ERA5, ERAI, GPCC, GPCP) in solid lines.

station. Arusha station has the same altitude but is located in the north. Arusha lies closer to the equator. This could influence whether an area experiences a bimodal rainfall pattern or not, as it is created by the movement of the ITCZ twice over the area. The southern location Kondoa might only experience the ITCZ once and for a longer period, explaining no short dry season.

The variation in values among the datasets is largest during the long rainy season (Figure A2; Table A1). The datasets show smallest differences during the long dry season, with ERA5 being the outlier. ERA5 values are more than twice as high compared to all other datasets during this period. This dataset is also the outlier in December through March, with smaller values than other datasets. Other outliers are Kondoa in February and Arusha in May. The in-situ and precipitation product datasets vary among the same range. Only during March and April most in-situ datasets (4 of the 6) have higher values than the precipitation product datasets.

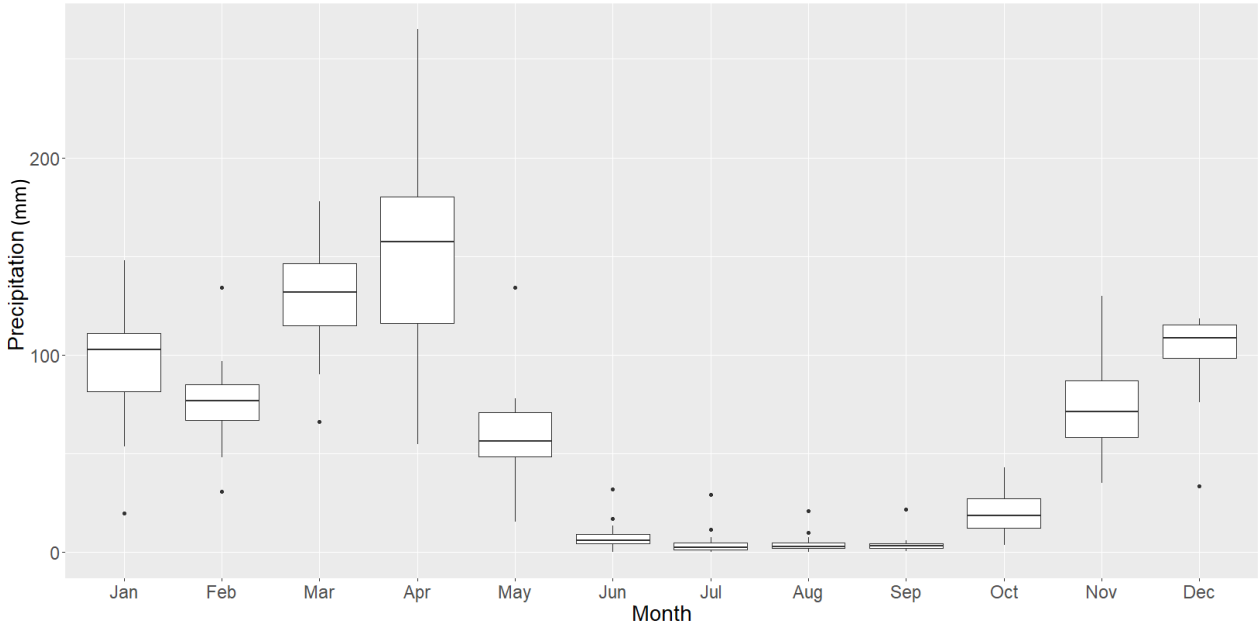

Figure A2: Boxplots showing the distribution of monthly average precipitation values among the datasets.

Table A1: Minimum and maximum average monthly precipitation value among the datasets. The corresponding dataset of these values are also shown. Absolute and relative difference between minimum and maximum monthly precipitation.

	Minimum (mm)	Minimum Dataset	Maximum (mm)	Maximum Dataset	Absolute difference (mm)	Relative difference (%)
Jan	19.8	ERA5	147.7	Kondoa	127.9	86.6
Feb	30.7	ERA5	134.1	Kondoa	103.4	77.1
Mar	66.1	ERA5	177.6	Mbulu	111.5	62.8
Apr	54.7	ERAI	264.9	Arusha	210.2	79.4
May	15.4	ERAI	134.1	Arusha	118.7	88.5
Jun	0	Kondoa	32.1	ERA5	32.1	-
Jul	0.1	Kondoa	29.1	ERA5	29	99.7
Aug	0	Kondoa	21	ERA5	21	-
Sep	0.4	Kondoa	21.7	ERA5	21.2	97.9
Oct	3.6	Kondoa	43.1	ERA5	39.5	91.6
Nov	35.1	Kondoa	129.7	Arusha	94.6	73
Dec	33.4	ERA5	118.4	Mbulu	85	71.8

The variation in annual total rainfall is visible in Figure A3 and A4. Total annual precipitation is not calculated in datasets for years with missing values. The range of annual precipitation provided by the dataset varies through the years (Figure A4). As can be seen in Figure A3, the ERA-Interim and ERA5 datasets overall have the lowest annual precipitation values. Multiple in-situ datasets give outliers due to relatively high values. CHIPRS, CRU, GPCC, GPCP, Karatu and Monduli datasets seem to follow the same pattern through the years.

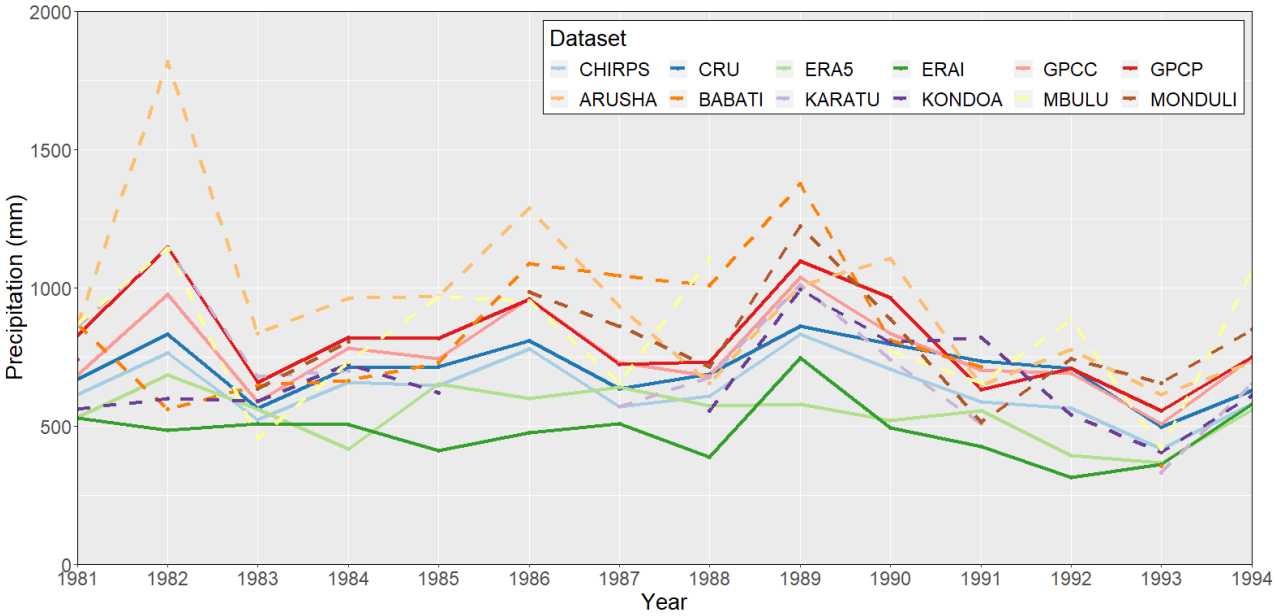

Figure A3: Annual total precipitation (mm) from 1981 to 1994 for all datasets. In-situ datasets (Arusha, Babati, Karatu, Kondoa, Mbulu, Monduli) in dashed lines. Precipitation products (CHIRPS, CRU, ERA5, ERAI, GPCC, GPCP) in solid lines.

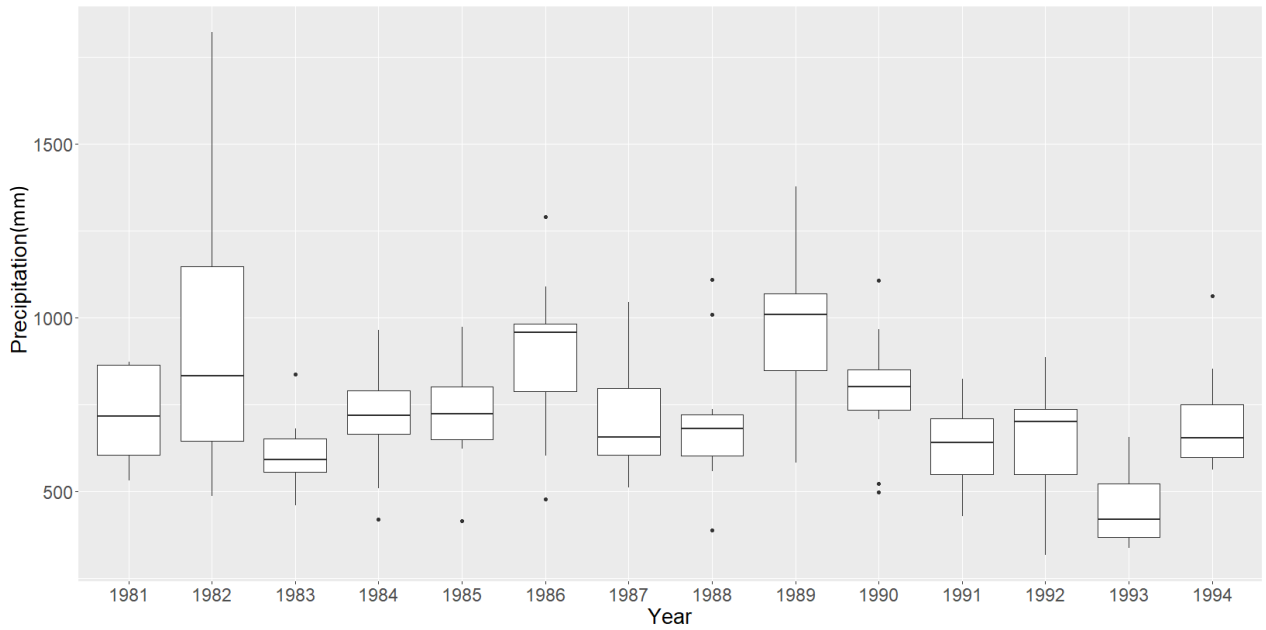

Figure A4: Boxplots showing the distribution of annual total precipitation values among the datasets.

Dataset inter-comparison

Table A2 shows the coefficient of determination (R^2) and Root Mean Square Error (RMSE) between the datasets. R^2 indicates the proportion of variance in one variable that is explained by linear regression and the other variables. It ranges between 0 and 1. A good fit is expressed by a high R^2. It can be used a measure of similarity between the datasets. If the datasets are equal, the R^2 would be 1. The RMSE shows how concentrated the data is around the linear regression line between the datasets. Low values indicate less difference between the values of the datasets and thus a better fit.

The R^2 and RMSE show a good fit between most precipitation products. CHIRPS, CRU, GPCC and GPCP show a good fit among each other (R^2>0.84, RMSE<30.78). ERA-Interim and ERA5 show poorer fits with CHIRPS, CRU, GPCC and GPCP. R^2/RMSE values range between 0.54-0.76/31.78-54.94 for ERA-Interim and 0.15-0.34/53.96-60.43 for ERA5. ERA-Interim and ERA-5 show the least similarity according to the R^2 of 0.03. Among the in-situ datasets there are overall poorer R^2 and RMSE values, indicating less similarity. Arusha and Kondoa datasets display in general the poorest values in connection to other datasets and each other. Comparing the precipitation products with the in-situ datasets, it stands out that ERA5 shows the least similarity with the in-situ datasets (< 0.43/ >57.16). ERA-Interim also has poor R^2 and RMSE values with other in-situ datasets (<0.52), except for with Kondoa (0.71/57.52). Arusha stands out as the station that shows poorest results when compared with precipitation products CHIRPS, CRU and GPCC. Only in comparison with GPCC Kondoa shows a lower R^2 than Arusha, but it also has a lower RMSE. Babati, Karatu, Kondoa, Mbulu and Monduli overall show a good fit with CHIRPS, CRU, GPCC, GPCP. This could be due to the similarity of the GPCC and GPCP. Despite this, comparison with Kondoa shows that this similarity is not absolute, as can be seen with R^2 and RMSE values for Kondoa versus GPCC and GPCP (0.72/49.93 and 0.55/59.66 respectively).

Table A3 shows F-test and t-test results between all datasets. The performed t-test did take into account whether variances were equal or not. Among the product datasets, both variances and means are equal for CRU compared to CHIRPS, GPCC and GPCP, and GPCC compared to GPCP. Among the in-situ datasets all means are equal. However, Arusha has significantly different variance than all other datasets. Babati and Karatu also have different variances. The other combinations show both equal means and variances. Karatu and Monduli are the only in-situ datasets with equal variances and means with precipitation products. ERA5 and ERA-Interim show no equal variances and/or equal means with many of the other datasets. When comparing Table A2 and A3, it is clear that equal means and/or variances between datasets does not necessarily imply good R^2 and RMSE values and vice versa. Still, GPCC, GPCP and CRU are the most similar datasets as these show good R^2 and RMSE values and equal variances and means among each other.

Table A2: Dataset inter-comparison over the period 1981-1994, showing R^2 and RMSE. Dark blue colours indicate a good fit and dark red indicates a poor fit.

		Precipitation products						In-situ datasets					
	RMSE\R²	CHIRPS	CRU	ERA5	ERAI	GPCC	GPCP	ARUSHA	BABATI	KARATU	KONDOA	MBULU	MONDULI
P Products	CHIRPS		0.94	0.15	0.76	0.94	0.84	0.37	0.70	0.64	0.75	0.72	0.62
	CRU	16.52		0.21	0.69	0.96	0.90	0.46	0.73	0.65	0.73	0.72	0.68
	ERA5	53.96	54.90		0.03	0.21	0.34	0.38	0.18	0.43	0.03	0.27	0.32
	ERAI	31.78	40.17	57.91		0.69	0.54	0.16	0.52	0.35	0.71	0.39	0.40
	GPCC	20.51	15.28	60.43	45.14		0.93	0.48	0.76	0.66	0.72	0.72	0.72
	GPCP	30.78	22.89	58.25	54.94	17.64		0.63	0.73	0.73	0.55	0.72	0.78
In-situ datasets	ARUSHA	85.65	77.80	90.39	104.85	75.33	64.11		0.29	0.53	0.16	0.39	0.50
	BABATI	53.02	48.34	81.21	69.45	43.65	45.54	89.69		0.53	0.57	0.60	0.57
	KARATU	43.42	41.79	57.16	61.86	41.81	38.29	71.99	61.70		0.30	0.72	0.58
	KONDOA	48.56	47.59	85.97	57.52	49.93	59.66	105.39	64.59	72.13		0.40	0.36
	MBULU	47.74	45.00	73.56	70.94	42.52	41.76	81.81	54.96	45.71	72.62		0.53
	MONDULI	48.66	43.02	67.97	66.43	39.03	34.76	72.13	56.98	52.03	73.15	55.72	

Table A3: T-test and F-test statistics between the datasets. T-test: green indicates significantly equal means, blue indicate significantly different means (α=0.95, p-value>0.05). F-test: darker colours indicate significantly equal variances, lighter colours indicate significantly different variances (α=0.95, p-value>0.05). So dark green means significantly equal means and variances.

		Precipitation products						In-situ datasets					
		CHIRPS	CRU	ERA5	ERAI	GPCC	GPCP	ARUSHA	BABATI	KARATU	KONDOA	MBULU	MONDULI
P Products	CHIRPS												
	CRU												
	ERA5												
	ERAI												
	GPCC												
	GPCP												
In-situ datasets	ARUSHA												
	BABATI												
	KARATU												
	KONDOA												
	MBULU												
	MONDULI												

Use of datasets in further analysis

In the comparison of the seasonal cycle and annual precipitation values among the datasets the discrepancy of ERA5 and ERA-Interim came forward. ERA5 shows abnormally high precipitation values during boreal summer compared to the other datasets. ERA-Interim does not show the presence of the bimodal rainfall pattern and has the noticeably lowest annual precipitation values. The discrepancy is also evident in R^2 and RMSE values and in F- and T- statistics. Therefore, ERA5 and ERA-Interim will not be included in further analysis. The average will be taken of CHIRPS, CRU, GPCC and GPCP datasets. This new time series will be called the Reanalysis dataset. The average of all in-situ datasets will be used to form the In-situ dataset. Though showing discrepancies, Arusha and Kondoa are included as the in the average rainfall over the catchment is desired. Comparison of the datasets gives a good fit (R^2=0.87). In general, the In-situ dataset shows higher values than the Reanalysis dataset (Figure A5). All analyses in this research are executed with both the Reanalysis dataset and In-situ dataset. The results of these analyses will be compared to see whether there is large difference between the use of in-situ data or precipitation products.

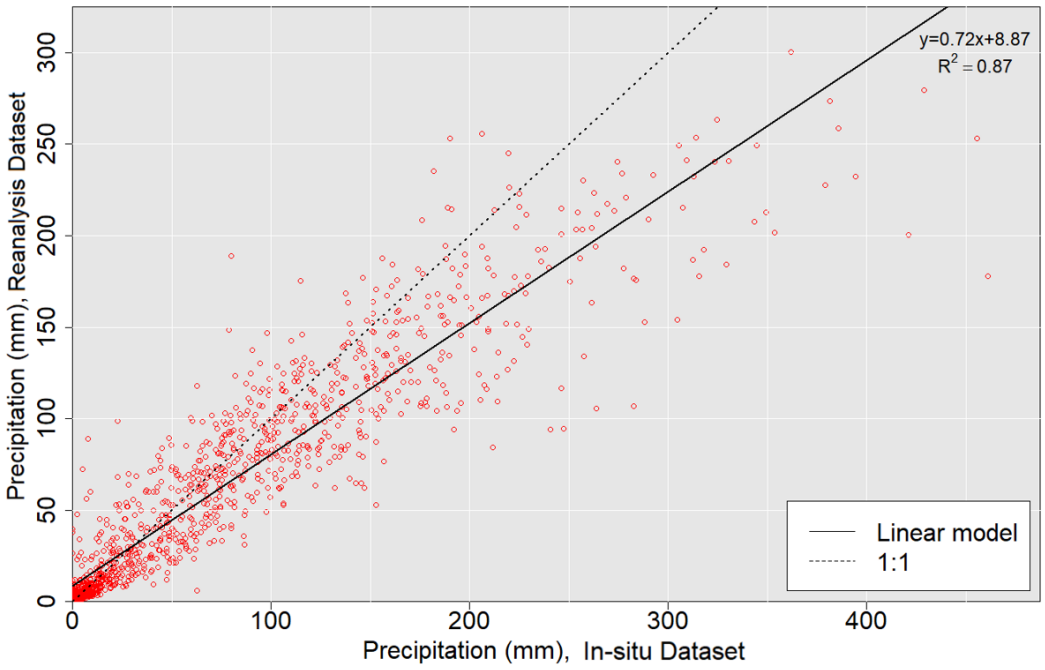

Figure A5: Scatterplot between the In-situ and Reanalysis datasets. Regression line and 1:1 line are also given.

Appendix B: Lake Manyara surface area observations

Table B: Surface area of Lake Manyara (km2) per observation.

Year	Jan	Feb	Mar	Apr	May	Jun	Jul	Aug	Sep	Oct	Nov	Dec	Images /year
1984											125.3		1
1985													0
1986													0
1987													0
1988													0
1989													0
1990													0
1991	142.9												1
1992													0
1993													0
1994												69.6	1
1995		197.3											1
1996													0
1997													0
1998													0
1999											547.1		1
2000		488.6							490.2			455.8	3
2001	462.8	481.8									447.9	456.0	4
2002	455.9	454.4									132.6	313.5	4
2003	452.4		361.2									223.6	3
2004													0
2005		95.5							13.9				2
2006													0
2007													0
2008									336.5				1
2009	96.7		93.1			279.5			18.1		113.3	53.7	6
2010	255.0									37.9		170.9	3
2011	248.9										41.9		2
2012		326.7						18.7		69.5			3
2013	58.2	75.8				309.8	308.0	305.9	286.8	390.8	224.3	172.7	9
2014	153.1	180.9		237.3			290.1	188.7		106.8	136.8	142.3	8
2015	100.7	129.5	83.8			362.6		218.0	217.9	114.4	214.2	224.3	9
2016	235.0	341.1	319.1					290.6		57.9	170.7	347.1	7
2017	37.2	231.4	304.3					81.1	23.9	120.8	260.3	278.9	8
2018	291.1	242.2			436.5	417.0				216.9		401.4	6
Total images	13	12	5	1	1	4	2	6	7	8	11	13	83

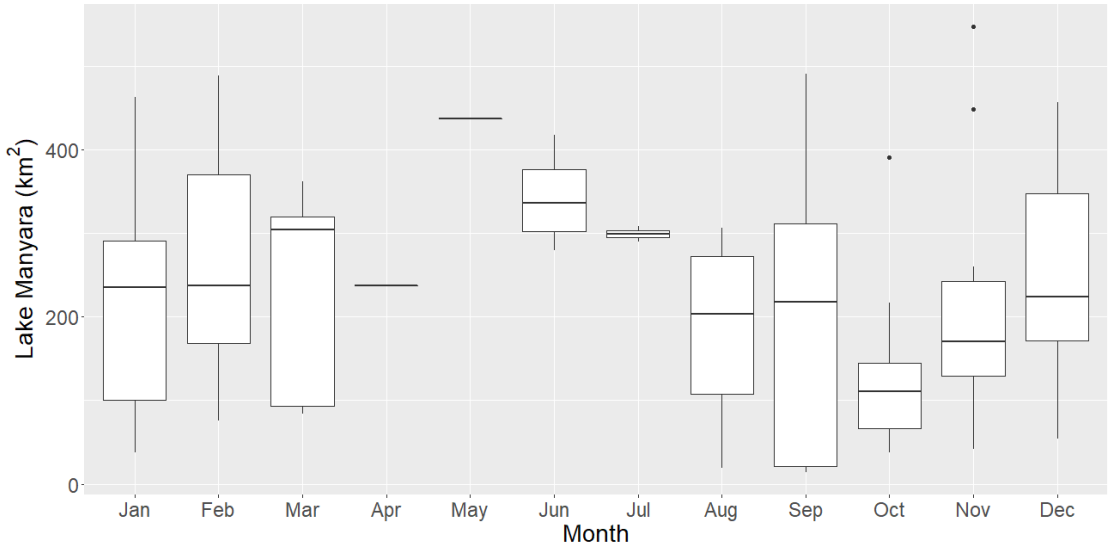

Figure B: Boxplots showing the distribution of surface area values of Lake Manyara per month of the year.

Appendix C: Yearly SPI-3 and SPEI-3 rainy seasons

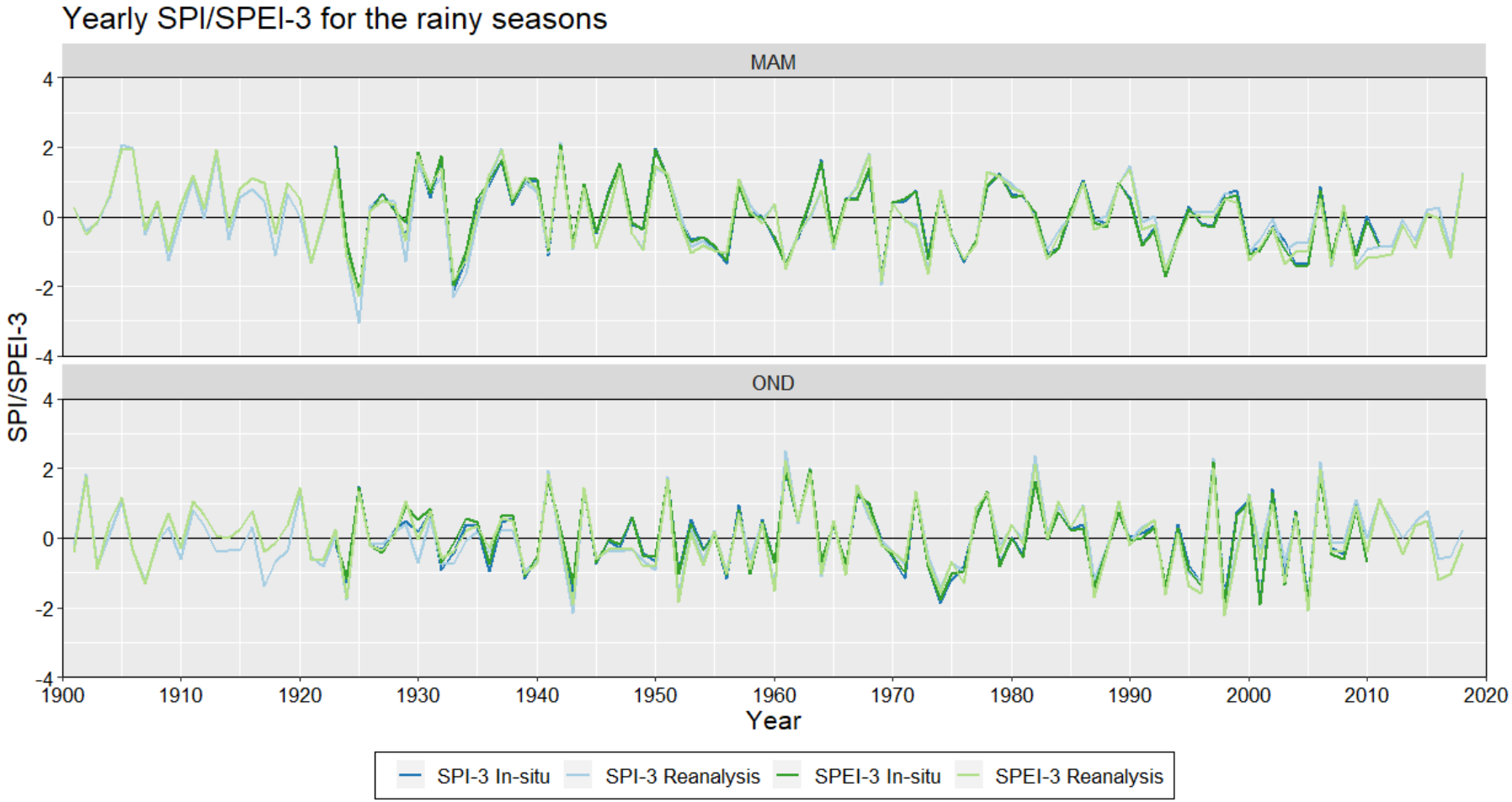

Figure C: Yearly SPI-3 and SPEI-3 values representing the long (March-May/MAM) and short (October-December/OND) rainy seasons.

Appendix D: Teleconnection correlations of the other months

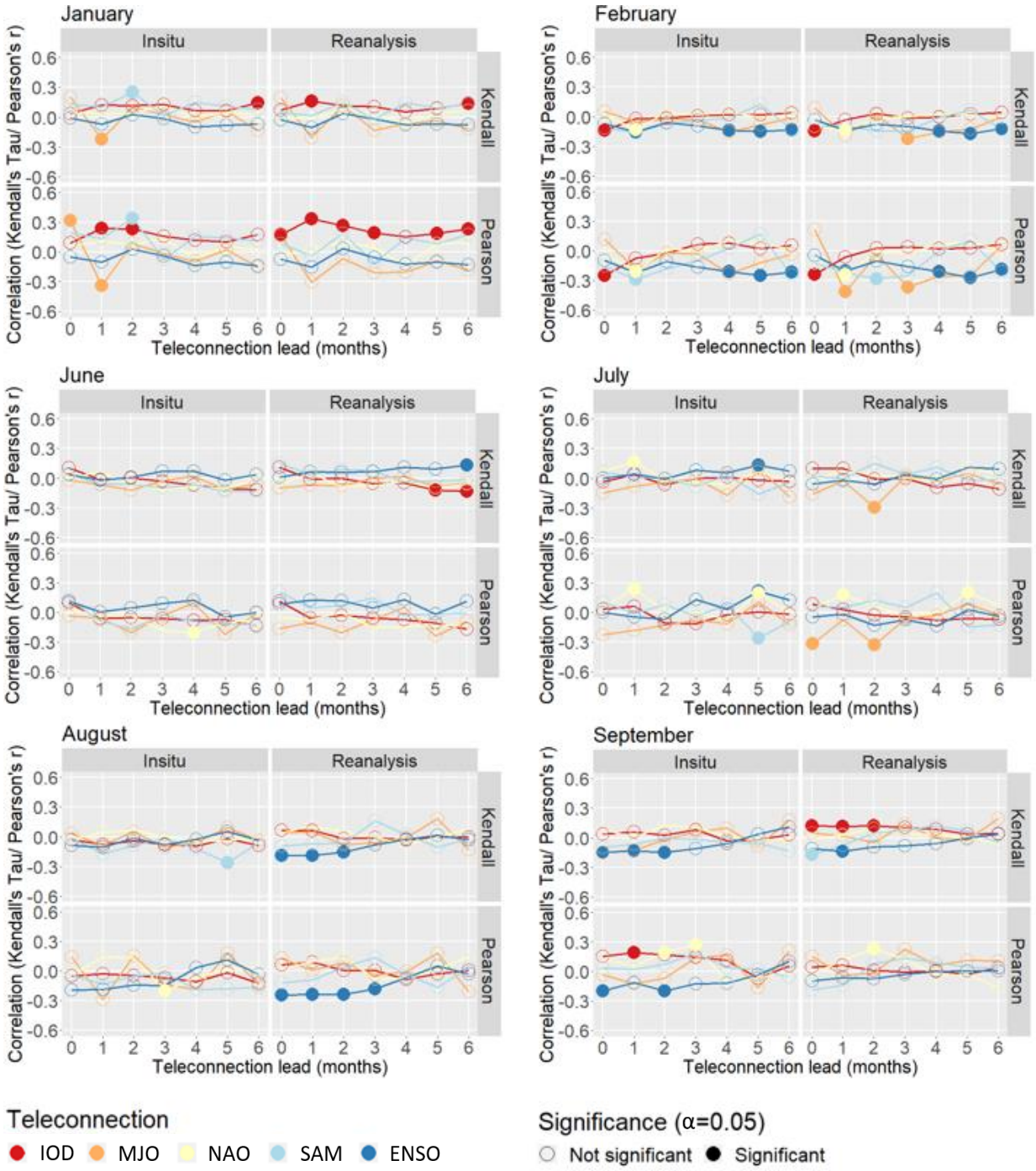

Figure D: Correlations between rainfall and teleconnection indices with a maximum lead of 6 months for the separate months of the dry seasons.